The Paton WELDING JOURNAL

May 2000 # 5

English translation of the monthly «Avtomaticheskaya Svarka» journal published in Russian since 1948

«The Paton Welding Journal» monthly is published by the E.O. Paton Electric Welding Institute of the National Academy of Sciences of Ukraine with the support rendered by the International Association «Welding».

Promotion group:
V.N.Lipodaev, V.I.Lokteva
A.T.Zelnichenko (Exec. director)
Translators:
S.A.Fomina, I.N.Kutianova, T.K.Vasilenko
Editorial and advertising offices
are located at PWI, Dept. 51, 11, Bozhenko str., 03680, Kyiv, Ukraine.
Tel.: (38044) 227 67 57
Fax: (38044) 268 04 86
E-mail: paton@i.kiev.ua

Subscriptions:
$460, 12 issues

«The Paton Welding Journal» Website:
http://www.nas.gov.ua/pwj

CONTENTS

SCIENTIFIC AND TECHNICAL

MAKHNENKO V.I., VELIKOIVANENKO E.A., MAKHNENKO O.V., ROZYNKA G.F. and *PIVTORAK N.I.* Investigation of effect of phase transformations on residual stresses in circumferential welding of pipes 2

KUZMENKO V.G., GALINICH V.I., TOKAREV V.S., STUKALO V.A. and *SOKOLSKY V.E.* Study of properties of slag melts for grounding the compositions of welding fluxes. Part II. Thermodynamic characteristics 8

MARKASHOVA L.I., GRIGORENKO G.M., KHARCHENKO G.K., ARSENYUK V.V., GRIGORENKO S.G. and *BOGAICHUK I.L.* Structure of the ferrite band formed in the joint zone of ferritic-pearlitic steels in vacuum pressure welding 14

NIKIFOROV N.I., SUKHININ G.K., KREKTULYOVA R.A., BEZHIN O.N. and *GUBENKO L.V.* Results of numerical and full-scale experiments on high-speed oxygen cutting of metals 19

CHIGAREV V.V. and *USTINOV A.V.* Design-experimental estimation of the possibility of reduction of the HAZ metal cooling rate in wet underwater welding 24

SAVITSKY M.M., KULIK V.M. and *BURSKY G.V.* Peculiarities of arc treatment of quenching steels without melting 30

INDUSTRIAL

ZYAKHOR I.V. Peculiarities of friction welding of dissimilar metals and alloys 36

SNISAR V.V., DEMCHENKO E.L., BREDNEVA O.I. and *IVANCHENKO E.V.* New electrodes for welding and surfacing of steel 110G13L 45

PROKOFIEV A.S. and *PISMENNY A.S.* Technology of braze welding of flanges to tubes 48

KHASKIN V.Yu., PAVLOVSKY S.Yu., GARASHCHUK V.P., SHELYAGIN V.D., TSARYUK A.K., SOLOMIJCHUK T.G. and *CHIZHSKAYA T.G.* Properties of hypereutectoid complex-alloyed steels after laser heat-treatment 51

BRIEF INFORMATION

CHIGAREV V.V. and *MALINOV V.L.* Selection of sparsely-alloyed surfacing materials for different impact-abrasive conditions 55

MARKASHOVA L.I., ARSENYUK V.V., OPARA V.S., ONATSKAYA N.A. and *REZNIKOVA L.Ya.* Effect of hydroelectric pulse treatment on structure of welded joint metal 58

NEWS

E.O. Paton Electric Welding Institute Technology Park 60

INVESTIGATION OF EFFECT OF PHASE TRANSFORMATIONS ON RESIDUAL STRESSES IN CIRCUMFERENTIAL WELDING OF PIPES

V.I. MAKHNENKO, E.A. VELIKOIVANENKO, O.V. MAKHNENKO, G.F. ROZYNKA and **N.I. PIVTORAK**
The E.O.Paton Electric Welding Institute, NASU, Kyiv, Ukranine

ABSTRACT

The effect of microstructural changes, caused by welding thermal cycle, on residual stresses within the zone of a multipass circumferential butt weld in X65 steel pipe is investigated using numerical methods. Two versions of welding the pipe wall of 19 mm thickness for 3 and 8 passes are considered. It is shown that allowance for microstructural changes in metal of weld and HAZ at different energy inputs of welding leads to the increase in non-uniformity of distribution of mechanical properties and residual stresses in weld zone.

Key words: *numerical investigation, microstructural changes, circumferential butt weld, multipass welding, heat-affected zone, triaxial stressed state.*

At present the welded structures made from high-strength steels, whose welding requires a comprehensive testing of technology from different points of view, including that of expected residual stresses (strains), find more and more wide spreading. It is natural that there is a tendency to make the most use of the calculating methods in parallel with the experiments [1 – 3, etc].

The calculating methods based on observation of development of elastic-plastic deformations during welding heating and cooling are used for the above-mentioned steels to study the changes in a microstructural composition in weld and HAZ, because the welding stresses and their distribution depend greatly on it.

Kinetics of microstructural changes in weld and HAZ during welding steels is a rather complicated process in general, as its adequate description with mathematical means encounters great difficulties. Now, it is most real to construct the models on the basis of appropriate experimental diagrams of anisothermal decay of austenite (ADA) and to concentrate attention to those transformations which influence remarkably the physical properties used in a calculating scheme. The most sensitive physical properties from these positions [3] are the volumetric effects and material resistance to deforming (yield strength $\sigma_y(T)$ at the given temperature).

Conception about the effect of characteristic constituents of the microstructure of structural steels on volumetric effects is given by the following results [4] as related to volume $\gamma_j(T)$ of one gram of material in a given state (j = a, m, f, b, p) at an appropriate temperature:

austenite –

$$\gamma_a \cong 0.12282 + 8.36\cdot10^{-6}\,(T + 273) + 2.15\cdot10^{-6}\,C,\ \mathrm{cm^3/g},$$

martensite –

$$\gamma_m \cong 0.12708 + 4.448\cdot10^{-6}\,(T + 273) + 2.79\cdot10^{-6}\,C,\ \mathrm{cm^3/g},$$

ferrite, bainite, pearlite –

$$\gamma_{fbp} \cong 0.12708 + 5.528\cdot10^{-6}\,(T + 273),\ \mathrm{cm^3/g},$$

where C is the carbon content, %.

It is seen from these data that there is the most essential difference between the specific volumes in austenite transformation into martensite within the region of low temperatures. The austenite transformation into ferrite at 600 – 700 °C and, the more so, ferrite into austenite at temperatures above 750 °C is not accompanied by a noticeable jump of difference in specific volumes.

A knowledge of a relative content of j-th microstructure $V_j(T)$ in unit mass at temperature T ($\Sigma V_j(T) \equiv 1$) allows calculation of function of free elongations at temperature changes:

$$\varphi(T) = \frac{\sum_j V_j(T)\,\gamma_j(T) - \sum_j V_j(T_0)\,\gamma_j(T_0)}{3\sum_j V_j(T_0)\,\gamma_j(T_0)}, \quad (1)$$

where T_0 is the initial temperature.

Figure 1 gives a conception about the effect of microstructure on the resistance of structural steel to deforming. It is seen from these data that the difference in resistance of separate structural constituents to deforming is rather noticeable. With value $\sigma_y^j(T)$ it is possible to synthesize $\sigma_y(T)$ with a sufficient accuracy for steel at different content of $V_j(T)$:

$$\sigma_y(T) = \sum_j \sigma_y^j(T) V_j(T). \quad (2)$$

To confirm this, Figure presents a curve $\sigma_y(T)$ at $V_b = 0.4$ and $V_f = 0.6$, calculated by formula (2) taking into account the experimental data. It should be noted that values $\sigma_y^j(T)$ for a wide range of chemical composition of steels preserve, at least approximately, a constant dependence on temperature for ratio $\sigma_y^j(T)/\sigma_y^j(20\ ^\circ C)$, that facilitates greatly the search for a necessary information in case of absence of data (of types given in Figure 1) for a definite chemical composition of steel. As to $\sigma_y^j(20\ ^\circ C)$, then in case of absence of experimental data it is possible to use different approximated regression relationships. Thus, for example, in [5] for the type of steel (%)

$$\begin{gathered} C \le 0.3;\ Mn \le 2;\ Si \le 0.8;\ Cr \le 2;\ Mo \le 1, \\ Ni \le 2;\ V \le 0.3;\ Ti \le 0.06;\ Al \le 0.06, \\ Nb \le 0.1;\ W \le 0.5 \end{gathered} \quad (3)$$

the ratios

$$\sigma_y^m(20\ ^\circ C) = 602 + 2150\,C + 500\,Mo,\ MPa,$$

$$\sigma_y^b(20\ ^\circ C) = 500 + 460\,C - 120\,C^2 + 150\,V + 360\,Mo,\ MPa,$$

$$\sigma_y^{fp}(20\ ^\circ C) = 187 + 92\,C + 47\,Mn + 90\,V,\ MPa$$

in combination with values $\sigma_y^j(T)$ are worthy of attention (Figure 1). It follows from the above-mentioned that at known kinetics of temperature changing in weld and HAZ, the characteristics of the material sensitive to phase changes under the action of a thermal cycle of welding, required for calculation of welding stresses (strains) are determined by formulae (1) and (2), if the kinetics $V_j(T)$ is known in each point of the joint examined. In different works [1, 5, 6, etc.] a large attention is now paid to the construction of appropriate models. The most design proposals are based on assumption that at the stage of heating the change in initial microstructural state occurs only at reaching sufficiently high temperatures (above A_3), i.e. for steels — at temperatures of about $T = 850 - 900$ °C.

Respectively, the region $T_{max}(x, y, z) \ge T_*$ defines the zone where the phase transformations at the stage of heating and cooling lead to the change in V_j as compared with the initial state.

From the mathematical point of view this assumption for a simple cycle of heating-cooling can be formulated as follows:

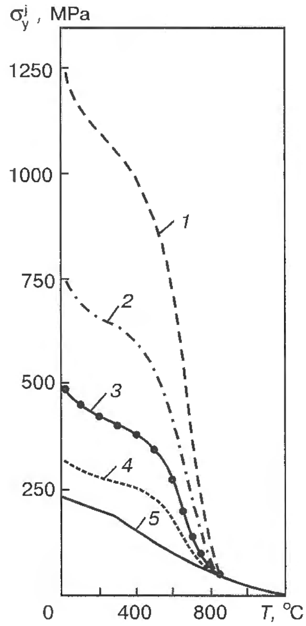

Figure 1. Relationship between the yield strength of steel A-538 and temperature and microstructural state: *1* — $V_m = 1$; *2* — $V_b = 1$; *3* — $V_b = 0.4$; $V_f = 0.6$; *4* — $V_f = 1$; *5* — $V_a = 1$.

$$T_{max} < T_*\ dV_j \equiv 0,$$
$$T_{max} \ge T_* \begin{cases} T > T_*: V_a = 1.0,\ V_m = V_f = V_p = 0, \\ T \le T_* \text{ and } \dfrac{\partial T}{\partial t} > 0: dV_j \equiv 0, \\ T \le T_* \text{ and } \dfrac{\partial T}{\partial t} < 0: dV_j = f_j(T). \end{cases} \quad (4)$$

In formula (4) the function $f_j(T)$ is determined by an appropriate diagram of the austenite transformation under the conditions of a continuous cooling or with the help of equivalent calculating relationships [5, 7, etc.]. The second way is rather popular due to its convenience in realization, in spite of its approximation. Authors of the article also follow this way by assuming that the kinetics of austenite transformation, which defines $V_j(T)$ can be estimated on the basis of known temperatures of start T_s^j and end T_e^j of appearance of the given microstructure (j = f, b, p, m), and also value V_j^{max} which corresponds to a real thermal cycle for the steel of a definite composition, in combination with some kinetic relationship of the following type:

$$V_j(T) = V_j^{max}\left\{1 - \exp\left(a_j \frac{T_s^j - T}{T_s^j - T_e^j}\right)\right\}$$

$$\text{at } T_s^j \ge T \ge T_e^j,$$

$$V_j(T) = 0 \text{ at } T > T_s^j, \quad (5)$$

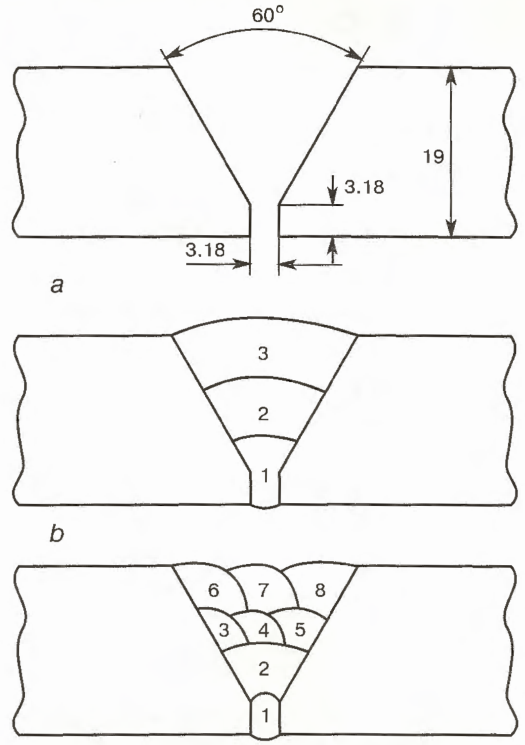

Figure 2. Shape of edge preparation (a) and sequence of groove filling in welding using version I (b) and II (c).

$$V_j\,(T) = V_j^{max} \text{ at } T < T_e^j,$$

where $a_j = -(2.5 - 3.0)$.

Values T_s^j and T_e^j at the presence of diagram ADA [8] for the given steel are selected without any difficulties, because they are not sensitive to small changes in chemical composition, and also to a cooling rate within the temperature interval 800 °C > T > 500 °C. To determine V_j^{max} the models of [5] developed for low-alloyed steels of a high-strength type (3) are worthy of attention:

$$V_m^{max} = 0.5\left[1 + \mathrm{erf}\left(\frac{\ln\Delta t_{8/5} - \ln\Delta t_m^{50}}{\sqrt{2}\ln S_m}\right)\right],$$

$$V_{fp}^{max} = 0.5\left[1 + \mathrm{erf}\left(\frac{\ln\Delta t_{8/5} - \ln\Delta t_{fp}^{50}}{\sqrt{2}\ln S_{fp}}\right)\right], \qquad (6)$$

$$V_f^{max} = 0.5\left[1 + \mathrm{erf}\left(\frac{\ln\Delta t_{8/5} - \ln\Delta t_f^{50}}{\sqrt{2}\ln S_f}\right)\right],$$

$$V_b^{max} = 1 - V_m^{max} - V_{fp}^{max};\;\; V_p^{max} = V_{fp}^{max} - V_f^{max}.$$

Here $\Delta t_{8/5}$ is the duration of material cooling within the temperature interval 800 – 500 °C; Δt_m^{50}, Δt_{fp}^{50}, Δt_f^{50}, S_m, S_{fp}, S_f are the parameters of model. In addition, Δt_j^{50} corresponds to the duration of cooling $\Delta t_{8/5}$, at which $V_j^{max} = 0.5$, and Δt_j^{85} – to values $\Delta t_{8/5}$, at which $V_j^{max} \approx 0.85$, then

$$S_m = \frac{\Delta t_m^{50}}{\Delta t_m^{85}};\; S_{fp} = \left(\frac{\Delta t_{fp}^{50}}{\Delta t_{fp}^{85}}\right)^{-1} S_f = \left(\frac{\Delta t_f^{50}}{\Delta t_f^{85}}\right)^{-1}$$

This is a physical interpretation of the above-described parameter. In [9] the regression relations which associate these parameters with a chemical composition of the steel are suggested on the basis of statistic processing of different compositions of group (3).

Below, the results of application of the above-described approach in combination with a numerical procedure of study of kinetics of temperatures, stresses and strains are given from [10] for a case of welding circumferential weld of a cylindrical shell of a radius R = 190 mm and wall thickness δ = 19 mm made of a pipe steel of X65 type of the following chemical composition, %: C – 0.10; Mn – 1.6; Si – 0.4; Nb – 0.07; V – 0.07; Ti – 0.03. The filler metal was of the same composition as the parent metal.

Initial state of the pipe material: $V_f = 0.6$; $V_b = 0.4$. Thermophysical properties (λ – heat conductivity; $c\gamma$ – volume heat capacity) and elastic characteristics (E – Young's modulus) were taken depending on the temperature given in Table 1. Two versions of welding the butt joint were considered (Figure 2): I – for three passes (1 – 3) at the conditions from Table 2; II – for eight passes (1 – 8) at lower heat inputs.

Figure 3 (z – coordinate in shell length, r – in radius) gives the estimated data for two versions in relation to microstructural state of section of the welded joint in the zone heated above T_* = 900 °C after completion of welding. In addition, the pause between adjacent passes provided a full cooling to the temperature T_0 = 20 °C. In the rest part of the welded joint heated below T_* the initial microstructure $V_f = 0.6$ and $V_b = 0.4$ is preserved (see Figures 3 and also 4 – 6 in colour inserts).

It is seen from these data that for version I in the zone heated above T_* a ferritic-bainitic microstructure is preserved. However, unlike the initial state the content of ferrite is decreased and the content of bainite is increased. In addition, the non-uniformity of distribution of these constituents in weld section is comparatively small: $V_f = 0.40 - 0.15$, $V_b = 0.7 - 0.4$.

For version II the final microstructure in the zone heated above T_* is bainitic-martensitic. Here, V_b is changed within the range from 0.2 to 0.9, and V_m from 0.1 to 0.8, respectively. The microstructural inhomogeneity is more pronounced, that is caused by a larger amount of passes at low heat inputs, i.e. lower values $\Delta t_{8/5}$ and sizes of zones $T_{max} > T_*$. It is characteristic that in the zone of

Table 1

T, °C	$\lambda \cdot 10^2$, W/(cm·°C)	$c\gamma$, J/(cm^3·°C)	$E \cdot 10^{-5}$, MPa
20	52.0	3.76	2.08
100	50.8	3.80	2.03
150	49.4	3.84	2.01
200	47.9	3.88	1.99
250	46.1	3.94	1.97
300	44.2	4.01	1.96
350	43.4	4.08	1.92
400	42.5	4.15	1.88
450	41.2	4.24	1.80
500	40.0	4.33	1.72
550	38.0	4.44	1.63
600	36.0	4.55	1.53
650	34.2	4.74	1.48
700	32.5	4.96	1.43
750	30.2	5.22	1.37
800	28.0	5.48	1.30
850	27.0	5.48	1.19
900	26.0	5.48	1.08
950	26.5	5.45	0.95
1000	27.0	5.42	0.82
1050	28.0	5.40	0.57
1100	29.0	5.38	0.32
1150	29.5	5.37	0.20
1200	30.0	5.36	0.07

Note. Coefficient of surface heat dissipation $\alpha_k = 2.08 \cdot 10^{-3}$ W/(cm^2·°C).

Table 2

No. of version	No. of passes	I_w, A	U_a, V	V_w, mm/s	Method of welding	q_{inp}, J/mm	F, mm^2
I	1	133	15	4.02	A	249	18
	2	183	35	3.18	B	2014	68
	3	280	35	3.18	B	3082	104
II	1	100	20	4.02	C	373	14
	2	192	25	4.02	C	896	3
	3	100	20	3.18	C	472	15
	4	85	20	3.18	C	401	14
	5	140	20	2.03	C	1034	32
	6	120	20	2.03	C	886	28
	7	120	20	2.03	C	886	28
	8	150	20	2.03	C	1107	35

Note. A — argon-arc non-consumable electrode welding, efficiency is 0.5; B — arc welding in CO_2, efficiency is 0.7; C — consumable electrode arc welding in a gas mixture, efficiency is 0.75; F — area of a pass section.

a root weld (1st pass), at the expense of noticeable heat inputs of the 2nd pass the microstructure in both versions is rather soft, in spite of very small values of a heat energy q_{inp} for the 1st pass. It is natural, that before the 2nd pass the microstructure after the 1st pass contains a large amount of martensite both for the version I and for version II.

It should be noted that a noticeable microstructural inhomogeneity affects to a certain degree the stressed state and promotes the growth of degree of volume of residual stresses. This can be seen visually from the data of Figure 4, where the calculating values of radial stresses σ_{rr} (acting in the direction of wall thickness) are given for both versions with and without allowance for changing the initial microstructural state in welding.

It is seen from these data that for version I (Figure 4, *a*, *b*) the values of residual tensile stresses σ_{rr} without allowance for changing the microstructural state do not exceed 100 MPa. The allowance for the above-mentioned microstructural changes increases the level of residual stresses σ_{rr} to approximately 400 MPa. However, such level covers a relatively small area of the parent metal near the fusion boundary in the center across the wall thickness.

For the version II the volume effect is even more pronounced: stresses σ_{rr} are increased up to a level from 200 to 400 MPa for a large volume of the parent metal along the fusion boundary. The allowance for the microstructural changes leads approximately to a double increase in residual tangent stresses σ_{rz} for both versions.

These data show that, in spite of thin walls of the shell ($\delta/R = 0.1$) the residual stresses σ_{rr} and σ_{rz}, comparable with a yield strength of the parent metal ($\sigma_y = 500$ MPa) occur under typical conditions of the multipass welding. Therefore, these calculations should not be made on the basis of a hypotheses of a plane stressed state, when $\sigma_{rr} \equiv \sigma_{rz} \equiv 0$.

Residual stresses σ_{zz} and $\sigma_{\beta\beta}$ are most important for this type of joints. Appropriate calculating data for the versions I and II are given in Figures 5 – 8.

It is seen in Figures 5 and 7 that for the version I the level of residual stresses σ_{zz} without allowance for the microstructures changes (Figure 5, *a*) does not exceed 400 MPa. Here, at the external surface (Figure 7, *a*) the stresses σ_{zz} are negative and in the zone of a stress raiser caused by a weld reinforcement they reach −500 MPa. At the internal surface the stresses σ_{zz} in the weld zone are tensile and at the level of 300 MPa. Allowance for the microstructural changes (Figure 5, *b* and 7, *b*) intensifies the non-uniformity of distribution of stresses σ_{zz} in thickness in the zone of weld. Here, at the external surface the stresses σ_{zz} in the zone of a stress raiser are negative and close to the value −600 MPa.

At the internal surface they are tensile at the level of 400 MPa in the weld zone. For the version II (Figures 5, *c*, *d* and 7, *c*, *d*) the distribution of stresses σ_{zz} in the weld zone is asymmetric with

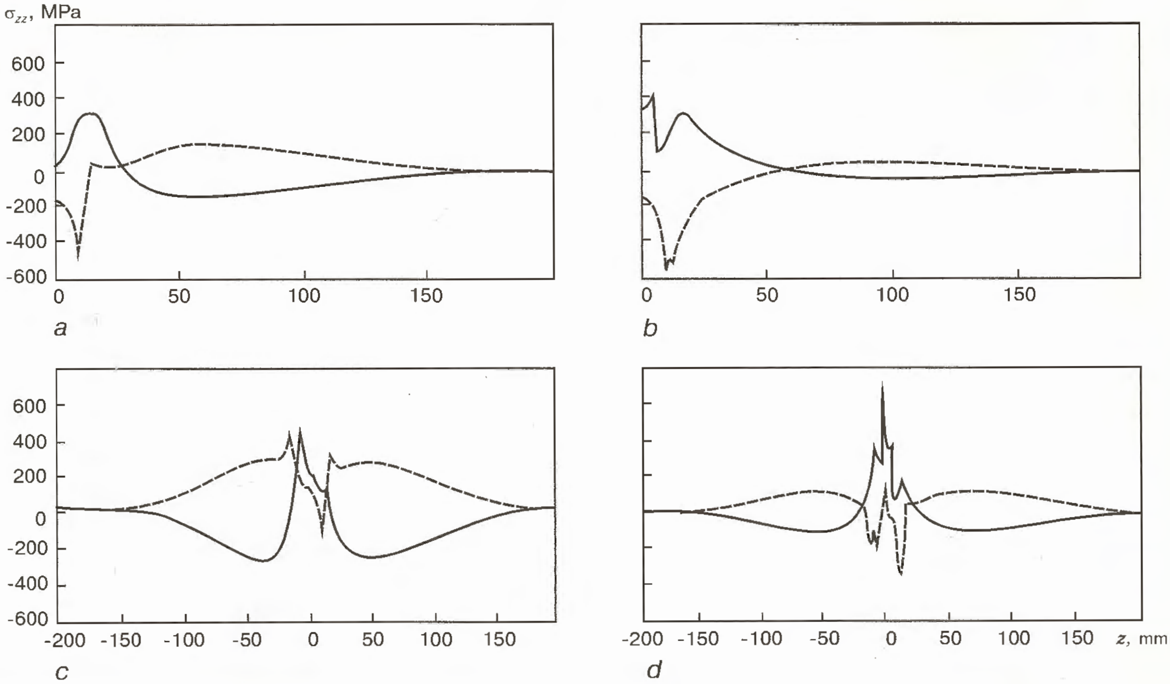

Figure 7. Diagrams of distribution of residual stresses σ_{zz} at internal and external of pipe for I (*a*, *b*) and II (*c*, *d*) versions without (*a*, *c*) and with (*b*, *d*) allowance for microstructural changes; ——— — internal surface; - - - - - - - - — external surface.

respect to the weld, especially, at the external surface. However, with increase in the distance from the axis it approaches symmetric distribution. Unlike the version I, here the role of bending deformations is less significant, because the maximum energy input of one pass is almost three times lower (Table 2). Due to this, the residual stressed state is close to that observed in plate of a corresponding thickness. Allowance for the microstructural changes intensifies the non-uniformity of distribution of stresses σ_{zz} in thickness (Figure 5, *c*, *d*).

The circumferential stresses $\sigma_{\beta\beta}$ (Figures 6 and 8) are highest and reach 600 MPa without allowance for the microstructural changes and 900 MPa with an allowance for the latter (Figure 6). The allowance for the microstructural

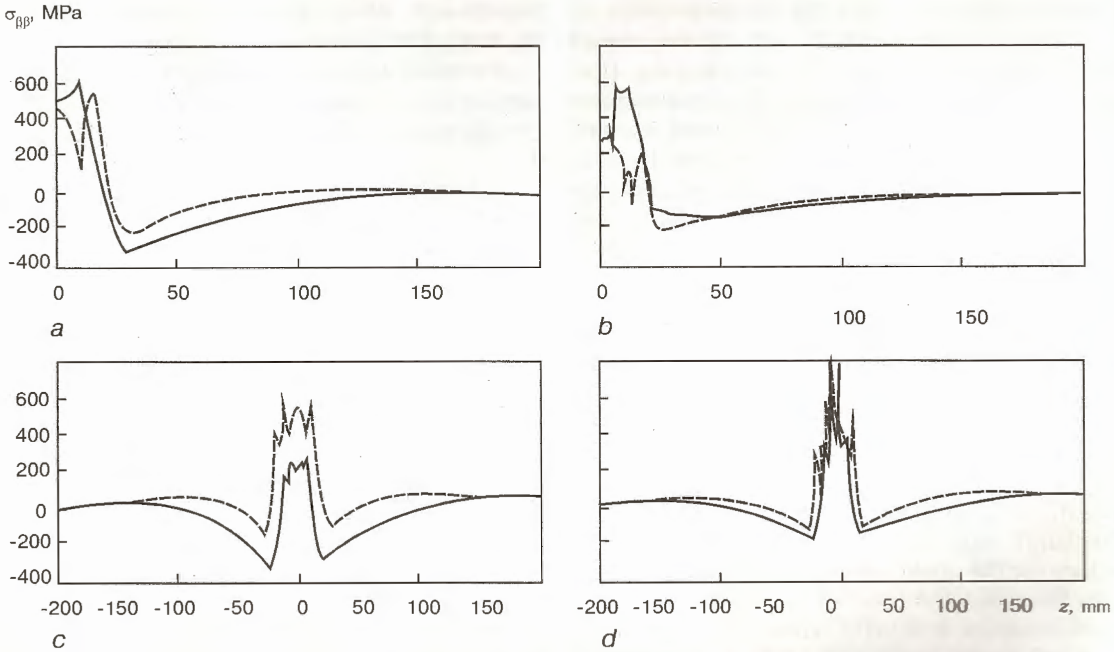

Figure 8. Diagrams of distribution of residual stresses $\sigma_{\beta\beta}$ at internal and external of pipe for I (*a*, *b*) and II (*c*, *d*) versions without (*a*, *c*) and with (*b*, *d*) allowance for microstructural changes; ——— — internal surface; - - - - - - - - — external surface.

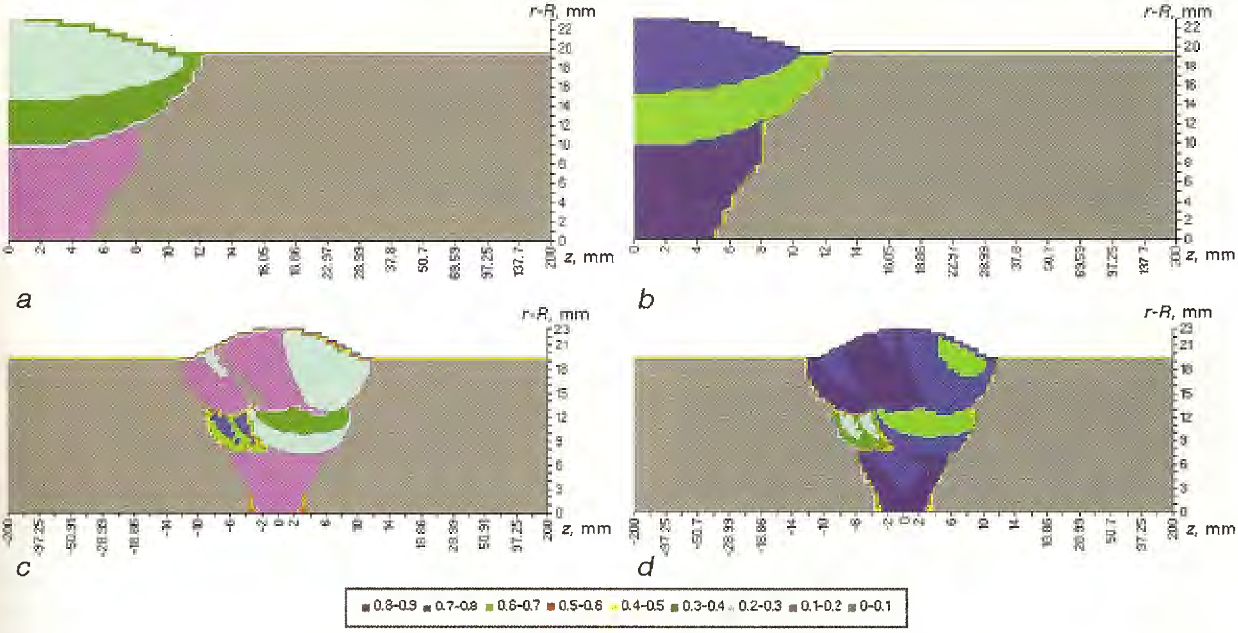

Рис. 3. Относительное содержание j-й микроструктуры в единице массы шва и околошовной зоны после сварки для I (a, b) и II (c, d) вариантов: a - $j=f$; b, d - $j=b$; c - $j=m$

Fig. 3. Relative content of j-th microstructure per unit mass of weld and HAZ after welding for I (a,b) and II (c,d) versions: a - $j=f$; b,d - $j=b$; c - $j=m$

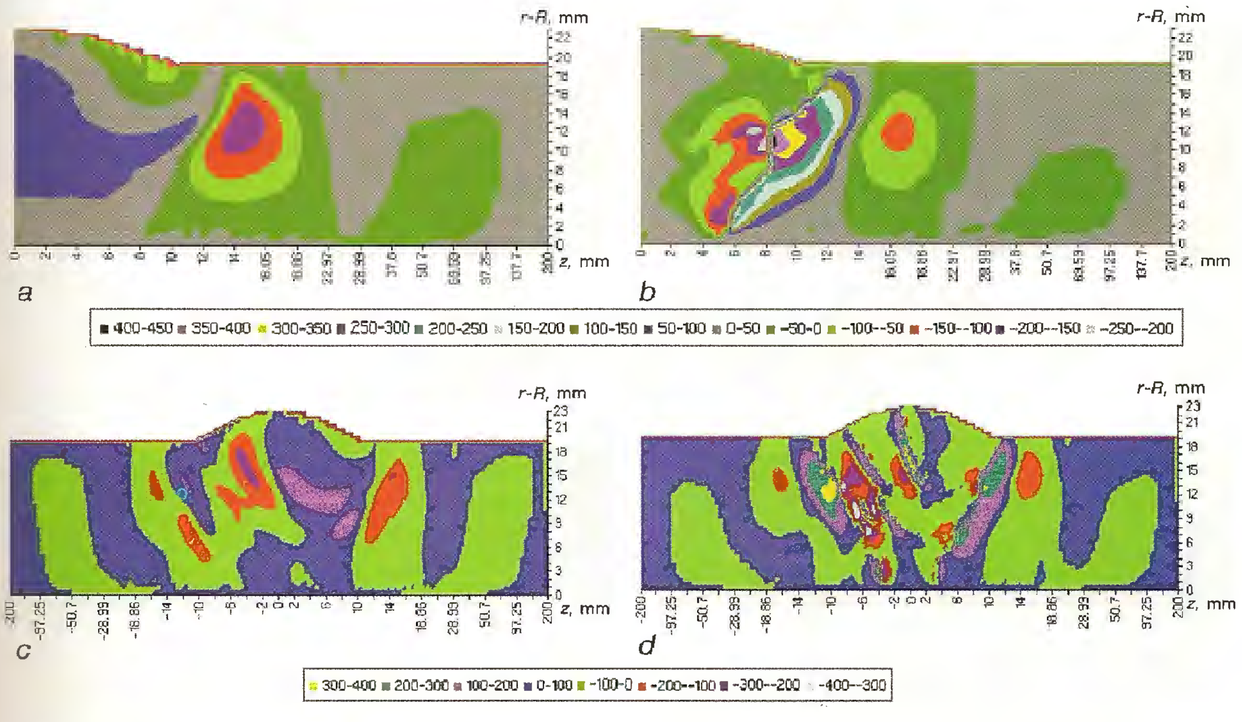

Рис. 4. Распределение остаточных радиальных напряжений σ_{rr} в поперечном сечении сварного шва для I (a,b) и II (c,d) вариантов без учета микроструктурных изменений (a, c) и с учетом (b,d)

Fig. 4. Distribution of residual radial stresses σ_{rr} in transverse section of weld for I (a,b) and II (c,d) versions without (a,b) and with (b,d) regard for microstructural changes

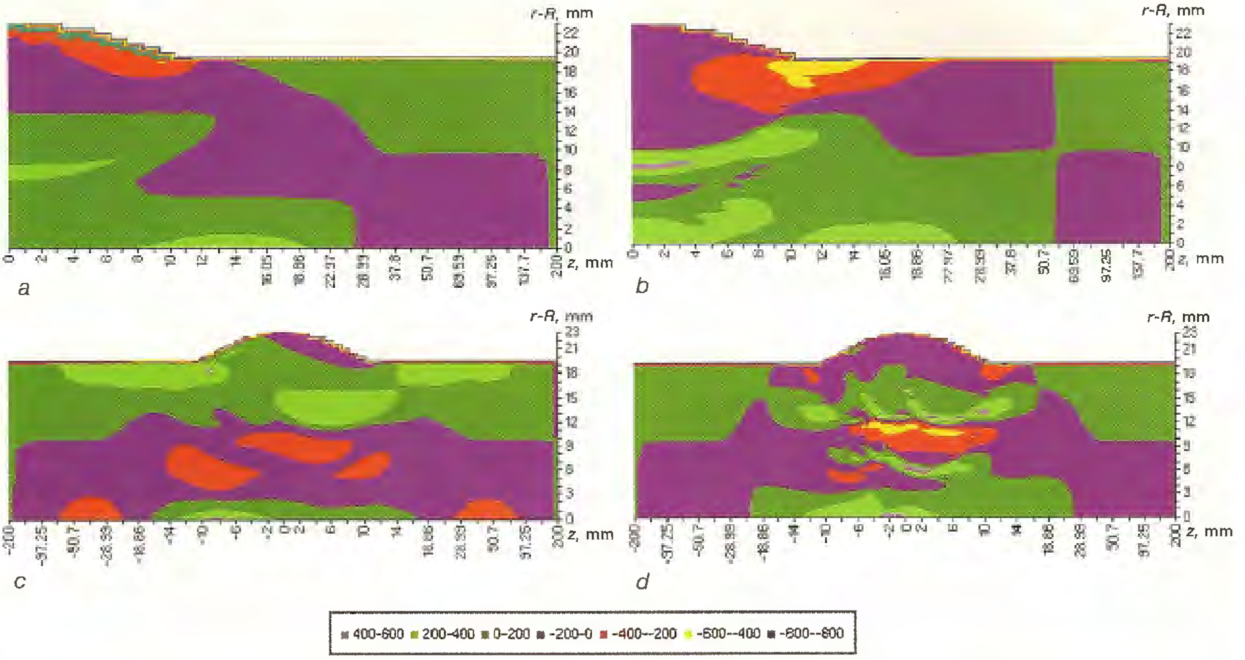

Рис. 5. Распределение остаточных поперечных (относительно сварного шва) напряжений σ_{zz} для I (a,b) и II (c,d) вариантов без учета микроструктурных изменений (a,c) и с учетом (b,d)

Fig. 5. Distribution of residual transverse (relative to weld) stresses σ_{zz} for I (a,b) and II (c, d) versions without (a,c) and with (b,d) regard for microstructural changes

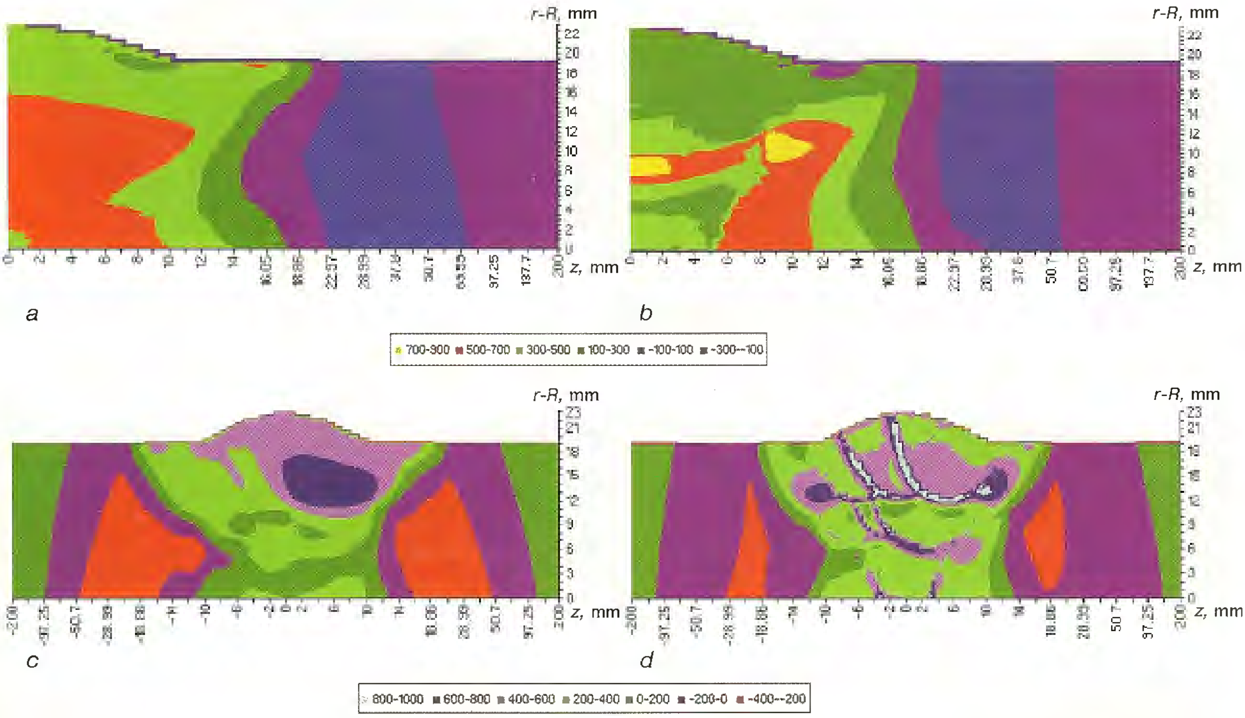

Рис. 6. Распределение остаточных окружных (продольных относительно сварного шва) напряжений $\sigma_{\beta\beta}$ для I (a,b) и II (c,d) вариантов без учета микроструктурных изменений (a,c) и с учетом (b,d)

Fig. 6. Distribution of residual circumferential (longitudinal relative to weld) stresses $\sigma_{\beta\beta}$ for I (a,b) and II (c,d) versions without (a,c) and with (b,d) regard for microstructural changes

changes increases the non-uniformity of distribution of $\sigma_{\beta\beta}$ in thickness, especially for version II. The relatively small energy inputs at version II specify the distribution of stresses $\sigma_{\beta\beta}$ at the internal and external surfaces (higher stresses at the external surface) typical for the multipass welding of plates.

CONCLUSIONS

1. Allowance for microstructures changes in weld and HAZ metal in circumferential butt welding of pipes of X65 type steel leads to the increase in non-uniformity of distribution of mechanical properties and residual stresses in the weld zone. The lower the energy input in welding, the higher the above-mentioned non-uniformity associated with a probability of appearance of regions with a high content of bainite and martensite. This leads to the growth of stress peaks, promotes the increase in a degree of volume of stressed state in deep layers due to the growth of constituents of a tensor of stresses directed across the thickness (σ_{rr}, σ_{rz}).

2. From the positions of a probability of formation of cold cracks the data obtained showed that the appearance of quenched structures do not only reduce the material resistance to the formation of similar defects but also to the increase of peaks of tensile stresses.

3. Selection of rational conditions of technology of welding is a rather actual problem for each definite case taking into account the large quantity of possible parameters of control of thermal cycles in welding similar joints (number of passes, methods and conditions of welding, preheating, duration of cooling before deposition of next layer, etc.). The feasibility of prediction of corresponding versions of combination of technological parameters can reduce radically the time and materials expenses for the solution of the above-mentioned problem.

REFERENCES

1. Ronda, J., Murakawa, H., Oliver, G. *et al.* (1999) Thermomechanical metallurgical model of welded steel. *Transact. of JWRI*, **2**, 93 – 114.
2. Raday, D. (1992) *Heat effects of welding*. Berlin: Springer-Verlag.
3. Grivnyak, I., Makhnenko, V.I. (1983) Application of calculation methods in study of steel weldability. In: *Paper of 2nd Symp. CMEA on Application of Mathematical Methods in Study of Weldability*. Sofia: VMEI.
4. Yuriev, S.F. (1950) *Specific volumes of phases in martensitic transformation of austenite*. Moscow: Metallurgizdat.
5. Kasatkin, O.G. (1990) Mathematical modelling of relationships between composition and properties of welded joints and creation of calculating-experimental system for optimizing main factors of welding low-alloyed structural steels. In: *Abstr. of thesis of Dr. of Sci. (Eng.)*. Kyiv.
6. Ueda, J., Murakawa, H., Luo, Ju.A. (1995) Computational model of phase transformation for welding processes. *Transact. of JWRI*, **1**, 95 – 100.
7. Jon, I., Salminen, A.S., Sun, Z. (1996) Process diagrams for laser beam welding of carbon manganese steels. *Welding J.*, **7**, 225 – 232.
8. Seyffarth, P. (1982) *Alas Schweiss — ZTU — Schaubilder*. Dusseldorf: VEB Verlag Technik.
9. Seyffarth, P., Kasatkin, O. (1982) Calculation of structural transformation in the welding process. *Doc. IIW-IX-82*.
10. Makhnenko, V.I., Velikoivanenko, E.A., Shekera, V.M. *et al.* (1998) Residual stresses in the zone of circumferential butt welds of austenitic steel. *Avtomaticheskaya Svarka*, **11**, 32 – 39.

STUDY OF PROPERTIES OF SLAG MELTS FOR GROUNDING THE COMPOSITIONS OF WELDING FLUXES.
Part II. Thermodynamic characteristics

V.G. KUZMENKO[1], **V.I. GALINICH**[1], **V.S. TOKAREV**[1], **V.A. STUKALO**[2] and **V.E. SOKOLSKY**[2]
[1]The E.O. Paton Electric Welding Institute, NASU, Kyiv, Ukraine
[2]T.G. Shevchenko National University, Kyiv, Ukraine

ABSTRACT

The method of isoperibolic calorimetry was used for evaluating the energy state (heat capacity, enthalpy of slag formation) of slags of $MnO-SiO_2-Me_xO_y$ (CaO, Al_2O_3, TiO_2) and welding fluxes of AN-348A, AN-60, ANTs-1, AN-26S, AN-47, AN-67A grades at 1923 K. Proceeding from the experimental data on heat of mixing the values of activity of oxides of manganese and silicon in the $MnO-SiO_2$ system and also in slags on this base were determined.

Key words: *welding slags, thermodynamic investigations, heat of mixing, activity of components.*

Calculation of a reactivity of components of molten slags is based on the assumption about formation in them of some coordinations of ions with a certain energy of interaction. The use of the latter in the calculations, based on the theory of regular solutions, is a decisive factor. To estimate the ionic interaction the calculation methods are usually used, including those which are based on experimental data for binary systems. In some cases they give results which are close to the practical results. The more exact data can be obtained by determination of heat effects directly in slags being studied.

We have measured the thermodynamic characteristics (heat capacity, heat content, enthalpy of slag formation) of three- and four-component slag systems and also of some real welding fluxes.

The investigations were performed using a high-temperature calorimeter with an isothermal sheath (isoperibolic calorimeter). The schematic diagram of this calorimeter is given in Figure 1 [1 – 4]. The procedure is based on study of heat processes proceeding in the calorimeter and described by the following equation of the heat balance:

$$C_c dT/dt = dQ_1/dt - dQ_2/dt,$$

where C_c is the total heat capacity of the container with a melt; dT is the difference between the current temperature of the melt and the temperature of the isothermal sheath; dt is the cycle duration. The left part of the equation shows changes in heat amount accumulated by a calorimeter contents in time. The first term of the right part of the equation denotes the power of radiation of a heat process, and the second term defines the rate of heat exchange with a sheath.

The principle of measurements using an isoperibolic calorimeter is based on recording changes in temperature of container contents during placing appropriate samples into it. The obtained time relationships of the temperature of a molten calorimetric bath (Figure 2) are the initial data for calculations of enthalpies of slags of a definite composition in the area of the heatexchanger configuration.

Data obtained from samples of a model slag (MS) and fluxes are presented in Table 1.

Table 2 shows results from determination of values of heat content and heat capacity of slags and fluxes, whose compositions are given in Table 1.

Experimental data for compositions of slags from Table 1 were approximated by a method of least squares using following equations:

$$\text{MS} \quad H_T - H_{298} = 1.925T - 1588, \tag{1}$$

$$\text{AN–348A} \quad H_T - H_{298} = 2.25T - 2479, \tag{2}$$

$$\text{AN–60} \quad H_T - H_{298} = 1.44T - 2755, \tag{3}$$

$$\text{ANTs–1} \quad H_T - H_{298} = 1.609T - 1345, \tag{4}$$

$$\text{AN–47} \quad H_T - H_{298} = 0.436T - 779, \tag{5}$$

$$\text{AN–67A} \quad H_T - H_{298} = 0.817T - 1045, \tag{6}$$

$$\text{AN–26S} \quad H_T - H_{298} = 2.78T - 3187. \tag{7}$$

The method of a regression analysis [5] at a homogeneity of dispersions of reproducibility of ordinates of a function measured was used for cal-

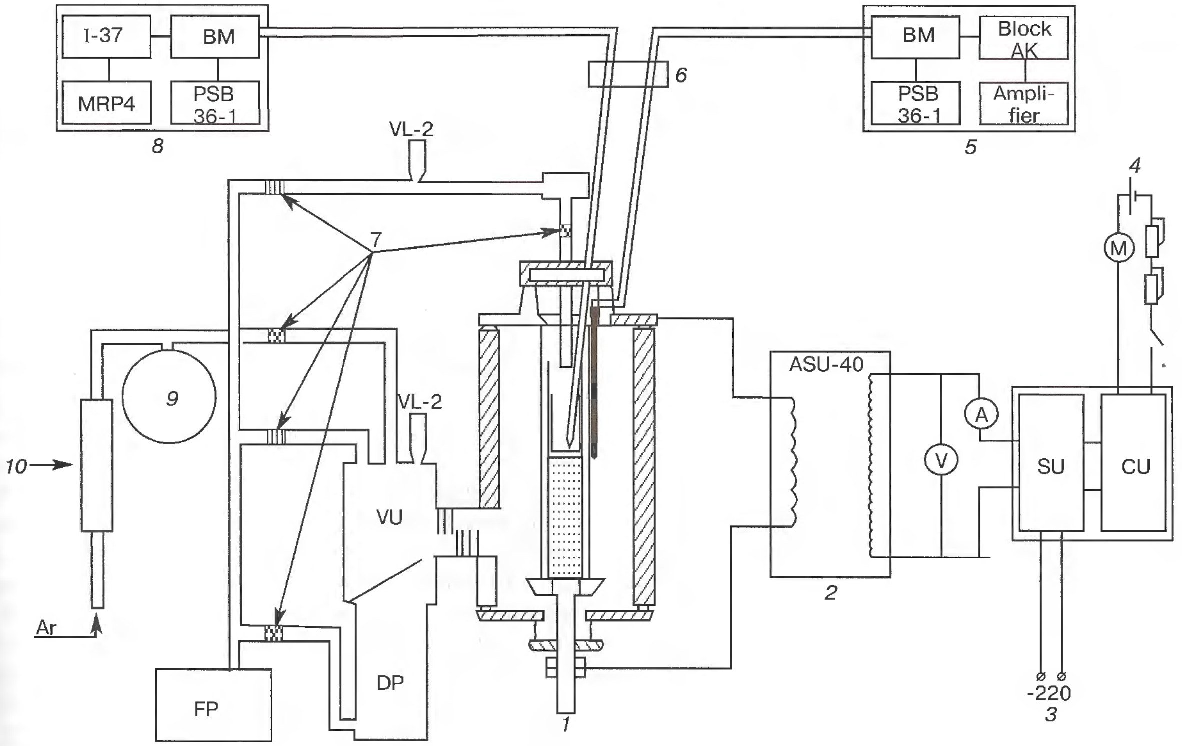

Figure 1. Schematic diagram of isoperibolic calorimeter for thermodynamic investigation of welding slags: *1* — high-temperature part of the calorimeter; *2* — step-down transformer; *3* — voltage controller; *4* — control circuit; *5, 8* — device for measuring temperature of heater and melt, respectively; *6* — zero-thermostat; *7* — vacuum valves; *9* — accumulating container; *10* — system of argon purification; I-37 — DC amplifier; BM — block of measurement; MRP4 — monitoring recording potentiometer; PSB36-1 — supply block of potentiometer; VL-2 — vacuum lamp; VU — vacuum unit; FP — forevacuum pump; DP — diffusion pump; autotransformer ASU-40; SU — supply unit; CU — control unit; block AK — self-balancing potentiometer of voltage.

culation of the enthalpy of melts shown in Table 1 and evaluation of confidence intervals for unknown functional relationship at a confidence probability $\alpha = 0.95$. The mean values of heat capacity were calculated by differentiating equations (1) – (7) with respect to the temperature (Table 2). The linear mode of changing the heat content depending on temperature indicates that the heat capacity of the slag does not depend on the temperature within the temperature interval which was investigated.

The present work included the study of effect of additions of some oxides on the energy of interaction in a slag system $MnO-SiO_2$ [6 – 8]. Figure 3 gives data about the heat of dissolution of SiO_2 and MnO in slags $MnO-SiO_2$–10 % CaO, $MnO-SiO_2$–30 % Al_2O_3, $MnO-SiO_2$–12 % TiO_2, and also in fluxes of grades AN-67A and AN-26S at 1923 K [2]. In the system examined an alternating mode of heat of their dissolution was observed depending on the amount of an added component (SiO_2 or MnO). The positive enthalpy of mixing in the region of compositions, which are rich in SiO_2, changes the sign for the negative one with an increase in MnO concentration.

In adding the basic fluxes to the slag with high SiO_2 content the subdivision of oxysilicon anions takes place up to formation of separate tetrahedrons of SiO_4^{4-} that requires additional consumption of energy and promotes increase in freedom of their thermal vibrations.

Thus, the introduction of such high-basicity oxide as CaO leads to a significant decrease in H_{SiO_2} and increase in H_{MnO}. The negative deviations from a perfect behaviour of H_{SiO_2} in a ternary system $MnO-SiO_2-CaO$ are, probably, associated with the formation in it of a short-range order which corresponds to the coordination of the Ca·SiO_2 type. This coordination has no tendency to accept a large amount of ions Mn^{2+} into its lattice and this explains, probably, the tendency to the increase in positive deviations from the perfect behavior of H_{MnO} obtained by us in melts $MnO-SiO_2-CaO$.

The addition of titanium oxide into the $MnO-SiO_2$ system leads to the shifting of molar enthalpies of SiO_2 dissolution to the region of more positive values, while the values of enthalpy of MnO

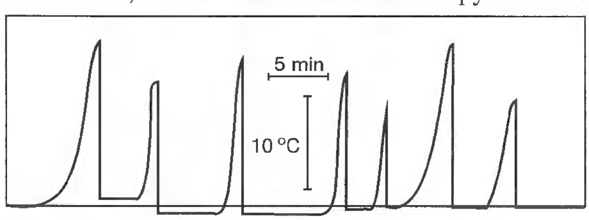

Figure 2. Characteristic curves of calorimetric experiments.

Table 1. Chemical composition of MS and standard fluxes

Flux grade	*Components, mass %*								
	SiO_2	MnO	CaO	MgO	Al_2O_3	CaF_2	TiO_2	ZrO_2	Fe_2O_3
MS	10.5	12.4	9.8	–	17.8	13.7	14.0	21.6	–
AN-348A	42.9	36.9	7.3	1.4	3.0	5.9	–	–	–
AN-60	43.6	38.0	6.3	1.3	2.2	7.3	–	–	0.2
ANTs-1	42.0	28.3	18.2	–	5.9	6.1	–	–	–
AN-47	30.2	15.0	14.9	7.1	9.8	15.4	5.8	2.1	–
AN-67A	13.3	16.4	8.2	–	39.0	16.6	6.3	–	–
AN-26S	28.1	3.8	5.6	16.4	20.4	25.1	–	–	0.5

become more negative. The behaviour of the above-mentioned components is explained by the fact that in system MnO–SiO_2–TiO_2 they tend antagonistically to the interaction with the manganese oxide. Such explanation is confirmed by the diagrams of phase equilibriums in the boundary binary systems.

Thus, in the state diagram of SiO_2–TiO_2 there is a wide region of unmixing of two liquid phases, while the formation of rather strong compounds is characteristic of other binary systems of a concentration triangle. Therefore, the antagonistic tendencies in SiO_2–TiO_2 system intensify the competition during interaction of oxides of silicon and titanium with a manganese oxide in ternary melts, thus leading to the decrease in H_{MnO}.

The modes of changing the concentration relationships of heat of dissolution of oxides of silicon and manganese in MnO–SiO_2 and MnO–SiO_2–Al_2O_3 systems are similar. Addition of aluminium oxide to the initial slag leads to some increase in heat of dissolution of dioxides of silicon and manganese. Nevertheless, the increase in concentration of Al_2O_3 up to 30 % leads to the decrease in heat of dissolution of manganese oxide in slag being rich with it. Probably, the replacement of silica by alumina promotes the formation of coordinations of a manganese spinel type ($MnO \cdot Al_2O_3$) in melts and strengthening of the appropriate bond.

Mutual effect of oxides of calcium, aluminium and titanium in melts of fluxes of AN-26S and AN-

Table 2. Experimental values of heat content and estimated heat capacities of MS and standard fluxes

MS			*AN-348A*			*AN-60*			*ANTs-1*		
T, K	$H_T - H_{298}$, *J/g*	∇, *J/g*	*T, K*	$H_T - H_{298}$, *J/g*	∇, *J/g*	*T, K*	$H_T - H_{298}$, *J/g*	∇, *J/g*	*T, K*	$H_T - H_{298}$, *J/g*	∇, *J/g*
C_{est} = 0.44 J/(g·K)			C_{est} = 2.25 J/(g·K)			C_{est} = 1.44 J/(g·K)			C_{est} = 1.61 J/(g·K)		
1858	1969	102	1600	1097	23	1600	1587	39	1640	1316	97
1865	2035	96	1650	1294	85	1650	1572	48	1747	1437	101
1883	2040	77	1715	1358	21	1715	1713	36	1793	1520	35
1906	2063	64	1797	1456	108	1797	1837	5	1835	1615	67
1933	2145	73	1867	1721	110	1867	1919	42	1877	1649	59
1953	2185	97	1918	1808	28	1918	2009	3	–	–	–
1971	2203	113	–	–	–						

AN-47			*AN-67A*			*AN-26S*		
T, K	$H_T - H_{298}$, *J/g*	∇, *J/g*	*T, K*	$H_T - H_{298}$, *J/g*	∇, *J/g*	*T, K*	$H_T - H_{298}$, *J/g*	∇, *J/g*
C_{est} = 0.44 J/(g·K)			C_{est} = 0.817 J/(g·K)			C_{est} = 2.77 J/(g·K)		
1638	1464	109	1617	2366	53	1600	1268	12
1695	1465	94	1675	2451	117	1650	1379	16
1749	1553	79	1753	2461	119	1715	1628	53
1793	1606	85	1793	2504	92	1797	1811	8
1835	1602	111	1836	2550	77	1867	2055	58
1877	1598	95	1877	2584	85	1918	2181	43
–	–	–	1971	2642	102	–	–	–

Note. Here, H_{298} are the experimentally established values of enthalpy of synthetic slags, ∇ is the errors in determination of these values, C_{est} is the estimated heat capacity. Each value of $H_T - H_{298}$ given in Table, was obtained by averaging at least five measurements, made at the same temperature.

67A grades [9] leads to the increase in heat of dissolution of oxides of silicon and manganese.

Results of investigation of a slag system $MnO-SiO_2$, including that with additions of third components are given in Table 3. They also comprise data about the partial molar enthalpies ΔH_i and activity a of oxides of silicon and manganese.

Activities of oxides of manganese and silicon (Tables 4 and 5) were calculated using experimentally established values of enthalpy of mixing the appropriate additions with melts of fluxes of AN-67A and AN-26S grades using the equation of a zero approximation of theory of regular solutions for the compositions given in Table 1.

It can be seen from Tables 4 and 5 and also from Figure 4 that the isotherms of activities in melts examined by us indicate a complex concentration relationship which is expressed in an alternating deviation from the laws of perfect solutions (Raoult's law). The main cause of these deviations is, probably, nonequivalence of ions in melts and the presence of a covalent bond between them.

In its structure the molten welding slags of a neutral and a weakly acid type can be referred to the solutions with a strongly-developed microheterogeneity of the chemical composition. More or less coarse oxysilicon or other anions are surrounded with single- and bivalent metals. The gradual increase in content of basic oxides in them promotes the subdivision of anions and leads, respectively, to the decrease in the degree of the melt heterogeneity.

The change in structure of melts is reflected in the nature of a concentration relationship of enthalpies of dissolution of components and also in their thermodynamic activity. In turn, the restructuring the slag structure and, thus, the change in values of activity of components influences greatly the mode of their interaction with the metal, in particular in reduction processes of silicon and manganese.

With the increase in the flux basicity, for example, in introduction of the calcium oxide, cations Ca^{2+} and anions O^{2-} appear in the melt together with cations Mn^{2+} and oxysilicon anions $Si_xO_y^{2+}$. This leads to the depletion of surface layers of slag with the oxysilicon anions and to the deterioration of silicon transition to the liquid metal.

The increase in the slag basicity, caused by decrease in silica in it, leads to the filling its surface layer with strong cations Mn^{2+} and to the corresponding intensification of manganese transition to the weld metal. In addition, the more manganese will transfer, the higher manganese content in slag and the lower content of the silicon dioxide. The inverse process of limiting the manganese transition to the weld at increase in content of the silicon dioxide in the flux is caused by the reduction in activity of the manganese oxide due to the formation of coordinations of the type of manganese silicates in slag.

Thus, the intensity of proceeding the silicon-reduction processes in submerged arc welding with a high content of the silicon dioxide can be limited

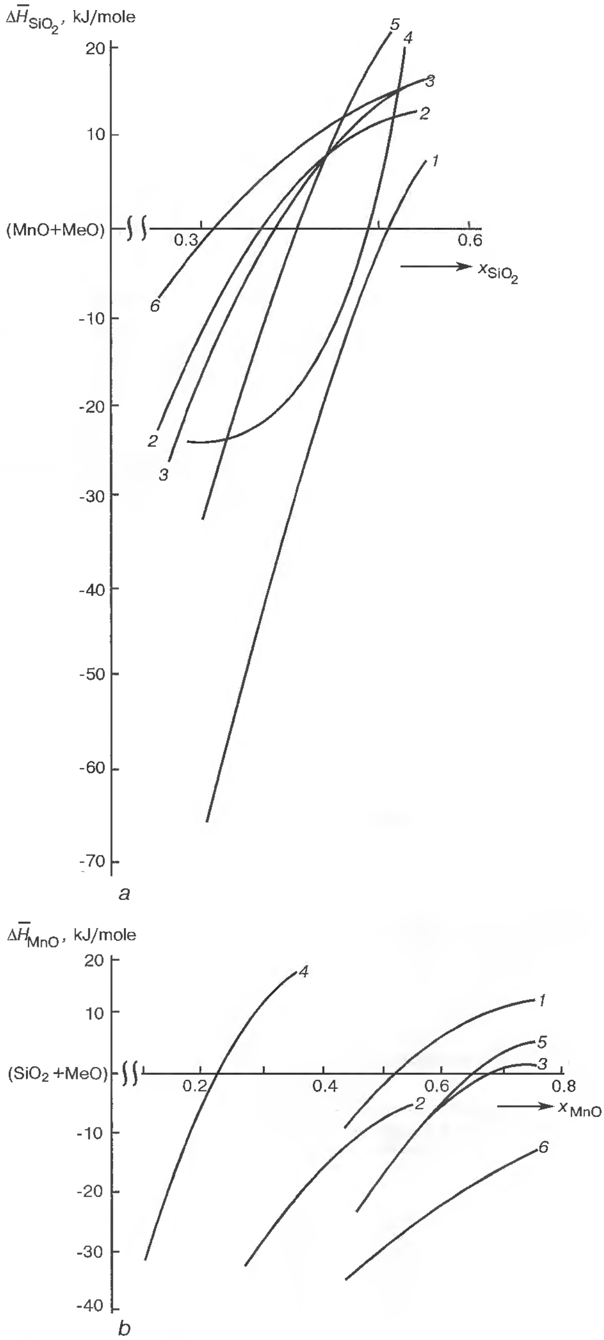

Figure 3. Partial molar enthalpies of dissolution of SiO_2 (*a*) and MnO (*b*) at 1923 K temperature in systems: *1* — $MnO-SiO_2$–10 % CaO; *2* — flux AN-67A; *3* — $MnO-SiO_2$–30 % Al_2O_3; *4* — flux AN-26S; *5* — $MnO-SiO_2$; *6* — $MnO-SiO_2$–12 % TiO_2.

Table 3. Values of partial molar enthalpies $\Delta\bar{H}_i$ (J/mole) and activity of MnO and SiO_2 in trenary melts $MnO-SiO_2-MeO$

x_{SiO_2}	$MnO-SiO_2$		$MnO-SiO_2$–10 % CaO		$MnO-SiO_2$–30 % Al_2O_3		$MnO-SiO_2$–12 % TiO_2	
	$\Delta\bar{H}_{SiO_2}$	a_{SiO_2}	$\Delta\bar{H}_{SiO_2}$	a_{SiO_2}	$\Delta\bar{H}_{SiO_2}$	a_{SiO_2}	$\Delta\bar{H}_{SiO_2}$	a_{SiO_2}
0.25	−58500	0.009	−88730	0.001	−47500	0.012	−7800	0.153
0.30	−34100	0.036	−67470	0.004	−24700	0.064	−1710	0.270
0.35	−16900	0.122	−48400	0.017	−10100	0.280	3530	0.436
0.40	−1900	0.450	−31520	0.056	900	0.420	8030	0.661
0.45	10800	0.886	−16830	0.157	8760	0.778	11700	0.935
0.50	21260	1.889	−4340	0.381	13860	1.189	14600	1.245
0.55	29410	3.457	5960	0.798	16590	1.551	16700	1.562
x_{SiO_2}	$\Delta\bar{H}_{MnO}$	a_{MnO}	$\Delta\bar{H}_{MnO}$	a_{MnO}	$\Delta\bar{H}_{MnO}$	a_{MnO}	$\Delta\bar{H}_{MnO}$	a_{MnO}
0.25	5000	1.03	11700	1.56	1200	0.81	−13170	0.44
0.30	2800	0.84	11050	1.40	180	0.71	−15250	0.36
0.35	−480	0.63	9320	1.16	−1880	0.58	−19480	0.30
0.40	−4800	0.44	6570	0.91	−5200	0.43	−22850	0.24
0.45	−10200	0.29	2800	0.66	−10140	0.29	−26380	0.19
0.50	−16700	0.18	−1990	0.44	−16850	0.17	−30000	0.15
0.55	−24280	0.10	−7800	0.28	−25630	0.09	−33570	0.12

Table 4. Thermodynamic activity of MnO in melts of welding fluxes of AN-67A and AN-26S grades at 1923 K

x_{MnO}	*$MnO-SiO_2$ system*			*Flux AN-67A*			*Flux AN-26S*		
	$\Delta\bar{H}_{MnO}$, J/mole	a_{MnO}	γ_{MnO}	$\Delta\bar{H}_{MnO}$, J/mole	a_{MnO}	γ_{MnO}	$\Delta\bar{H}_{MnO}$, J/mole	a_{MnO}	γ_{MnO}
0.10		No data			No data		−31100	0.01	0.14
0.20				−45540	0.01	0.05	−5300	0.14	0.72
0.25	5000	1.03	1.36	−36300	0.03	0.10	3800	0.32	1.27
0.30	2800	0.84	1.20	−28300	0.05	0.17	10700	0.59	1.95
0.35	−480	0.63	0.97	−21600	0.09	0.26	15580	0.93	2.65
0.40	−4800	0.44	0.73	−16060	0.15	0.35			
0.45	−10200	0.29	0.53	−11500	0.22	0.49			
0.50	−16700	0.18	0.32	−7800	0.31	0.61		No data	
0.55	−24280	0.10	22	−5000	0.40	0.73			
0.60		No data		2900	0.50	0.83			

Note. Here, γ is the activity coefficient.

Table 5. Thermodynamic activity of SiO_2 in melts of welding fluxes of AN-67A and AN-26S grades at 1923 K

x_{SiO_2}	*$MnO-SiO_2$ system*			*Flux AN-67A*			*Flux AN-26S*		
	$\Delta\bar{H}_{SiO_2}$, J/mole	a_{SiO_2}	γ_{SiO_2}	$\Delta\bar{H}_{SiO_2}$, J/mole	a_{SiO_2}	γ_{SiO_2}	$\Delta\bar{H}_{SiO_2}$, J/mole	a_{SiO_2}	γ_{SiO_2}
0.20		Not determ.		47060	0.01	0.05		Not determ.	
0.25	−53500	0.01	0.03	−29880	0.04	0.15			
0.30	−34100	0.04	0.12	−16030	0.11	0.37	−24000	0.07	0.22
0.35	−16900	0.12	0.34	−5200	0.25	0.72	−23870	0.08	0.22
0.40	−1900	0.45	1.12	2910	0.48	1.20	−19680	0.12	0.29
0.45	10800	0.89	1.97	8620	0.77	1.71	−10360	0.23	0.52
0.50	21260	1.89	3.77	12230	1.07	2.15	5180	0.69	1.38
0.55			Not determ.				28000	3.16	5.75

Note. Here, γ is the activity coefficient.

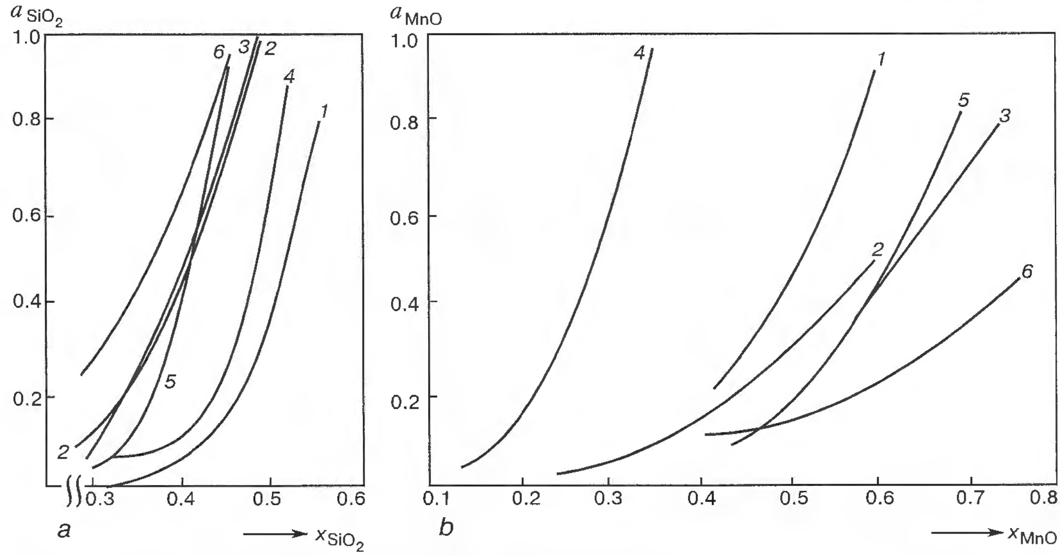

Figure 4. Activity of SiO_2 (*a*) and MnO (*b*) at 1923 K temperature in systems (see designations in *1* – *6* in Figure 3).

by the decrease in its thermodynamic activity with introducing the basic oxides.

The results of investigation of reactivity of components of fluxes of AN-67A, AN-26S and slags of $MnO-SiO_2$ system show that the intensity of proceeding the silicon-reduction process will be minimum when the flux of the AN-26S is used as the most basic flux.

CONCLUSIONS

1. The application of a method of an isoperibolic calorimetry provides the more comprehensive information about the ionic interactions when slag systems and welding fluxes in the molten state are investigated.

2. Energy of interaction in the system $MnO-SiO_2-Me_xO_y$ (10 % CaO, 12 % TiO_2, 30 % Al_2O_3) and in fluxes of AN-67A and AN-26S was studied by measuring the heat of mixing. The activity of MnO and SiO_2 was determined in the objects examined at 1923 K temperature.

3. Isotherms of activity of manganese oxide and silicon dioxide in melts examined show a complex concentration relationship which is expressed in an alternating deviation from the laws of perfect solutions (Raoult's law) and reflects the corresponding changes in their structure. The main cause of these deviations is, probably, the energy unequivalence of ions in melts and the presence of a covalent bond between them.

REFERENCES

1. Kubashevsky, O., Olkokk, S.B. (1982) *Metallurgical thermochemistry*. Moscow: Metallurgia.
2. Stukalo, V.A., Neshchimenko, N.Ya., Batalin, G.I. *et al.* (1984) Thermodynamic properties of melts of SiO_2–MnO system. *Izv.AN SSSR, Inorganic Materials*, **5**, 811 – 814.
3. Stukalo, V.A., Neshchimenko, N.Ya., Kurach, V.P. *et al.* (1983) Temperature dependence of enthalpy H_T–H_{298} of oxide melts of system MnO–SiO_2. *Avtomaticheskaya Svarka*, **8**, 72 – 73.
4. Stukalo, V.A., Neshchimenko, N.Ya., Batalin, G.I. *et al.* (1988) Temperature dependence of enthalpy H_T–H_{298} of synthetic slags used in welding structural steels. *UKh. J.*, **1**, 27 – 29.
5. Spiridonov, V.P., Lopatkin, A.A. (1970) *Mathematical processing of physical-chemical data*. Moscow: Moscow State University.
6. Stukalo, V.A., Neshchimenko, N.Ya., Galinich, V.I. *et al.* (1991) Thermodynamic properties of melts of MnO–SiO_2–CaO system. *DAN SSSR, Melts*, **3**, 112 – 114.
7. Stukalo, V.A., Patseliy, N.V., Neshchimenko, N.Ya. *et al.* (1991) Thermodynamic properties of components of liquid fluxes of MnO–SiO_2–TiO_2 system. *Avtomaticheskaya Svarka*, **6**, 23 – 25.
8. Stukalo, V.A., Neshchimenko, N.Ya., Patseliy, N.V. (1991) Thermodynamic properties of MnO and SiO_2 in melts of MnO–SiO_2–Al_2O_3 system. *Izv. AN SSSR, Inorgenic Materials*, **4**, 755 – 757.
9. Stukalo, V.A., Neshchimenko, N.Ya., Tokarev, V.S. *et al.* (1996) Thermodynamic properties of melts of welding flux AN-67A. *Avtomaticheskaya Svarka*, **2**, 25 – 27.

STRUCTURE OF THE FERRITE BAND FORMED IN THE JOINT ZONE OF FERRITIC-PEARLITIC STEELS IN VACUUM PRESSURE WELDING

L.I. MARKASHOVA, G.M. GRIGORENKO, G.K. KHARCHENKO, V.V. ARSENYUK, S.G. GRIGORENKO and **I.L. BOGAICHUK**
The E.O. Paton Electric Welding Institute, NASU, Kyiv, Ukraine

ABSTRACT

Results of examination of peculiarities of structure and conditions of a ferrite band formation in the zone of joining ferritic-pearlitic steels during vacuum pressure welding are presented. It is shown that two types of ferrite are formed in the zone of welding which are distinguished by several features. It is established that decarburization of metal layers adjacent to the surface to be welded and thermodynamic instability of a pearlitic cementite in the high inner stress fields are the conditions which promote the formation of ferrite bands.

Key words: *vacuum pressure welding, ferrite band, cementite platelets, dislocation density, self-cleaning of surfaces.*

The researchers have more than once noted [1 – 5] the formation of a ferrite structure in the butt zone in pressure welding of ferritic-pearlitic steels. Sometimes, a lowering of mechanical properties, especially under impact loads is associated with this ferrite band (FB) [1, 3, 4]. FB formation is usually attributed either to metal decarburization [2], or to the presence of oxide inclusions [5].

Unfortunately, FB whose size in the transverse cross-section is 10 to 20 μm, are practically inaccessible for study with the regular methods of investigation. Therefore, considering the limited information on what extended ferrite precipitates are like in pressure welding, the problem of a more detailed study of the features of the texture and conditions of such structures formation was posed.

Studied were joints of low-alloyed pipe steel X60, made by pressure welding under vacuum in the following mode: $T_w = 1000$ °C; $P_{w.f} = 3$ kJ (deformation $\varepsilon \approx 20.4$ %). Upsetting was 10 mm. The steel composition, wt.%, was as follows: C — 0.11; Mn — 1.5; Si — 0.42; Cr — 0.02; V — 0.14; Ni — 0.04; Cu — 0.04; S — 0.018; P — 0.014 and O — 0.0075.

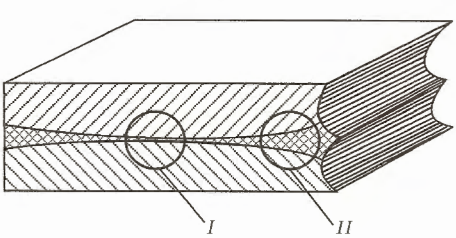

Figure 1. Schematic of location and dimensions of the FB: *I*, *II* — zones of narrow ($\delta \approx 5 - 10$ μm) and wide ($\delta \approx 20 - 25$ μm) bands, respectively.

A number of investigation methods were used to do this work, including optical, analytical scanning, as well as transmission microdiffraction electron microscopy in the instruments of Versamet company (Japan), scanning electron microscope SEM-500 of Philips company (Holland) and transmission electron microscope JEM-200 CX JEOL company (Japan) at the accelerating voltage of 200 kV.

The samples for optical investigations were prepared by standard methods of polishing and etching, *HV* microhardness measurements were taken at 25 g load.

The foils for direct investigation of FB structural-phase state in the transverse sections relative to the joint plane, were prepared successively by mechanical, preliminary electrolytic and then ion thinning of the object by ionised beams in argon.

The procedure of local thinning of the objects under study was used, in view of the small dimensions of FB [6].

Optical metallographic examination (Figures 1, 2) in the joint zones characterised by different thickness of FB, showed that at the same distance from the surface of initial contact but with different FB thickness, the larger grain size D_{gr} is found in the zone adjacent to the interlayer of a greater thickness (Figure 3, curve *1*). With increase of distance l from the surface of initial contact D_{gr} changes non-uniformly, namely grain refinement is found at $l \approx 50$ μm, and grain coarsening at $l = 100 - 1000$ μm, while at $l \approx 4000$ μm, D_{gr} becomes close to the base metal grain size (Figure 3, curve *2*). One can see that D_{gr} starts changing significantly at the distance of 50 μm from the contact surface. Note that the process of common grain

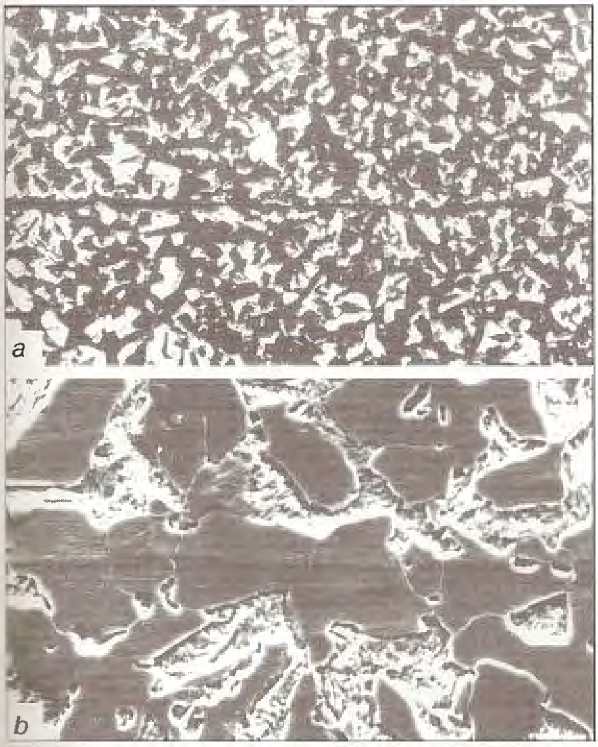

Figure 2. Optical image of the structure of the ferrite band in the joint zone: *a* — ×170; *b* — ×100.

formation is active in the welding zone, which is accompanied by the intergranular boundaries growing through the ferrite interlayer (Figure 2, *b*). Microhardness measurement in different structural constituents, namely in ferrite, pearlite with the changing structure of cementite platelets (Figure 4) shows that its minimal values are found directly in the area of contact. In this case a non-uniformity of microhardness values is noted for different structural states of pearlite, namely an abrupt drop is recorded in those pearlite regions in which decomposition of cementite platelets and formation of isolated ferrite areas are found, whereas higher values are characteristic of pearlite with a clearly visible laminated structure.

A more detailed direct examination by transmission electron microscopy of the structural-phase state of the interlayer proper, as well as the change of this state by the depth of the heat-affected zone (closer to the base metal) revealed the following. The base metal structure consists of ferrite and pearlite grains in approximately equal proportion by volume. In pearlite grains the thickness of ferrite interlayers is 0.15 to 0.20 μm, while the thickness of cementite platelets is 0.05 to 0.10 μm (Figure 5, *a*).

Closer to the contact surface (at ≥ 1000 μm distance) some pearlite grains show partial dissolution of extended cementite platelets (Figure 5, *b* – *e*). This results in carbide particles of predominantly rod shape of 0.05 × 0.15 μm size forming in the place of the dissolving cementite platelets. Rod carbides, as a rule, preserve the orientation of the

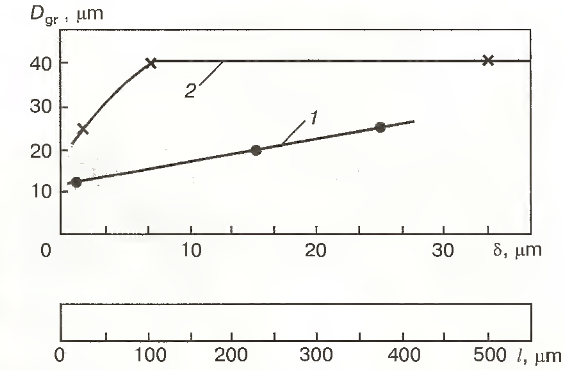

Figure 3. Change of the grain size of the ferrite band (*1*) and beyond it (*2*) by the depth of the welding zone.

initial cementite platelets. The pearlite structure at the initial stages of dissolution become similar to that of upper beinite which is known to have the characteristic feature of the presence of a chain of rod carbides serving as a fringe for the ferrite fragments of an extended shape (Figure 5, *d, e*).

It is characteristic that the process of decomposition — dissolution of pearlitic cementite proceeds under the action of considerable local internal stresses, the evidence of which is a high density of dislocations formed in intercementite ferrite interlayers, as well as their active displacement in the crystallographic slip systems (Figure 5, *b, c*).

At 350 to 550 μm distance from the contact surface an increase in the volume fraction of dissolved cementite is found, which is accompanied by dispersion and spheroidization of residual particles of cementite whose dimensions are 0.01 to 0.02 μm (Figure, 5 *e, f*).

As regards ferrite grains, the changes in this component of ferritic-pearlitic structure are related, primarily, to the change of density, as well as the pattern of distribution of crystalline lattice defects. So, at ≈ 1000 μm distance from the contact

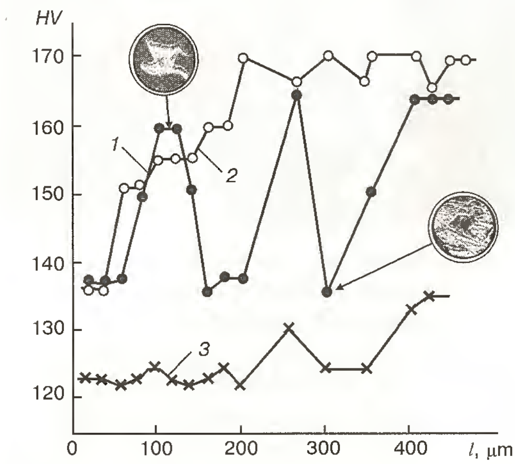

Figure 4. Change of microhardness deeper into the base metal from the ferrite band: *1* — region of decomposition of cementite platelets in pearlite; *2* — region of preserved laminated structure in pearlite; *3* — ferrite components of the structure.

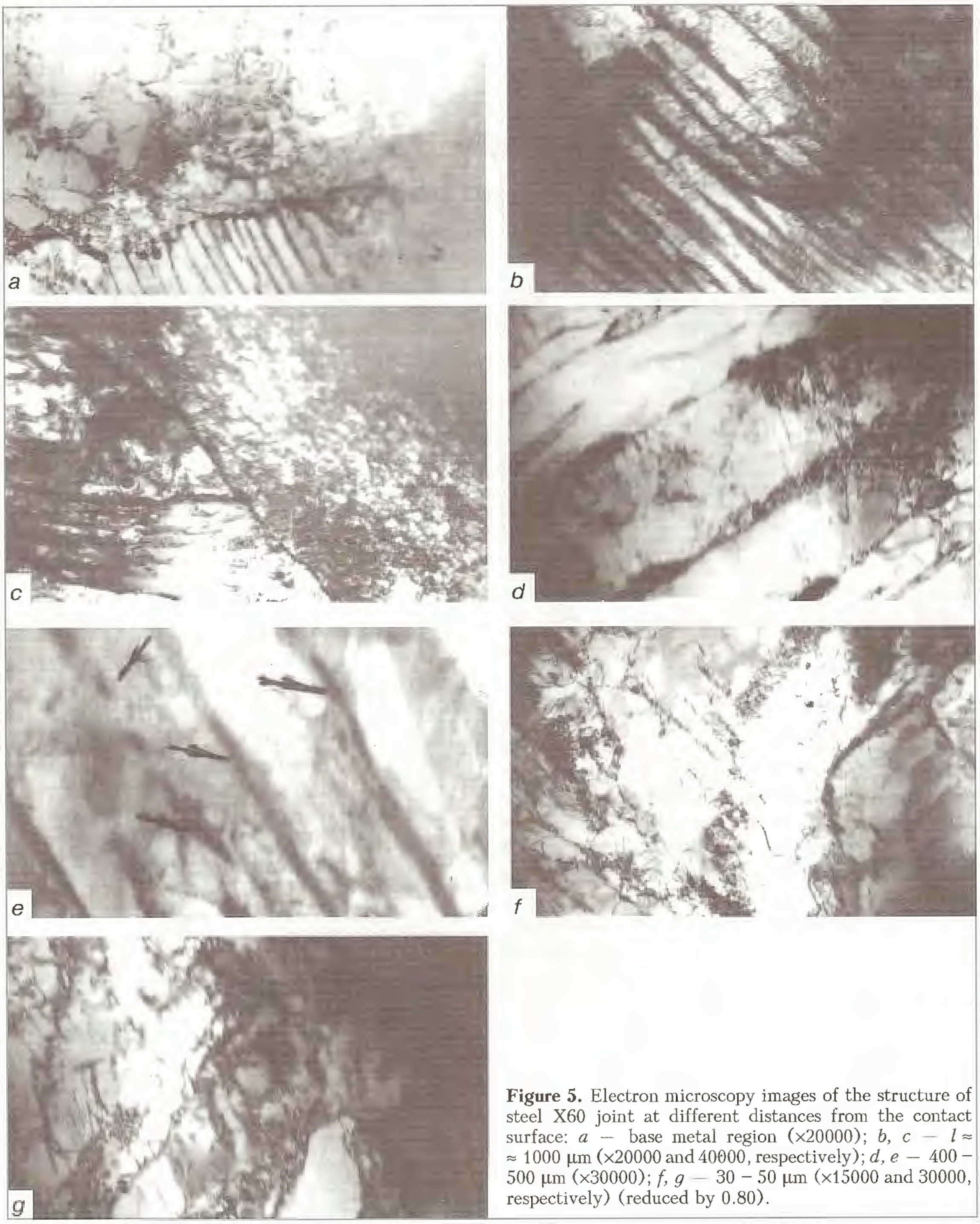

Figure 5. Electron microscopy images of the structure of steel X60 joint at different distances from the contact surface: *a* — base metal region (×20000); *b, c* — $l \approx 1000$ μm (×20000 and 40000, respectively); *d, e* — 400 – 500 μm (×30000); *f, g* — 30 – 50 μm (×15000 and 30000, respectively) (reduced by 0.80).

surface, a certain increase in the dislocation density up to the order of 10^{10} cm^{-2} with their chaotic distribution is found (Figure 5, *b, c*). Closer to the contact surface, the crystalline lattice defects become redistributed and ordered, and substructural elements of various types, namely fragments, recrystallization centers, etc. are formed. One can see that processes of a relaxation nature, namely polygonization, recrystallization prevail in the volumes of the deformed initial ferrite grains of the above welding zone (Figure 5, *f, g*).

Directly in the welding zone the structure practically completely consists of ferrite grains (optically observed FB), but characteristically, of two types, essentially differing by several parameters, namely density and distribution of dislocations, presence of a special segregation contrast and density of carbide phase precipitations (FP).

So, ferrite grains of the first type differ by a comparatively low dislocation density of $\approx (4 - 6)\cdot 10^9$ cm^{-2} and the absence of segregation contrasts, which is confirmed by a clear image of iso-

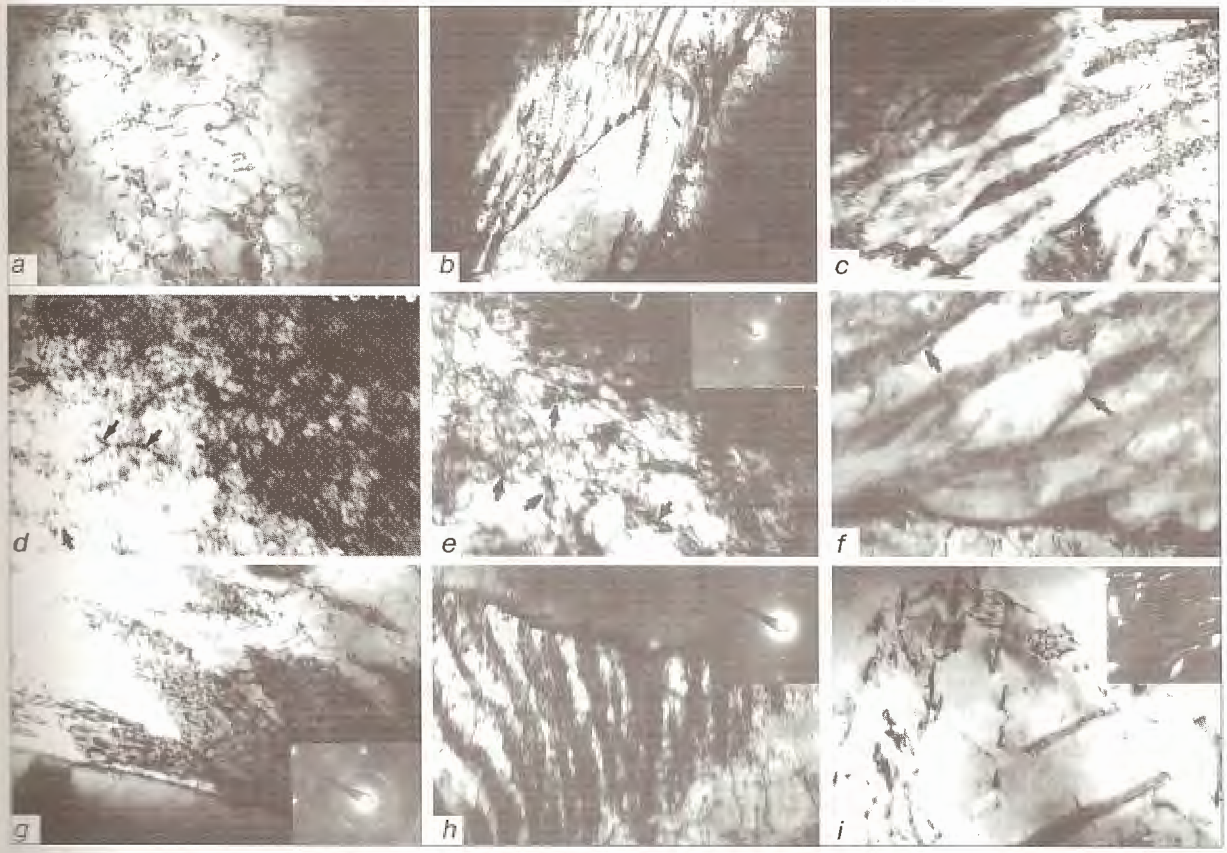

Figure 6. Structure of the ferrite band: *a* — ferrite of the first type (×20000); *b* — general view of pearlite and ferrite (×20000); *d, e* — ferrite of the second type with the characteristic high density of dislocations and clusters of disperse carbides (marked by arrows) (×20000 and 30000, respectively); *f* — segregation contrast in the traces of dissolved cementite platelets (×30000); *g* — acicular structures (×20000); *h* — traces of cementite platelets and microdiffraction reflections of residual carbide particles (arrows show dislocations in the place of the platelets and segregation clusters (×30000); *i* — light and dark field images of carbide particles in the ferrite band (×30000) (reduced by 0.60).

lated unit dislocations and their complexes (Figure 6, *a*). Traces of dislocation movement are also observed in the slip systems at different stages of formation of sub- and intergranular boundaries. The latter allows to make the conclusion that ferrite of the first type is similar to the ferrite of the base metal (matrix).

Ferrite grains of the second type are characterised by the following: 1) high density of ultradisperse carbide-type FP (0.005 to 0.200 μm) with particle spacing in FP distribution equal to 0.10 to 0.25 μm (Figure 6, *b, c*) at a high density of dislocations (10^{10} to 10^{11} cm^{-2}) (Figure 6, *d, e*); 2) dense segregation contrast on individual defects of the crystalline lattice, which, as a rule, creates a blurred dislocation image and has an obvious orientation which reproduces the orientation of the dissolved cementite platelets (Figure 6, *f*).

Note that in transmission electron microscopy investigations formation of acicular structures (similar to the structure of tempered martensite, bainite) with the needle size ≤ 3.0 μm, was often registered directly in the welding zone (Figure 6, *g*). Apparently, the appearance of thin line effects with a metal lustre along the welding zone, often found in the microsections (silvery line) is associated with formation of exactly this type of acicular structures.

It was established that the morphological features of carbide particles found in ferrite of the second type, are interrelated with the size of these carbides. So, the phases of minimal dimensions (0.005 to 0.010 μm) have a predominantly globular shape (Figure 6, *b, c*), while carbides of the rod or another irregular geometrical shape are of 0.01 to 0.05 μm or greater size (Figure 6, *d, e, i*).

Microdiffraction reflections from disperse FP show that their composition mostly corresponds to Fe_3C composition (Figure 6, *h*). Segregation clusters give off reflections of a circular type whose interpretation shows that the appropriate contrast is due predominantly to the presence of carbon (Figure 6, *f, g*).

Reflections from the matrix grains of ferrite in FB are clear enough, i.e. the structure is more or less relaxed and has no considerable internal stresses.

Thus, during welding changes associated predominantly with pearlitic cementite transformation, take place closer to the welding zone in the ferritic-pearlitic structure of the material being welded.

The transformation process consists of different stages of cementite platelet dissolution in the internal volumes of pearlite grains. As a result of such a dissolution, dense clusters of residual particles, namely ultradisperse carbides $(Fe_3C)_{pl}$, carbon segregations [C] form in the trace of the initial cementite platelets $(\mu Fe_3C)_p$, which is accompanied by a considerable increase of the density of dislocations up to the values of $(7-8)\cdot 10^{10}$ cm^{-2}. Thus, the physico-chemical reaction of pearlitic cementite transformation is implemented in the welding zone:

$$(Fe_3C)_{pl} \rightarrow (\mu Fe_3C)_p + [C] + \rho^{\uparrow},$$

where ρ is the dislocation density.

In this case ρ increase is found not only in the cementite platelet trace, but also in the bulk of intercementite ferrite interlayers (see Figure 5, *b*, *c*).

The reaction running in this direction reflects the process of dissolution (degradation) of the pearlitic structure. Various stages of this process are implemented judging by the morphological features and distribution of residual particles of the carbide phases. The structural state which is characterised by the presence of coarser carbides (their geometrical shape being irregular) corresponds to the initial stages. Now, the presence of ultradisperse carbides of a globular shape is indicative of the running of the more advanced stages of cementite platelet dissolution.

It is known that cementite dissolution is interrelated with the process of deep decarburization of the surface layer of the steels being welded [7] which starts already in the preheating period and is activated by the reaction of carbon with oxygen on the surface of the items being welded. Under the conditions of welding in air, a practically unlimited amount of oxygen is present which enters into the reaction with formation of carbon monoxide (CO).

In vacuum welding the oxygen present on the surface in the form of oxides and an adsorbed layer reacts with carbon. The reaction is intensified by the presence of vacuum. Such a process is known and described in publications [8] as self-cleaning of the surface, which goes on during welding. The carbon from the adjacent metal layers diffuses to the surface where it reacts with oxygen.

In a number of cases [9] not only a deep decarburization, but even oxygen increment in the metal near the contact surface can be found.

As was already noted, dissolution of cementite platelets in individual local sections of pearlite is also found at a considerable distance from the contact surface. As a rule, the structure in zones of this type is characterized by the presence of regions with a high level of local internal stresses. The proof of that is an intensive generation of dislocations and high activity of dislocation sliding (see Figure 5, *b, c*). Apparently, under certain conditions, the primary structure (or individual structural fragments) becomes thermodynamically unstable, this kind of instability arising predominantly along the local region of contact interaction of the surfaces being welded, where the level of plastic deformation is known to be the highest [10, 11].

CONCLUSIONS

1. The ferrite band consists of two types of ferrite, namely the one similar to the base metal ferrite in its structure and the transformed ferrite which is the product of transformation of the initial pearlite of the base metal into a conglomerate, consisting of ultradisperse FP of a carbide type, segregation clusters of carbon at a high bulk density of dislocations.

2. Transformed ferrite is characterized by a higher density of crystalline lattice defects, this being due to dislocations pileup under a braking impact of clusters of disperse particles of carbide type and carbon segregations.

3. The following conditions promote FB formation in pressure welding of ferritic-pearlitic steels: presence of surface oxide films in the welding area, whose reduction reactions activate the processes of decomposition of cementite platelets and their diffusion into the zone of free carbon reduction.

REFERENCES

1. Kuchuk-Yatsenko, S.I., Kazymov, B.I., Zagadarchuk, V.F. *et al.* (1980) Steel ductility in flash-butt welding. *Avtomaticheskaya Svarka*, **2**, 1 – 4, 8.
2. Orlov, B.A., Dmitriev, Yu.V., Chakalev, A.A. *et al.* (1975) *Flash-butt welding technology and equipment*. Moscow: Mashinostroyeniye.
3. Kazymov, B.I., Kuchuk-Yatsenko, S.I., Kasatkin, B.S. (1969) Features of fracture of flash-butt welded joints. *Avtomaticheskaya Svarka*, **11**, 31 – 33.
4. Kasatkin, B.S. (1958) On the mechanism of brittle fracture of steel. *Svarochnoye Proizvodstvo*, **6**, 24 – 28.
5. Falkevich, A.S. (1952) Investigation of gas pressure and electric pressure welding of pipelines. In: *High-efficient methods of welding in oil industry*. Moscow: Gostoptekhizdat.
6. Darovsky, Yu.F., Markashova, L.I., Abramov, N.P. *et al.* (1985) Methods of preparation for electron microscopy examination. *Avtomaticheskaya Svarka*, **12**, 60.
7. Gudremon, E. (1966) *Special steels*. Moscow: Metallurgia.
8. Kuchuk-Yatsenko, S.I., Kharchenko, G.K., Falchenko, Yu.V. *et al.* (1998) Self-cleaning from oxides of abutted surfaces in solid-phase welding with heating. *Avtomaticheskaya Svarka*, **2**, 20 – 23.
9. Malinochka, Ya.N., Shmelev, Yu.S., Olikhova, M.A. *et al.* (1981) Formation of oxides in hard steel in oxygen diffusion into it. *Izv. AN SSSR, Metally*, **5**, 110 – 119.
10. Markashova, L.I. (1990) Features of plastic deformation under pressure welding conditions. In: *Achievements and prospects of pressure welding development*. Moscow: PNILDSV.
11. Markashova, L.I., Kireev, L.S., Zamkov, V.N. (1997) Peculiarities of formation of an interfacial zone in pressure welding of dissimilar metals. *Welding Structures*, **8**, 137 – 147.

RESULTS OF NUMERICAL AND FULL-SCALE EXPERIMENTS ON HIGH-SPEED OXYGEN CUTTING OF METALS

N.I. NIKIFOROV[1], **G.K. SUKHININ**[1], **R.A. KREKTULYOVA**[2], **O.N. BEZHIN**[2] and **L.V. GUBENKO**[2]
[1]VNII Avtogenmash, Moscow, Russia
[2]Institute for Physical Problems of Materials Science, Siberian Division of Russian Academy of Sciences, Tomsk, Russia

ABSTRACT

The processes of oxygen cutting of metals are investigated in terms of raising their productivity. The methods of activation of oxidation are considered on the basis of construction and analysis of the equation of kinetics of the oxidation processes. It is suggested that the equation of the oxidation kinetics should be used in a general system of equations which model the heat and mass transfer processes occurring within the cut zone. The three-dimensional dynamic problem of heat and mass transfer was solved numerically using the explicit difference diagrams. Results of numerical and full-scale experiments are given. They confirm reliability of the computer models when used instead of the full-scale experiments for optimization of the oxygen cutting technology.

Key words: *oxygen cutting, attack angle, productivity, cut zone, oxidation kinetics, computerized experiments, numerical solution, difference diagram.*

Cutting is one of the basic operations used in machine-building. Oxygen cutting is among the most common technologies for severing metals into separate parts. Continual improvement of hardware for oxygen cutting, as well as affordability and high cost effectiveness of this method attract interest of scientists and engineers in terms of getting an insight into technological capabilities and raising productivity of the process for making metal tailored blanks.

In this connection, it should be noted that until recently the practical achievements in the field of oxygen cutting have been much ahead of the theoretical developments. In the work described in [1] an attempt was made to construct a general mathematical model for basic technological stages of oxygen cutting. This work is a continuation of the research first initiated in this area. It was aimed at theoretical investigation into the effect of various technological factors on an increase in the speed of oxygen cutting, as well as at experimental verification of individual theoretical postulates.

The problem thus formulated is solved using a mathematical model developed in [1]. For this, the main consideration is given to investigation of the following factors:

kinetics of the oxidation processes for the case of the oxygen jet interacting with the metal cut;

effect of the attack angle α, i.e. the angle between the cutting jet and the sample surface (Figure 1), on the cutting speed;

effect of the first two factors on surface finish within the cut zone.

Derivation of the equation of kinetics. In our work we limit our studies to consideration of iron as a basic component of steels. Based on the Wagner's concept [2], consider the oxidation processes to be the electrolytic ones, i.e. where an increase in thickness of the oxide film is caused by diffusion of charged particles (cations of oxygen atoms, anions of iron atoms and electrons). Transport of the charged particles is schematically shown in Figure 2. According to these concepts, motion of the charged particles can be identified as passage of the electric current through an electrolyte (oxide film). Designate electrochemical potential of the electrolyte as E, the number of the charged ions of iron as N_i, the number of the charged ions of oxygen as N_o and the number of electrons as N_e. Then, using the Faraday's law, formation of oxide dn for time dt can be expressed as follows:

$$\frac{dn}{dt} = \frac{1}{F}\frac{dE}{dr_0}, \qquad (1)$$

where F is the Faraday constant and r_0 is the impedance (electrolytic and electronic) of the oxide film. If we designate the cross section area of the

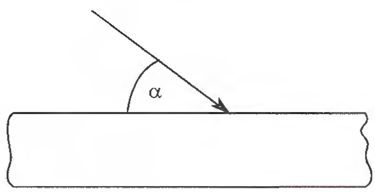

Figure 1.

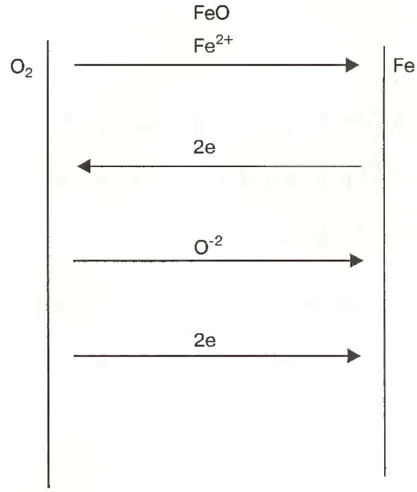

Figure 2.

oxide film as S and its thickness as h, we can write down that

$$r_0 = \frac{h}{S}\frac{1}{\sigma} = \frac{h}{S}\frac{N_i + N_o + N_e}{(N_i + N_o)\,N_e}\frac{1}{\sigma_0}, \tag{2}$$

where k is the specific electrical conductivity of oxide and σ_0 is the initial conductivity of oxide, which is a constant value.

At the same time, the electrochemical potential is known [3] to be a function of temperature and pressure:

$$E = E_0 + \frac{RT}{zF}\ln(P), \tag{3}$$

where R is the universal gas constant, z is the ion charge, T is the temperature, P is the pressure and E_0 is the certain initial value of the electrochemical potential. Allowing for relationships (2) and (3), the equation of kinetics will have the following form:

$$\frac{dn}{dt} = \frac{R}{zF^2}\frac{\sigma_0\,S\,(N_i + N_o)\,N_e}{N_i + N_o + N_e}\left(\frac{\partial T}{\partial h}\ln(P) + T\frac{1}{P}\frac{\partial P}{\partial h}\right). \tag{4}$$

It follows from this equation that the rate of growth of the oxide film is a complex non-linear function of temperature and pressure. Since during the process of oxygen cutting both parameters reach sufficiently high values, which continuously vary with time and thickness of the oxide film, in a general case the solution of this equation cannot be considered separately from solution of the entire systems of equations of heat and mass transfer as formulated in [1]. However, substantiation of mismatch of the problems of heat transfer and hydrodynamic flow given in [1] allows the relationship obtained to be qualitatively analysed.

Analysis of the equation of kinetics. Variations in temperature of the surface layer (oxide layer and adjoining thin metal layer) can be determined from solution of the unidimensional non-linear equation of thermal conductivity

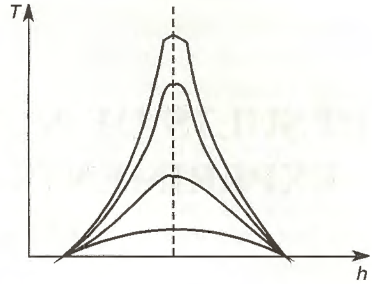

Figure 3.

$$\frac{\partial T}{\partial t} = \frac{\partial}{\partial h}\left(a\frac{\partial T}{\partial h}\right) + Q, \tag{5}$$

where a is the thermal diffusivity and Q is the heat released during oxidation.

It is well-known [4] that solution of this equation includes relationships shown in Figure 3, i.e. the so-called conditions with peaking. They result from the presence in equation (5) of fundamentally non-linear terms, which are a and Q for iron in the oxidation process. Because thermal diffusivity for iron at its melting temperature is almost 8 times lower than at the room temperature, the heat released in oxidation propagates in a hot metal at a much lower rate than in a cold metal. This leads to the fact that a peak-type increase in temperature occurs in local regions, thus causing an enhancement of oxidation of metal, according to equation (4). In turn, this causes an increase in the heat release and a rapidly increasing intensification of the oxidation process, providing that oxygen is fed to this region on time and in a required amount.

Consider now the effect of pressure of the oxygen jet on the kinetic processes. The function of pressure, $P\,(h, t)$, can be found from solution of the system of equations of the hydrodynamic flow [1]. For the unidimensional case, this system has the following form:

$$\begin{gathered}\frac{\partial H}{dh} = \frac{V}{V_0}, \quad V = \frac{1}{\rho}, \quad V_0 = \frac{1}{\rho_0}, \\ \frac{\partial U}{\partial t} = -\,V_0\frac{\partial\,(P + \mu)}{\partial h}, \quad U = \frac{\partial H}{\partial t}, \\ P = A\left(1 - \frac{V}{V_0}\right) + B\left(1 - \frac{V}{V_0}\right)^2,\end{gathered} \tag{6}$$

where H is the space coordinate in a direction of increase in film thickness; h is the mass coordinate; V_0 and V are the initial and specific volumes; U is the mass velocity; ρ_0 and ρ are the initial and current densities; μ is the dynamic viscosity; and A and B are the semi-empiric material constants determined from the experiment [5]. The first equation in system (6) expresses the law of conservation of mass, the second – the law of conservation of momentum and the third is the equation of state.

Set initial and boundary conditions in a general form

$$P(0, t) = P_0(t),$$
$$V_0(h, 0) = \varphi(h) = K_1 + K_2 h;\ K_1, K_2 = \text{const}, \quad (7)$$
$$K_1 = V_{0\mathrm{FeO}},\ K_2 = \frac{V_{0\mathrm{Fe}} - V_{0\mathrm{FeO}}}{h}.$$

Under the assumed conditions, pressure $P_0(t)$ applied to the surfaces is a resultant of all energy effects: impact of the oxygen jet, thermal expansion of the oxidized metal and thermal effect. According to the estimates, pressure that develops in a thin (with a thickness of several microns) subsurface layer is rather high, it amounts to about $(20-30)\cdot 10^2$ MPa. In this case the viscosity forces hardly have a marked effect on the total pressure. They determine dissipation of the mechanical energy at propagation of the pressure front [6]. Therefore, dynamic viscosity was ignored in further analysis.

It is assumed in conditions given in (7) that material of the subsurface layer with a thickness of h varies gradually from iron oxide to pure iron, following a linear rule. Values of specific volumes $V_{0\mathrm{FeO}}$ and $V_{0\mathrm{Fe}}$ are determined as inverse quantities of the corresponding density values ($V_0 = 1/\rho_0$). With the assumed limitations, the system of equations (6) and conditions (7) can be solved analytically. For this, we will use thermodynamic identity obtained in [7]

$$\frac{\partial U}{\partial V} = \left(-\frac{\partial P}{\partial V}\right)^{\frac{1}{2}}. \quad (8)$$

Allowing for this condition and the equation of state, the law of conservation of momentum can be re-written as follows:

$$\frac{\partial V}{\partial t} = -V_0^{\frac{1}{2}} \frac{\partial V}{\partial r}\left[K_1 + 2K_2\left(1 - \frac{V}{V_0}\right)\right]^{\frac{1}{2}}. \quad (9)$$

At a preset initial condition, solution of equation (9) is a solution of the Cauchy problem [8], which is set implicitly by the following relationship:

$$V = \varphi[h + f(V)t], \quad (10)$$

where:

$$f(V) = V_0^{\frac{1}{2}}\left[K_1 + 2K_2\left(1 - \frac{V}{V_0}\right)\right]^{\frac{1}{2}}. \quad (11)$$

As the solution in the explicit form is very cumbersome, we will give its graphic analogue (Figure 4). In this Figure, thickness of the subsurface layer is designated as h_1. The layer includes the

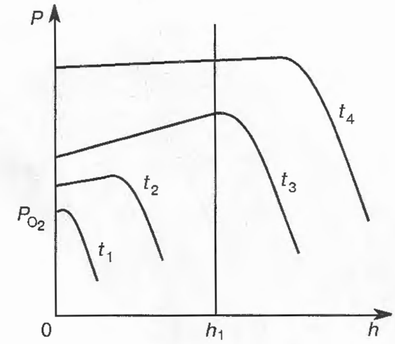

Figure 4.

entire zone of heterogeneity of the material being cut: from molten oxide (with a density of $\rho_0 \approx 4.7$ g/cm^3) to a substrate material (with a density of $\rho_0 \approx 7.85$ g/cm^3). The pressure distribution pattern for this layer is of a clear wavy character. At the initial time moment t_1, where the momentum has just been formed on the surface of the oxide film, its maximum pressure corresponds to pressure of the oxygen jet P_{O_2}. With time $t_1 < t_2 < t_3 < t_4$, its amplitude grows, as the acoustic impedance (ρc, where c is the sound velocity) of iron is approximately three times higher than that of the iron oxide melt. At the same time, part of the insident wave energy is reflected from iron layers with a higher density and goes back at the sound velocity to a free surface. Thus, pressure on the free surface also starts growing until it reaches the value equal to pressure in the base metal. The reverse wave formed inside the material promotes removal of the melt from the surface, as velocity of this wave is higher than the flow rate of the oxygen jet (to compare: sound velocity in steels is $\approx$ 5000 m/s, oxygen flow rate is $\approx 400-600$ m/s), and power of the wave increases with an increase in pressure applied to the surface.

Therefore, it follows from analysis of equation (4) that increasing the pressure of the oxygen jet promotes separation of the oxide film, rather than its growth, whereas increasing the temperature within the cut zone promotes a stable growth of the oxide film.

Results of computerized investigations. Qualitative analysis of methods for increasing the oxygen cutting speed was utilized to design computerized experiments to simulate actual technological processes. The work described in this article involved numerical solution of a three-dimensional dynamic problem of heat and mass transfer given in [1]. This statement of the problem made it possible to investigate the effect of the attack angle on the cutting speed and trace dynamics of formation of roughness under different cutting conditions. All the investigations were conducted on thin-sheet low-alloy steel. Sizes of the model samples were limited by the computation capabilities

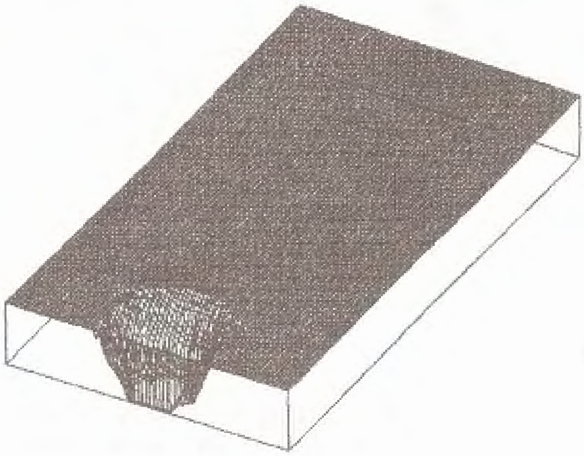

Figure 5.

of the available computer facilities and were as follows: thickness — not more than 4 mm, width 20 – 25 mm and length 40 – 60 mm. It should be noted that actual sizes of the samples cut are as a rule much in excess of those used in the model. However, the processes of thermal oxidation within the cut zone occur normally in a narrow region, which is determined by a diameter of the oxygen jet nozzle and diameter of the heating flame nozzle, which in this case are 0.6 and 6.0 mm, respectively. This is caused by the fact that the metal, as it is oxidized and melted, as well as a considerable part of the energy released during chemical reaction, are removed from the cut zone during cutting. Thus, the metal has time to be heated in width only to a distance of 2.0 – 2.5 mm from the cut edges (at thickness of the sheet equal to no more than 4 mm), which allows the gauge region to be limited to the said sizes. The computations were carried out using a difference diagram with a variable pitch: within the cut zone (4 – 5 diameters of the nozzle) the pitch was 0.1 – 0.2 mm and in the rest of the region it was 0.5 mm. The cutting speed was varied over a wide range: from 0.6 to 6.0 cm/s, and the angles α were varied from 10 to 90°. The oxidized and molten metal was forced removed from the computation region. The rate of removal was determined on the basis of the above-indicated laws of conservation.

Numerical computations showed that at a small attack angle ($\alpha = 10 - 30°$) and sufficiently high pressures of the oxygen jet (1 – 5 MPa) the cutting speed could be increased to 10 cm/s and more. However, in this case the above-noted centres of intensive oxidation are formed within the cut zone. This makes the cut zone wider and the cut edges very rough. The above-said is illustrated in Figure 5. In this case the cut width is 8 mm. It can be seen in the Figure that the centre with an increased oxidation rate, directed deep into the material, has already formed at the frontal part of the cut.

In this case, on the display we have a typical image of the sample surface within the cut zone and with a clearly defined boundary of the heat front, the three-dimensional representation of the cut zone proper, the sample regions where the oxidation process has not been completed as yet, and the geometrical sizes of the cut zone at a depth of 1.5 mm.

These and other computerized experiments showed that capabilities of oxygen cutting are far from being exhausted. In general, the feasibility exists for increasing cutting speed and improving the surface finish of the cut edges.

Experimental results. Experiments on high-speed oxygen cutting of low-alloy steel were carried out to verify the computations. Tests were done on steel sheets 3 – 10 mm thick. It was established that at small attack angles ($\alpha = 30 - 45°$) and at a cutting oxygen jet pressure of $P \approx 1$ MPa and higher the cutting speed appreciably increased (3 – 5 times). Thus, at a sheet thickness of 4 mm, it was 4.8 cm/s. However, as was predicted by the computations, the cut edges were extremely rough, the valleys were about 2 mm deep and the total cut width was about 8 mm.

The experiments also showed that the highest effect was provided by the use of the acute attack angles in cutting large-diameter pipes. Thus, in cutting the pipe with a diameter of 820 mm, wall thickness of 9 mm and the attack angle of $\alpha = 10°$, the cutting speed was 5.9 cm/s. Such a high productivity was ensured by the fact that the slag melt formed during cutting moved on the inside and outside surfaces of the pipe and heated the metal to a high temperature prior to cutting, which markedly enhanced the oxidation processes.

CONCLUSIONS

1. The equation of kinetics of oxidation of metals was derived. The qualitative analysis of applicability and efficiency of utilization of this equation as a supplement to simulation of the oxidation processes was conducted.

2. Computerized experiments were carried using the updated mathematical model. They allowed the methods of improving the quality and raising the productivity of cutting to be analysed.

3. Experimental studies on high-speed oxygen cutting were conducted, which confirmed reliability of the model representations.

4. The qualitative agreement between the full-scale and computerized experiments was proved. This makes it possible to use the computer models for development of new oxygen cutting processes and upgrading of those available.

REFERENCES

1. Nikiforov, N.I., Krektulyova, R.A. (1998) Mathematical modelling of the oxygen cutting process. *Svarochnoye Proizvodstvo*, **4**, 3 – 6.
2. (1989) *Theory of metallurgical processes*. Ed. by D.I. Ryzhonkov. Moscow: Metallurgia.
3. Davis, S., James, A. (1986) *Electrochemical dictionary*. Moscow: Mir.
4. Samarsky, A.A., Galaktionov, V.A., Kudryumov, S.P. *et al.* (1987) *Conditions with peakings in problems for quasi-linear parabolic equations*. Moscow: Nauka.
5. Zharkov, V.N., Kalinin, V.A. (1968) *Equations of state for solid bodies at high pressures and temperatures*. Moscow: Nauka.
6. Makarov, P.V., Skripnyak, V.A. (1983) Viscosity of iron in loading and unloading waves. In: *Mechanics of continuum*. Tomsk: Tomsk University Publ.
7. Krektulyova, R.A., Gerasimov, A.V. (1995) Three-dimensional propagation of impact pulse in condensed gradient media. In: *Numerical methods for solution of elasticity and plasticity problems*. Ed. by V.M. Fomin. Novosibirsk.
8. Farlow, S. (1995) *Equations with partial derivatives for scientific and engineering staff*. Moscow: Mir.

DESIGN-EXPERIMENTAL ESTIMATION OF THE POSSIBILITY OF REDUCTION OF THE HAZ METAL COOLING RATE IN WET UNDERWATER WELDING

V.V. CHIGAREV and **A.V. USTINOV**
Priazov State Technical University, Mariupol, Ukraine

ABSTRACT

Methods are considered for regulation of thermal cycle of the HAZ metal in coated-electrode arc welding directly in the water. A finite-element mathematical model of thermal processes is developed which allows forecasting the lowering of the cooling rate at the expense of thermal insulation of the heated surface of the metal being welded from the water.

Key words: *wet underwater welding, coated electrodes, thermal cycle, cooling rate, finite element method, experimental investigations, thermal processes.*

Wet underwater welding with coated electrodes is considered to be the most versatile and cost-effective method of performance of underwater operations in building and repair of metallic constructions. A wide acceptance of this process is hindered by poor quality of the joints [1]. In the water the metal cooling rates are by 10 to 15 times higher than in welding in air [2]. This causes an abrupt loss of ductile properties of the metal of the weld and the HAZ. In the joints of low-alloyed steels a combination of the quenching structures in the HAZ and an increased content of hydrogen can result in formation of cold cracks.

The rate of metal cooling under the water depends on many factors, part of which cannot be controlled, namely the item structural parameters (metal thickness and its position in space) and the properties of the environment (temperature, depth of the water, salt concentration in it, strong currents). The controllable parameters of the welding mode (electrode diameter, welding current, arc voltage, welding speed) permit the rate of the HAZ metal cooling to be varied in a rather broad range. In the temperature range of 800 to 500 °C it can change from 415 to 56 °C/s [3, 4]. Increase of arc power or decrease of welding speed lower the metal cooling rate. However, a high power of the arc or low speed of welding lead to an excess increase of the deposited metal mass. Rise of welding current causes undercuts in the base metal. The lower limit of the cooling rate which is achieved in welding, is rather far from the values providing equilibrium structures in welded joints of low-alloyed steels [5].

The cooling rate is lowered more effectively at the expense of heat insulation from the water of sections of the surface of the metal being welded [3, 4]. Weld surface insulation from the water significantly improves the thermal cycle of welding, making it closer to the shape characteristic for welding in air. Insulation of just the base metal surface adjacent to it, practically does not affect the cooling rate [3]. From other data [4], the thermal cycle of the HAZ metal becomes close to that achieved in air, exactly due to insulation of the surface adjacent to the weld and of the reverse side of the plate. The contradictory opinions on the optimal location of heat insulation are indicative of the complexity of the thermal processes occurring in underwater welding.

A mathematical model of thermal processes for the case of wet underwater welding was developed in order to evaluate the influence of the dimensions and location of heat insulation on the cooling rate. The thermal problem was solved for welding metal of medium-thickness most often used in ship-building and in off-shore construction. The initial data for the model construction were derived in welding in a laboratory unit. The high accuracy and reproducibility of the experiments were achieved by mechanized feed of the electrode and its displacement with a specified speed of welding. The direct connection of the welding cable to the electrode tip through the electrode holder reproduced the condition of current flowing inherent to coated-electrode manual welding process. The thermal cycles in the metal were recorded using chromel-alumel thermocouples of 0.2 mm diameter by a mirror-galvanometer oscillograph H-117/1 on light-sensitive UF-67 paper. A detailed description of the procedure of recording the thermal cycles in underwater welding is given in [6].

Underwater welding was performed on 200×300 mm plates 16 and 12 mm thick of 09G2 and 10KhSND steels at the depth of 0.3 m in flesh water at the temperature of 10 to 12 °C. ANO-4 coated electrodes of 4 mm diameter with hydraulic insulation were used, which proved a high arcing stability. Direct current of reverse polarity was used. The thermocouples were mounted in the region of the maximal HAZ temperatures on the surface at the weld edge. Such a schematic of measurement allows for the non-uniformity of temperature distribution in the plate cross-section. The gradient of maximal temperatures in the surface layer is 2.2 times higher in some cases than under the weld [6].

Application of the design-experimental model of thermal processes from study [3] does seem possible, as it is based on the numerical solution of the differential equation of heat conductivity for heat flow in a thin plate. In this case, it is assumed than the heat source should be linear, with the power distributed over the entire thickness [7]. Such a condition is not met in the medium-thickness metal in coated-electrode welding.

In the assumed model of thermal processes, the application of the arc heat to the base metal is performed in a section equal to the weld width (B) determined from the experimental data. From the point of application, the heat propagates in the metal by the heat conductivity law and, having reached the plate surface, is dissipated into the surrounding water. For wet underwater welding the boundary conditions of the 3rd kind are satisfied on the media interface [7]

$$a_{\mathrm{h}}\,(T_0 - T_{\mathrm{wat}}) + \lambda \left.\frac{\partial T}{\partial n}\right|_S = 0, \tag{1}$$

where a_{h} is the heat-transfer coefficient; S is the boundary surface of the body; T_0 and T_{wat} are the temperature on the metal and water surface, respectively; and λ is the metal heat conductivity factor.

In the presence of a heat-insulating material on the plate surface, the boundary condition of the 4th kind should be satisfied on their boundary

$$\lambda_1 \left.\frac{\partial T_1}{\partial x}\right|_S = \lambda_2 \left.\frac{\partial T_2}{\partial x}\right|_S, \tag{2}$$

where λ_1 and λ_2 are the coefficients of heat conductivity of the metal and the heat-insulating material, respectively.

Heat transfer beyond the heat-insulating material location zone and from its surface, proceeds by Newton's law and condition (1) is satisfied, i.e. mixed boundary conditions are in place. In order to simplify the thermal model, it was conditionally assumed that on the metal surface coated by the heat-insulating material, the convective heat transfer occurs by Newton's law into a layer of the low heat-conducting liquid which has the same heat-transfer coefficient as with air. During welding the liquid does not lose its properties, does not mix or dissolve in the water. Beyond the heat-insulating layer the heat-transfer coefficient is equal to the value found for the conditions of wet welding in its pure form. This problem was realized by the finite-element method (FEM) which permits solving physical problems described by differential equations and allowing for the boundary conditions [8]. When the calculation procedure was elaborated, it was assumed that the heat flow propagates in a plane normal to the weld axis, and the plate cross-section from one side of weld axis was considered in view of its symmetry, as shown in Figure 1. The thermophysical properties of the base metal were assumed to be independent of temperature and corresponded to the properties of low-carbon low-alloyed steel [9].*

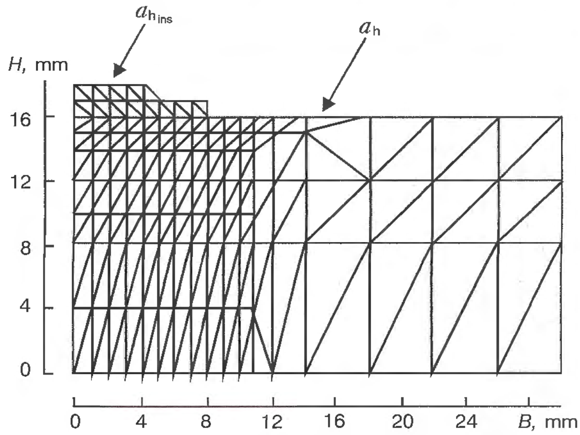

Figure 1. Design schematic of heat transfer by the FEM for underwater welding with heat insulation of the weld surface.

The heat-transfer coefficient was taken in the form of the 3rd degree polynomial. The polynomial coefficients were selected to provide the best correlation of the design and experimental thermal cycles, as well as distribution of maximal temperatures over the plate cross-section. Use of an averaged heat-transfer coefficient dependent on the metal surface temperature [3, 10] yields worse results. Proceeding from the published data [3, 4, 10], the effective efficiency of the process for coated-electrode wet underwater welding was taken to be 0.65. It should be noted that the two-dimensional diagram of heat propagation does not entirely correspond to the actual thermal pattern developing in a flat layer in surfacing with a mobile heat source. The three-dimensional diagram could improve the design accuracy in this case, but a too great complication makes its application problematic.

The thermal problem was initially solved for the case of bead deposition on 16 mm plate without

*S.P. Markov took part in the design work.

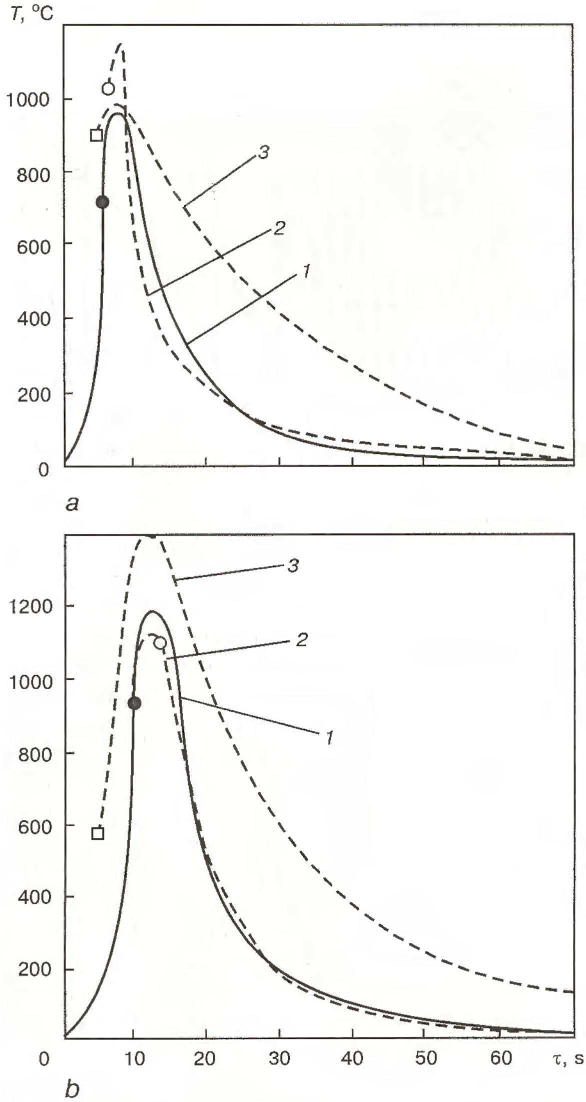

Figure 2. Thermal cycles of HAZ metal on plate surface (*a*) and under the weld (*b*); *1* — experimental; *2* — design under regular conditions; *3* — design in the presence of a heat-insulating layer.

the heat-insulating layer. Welding was performed at minimal current (150 ± 5 A) and speed (1.7 ± ± 0.1 mm/s), which corresponded to the process heat input q_i/v_w = 1.6 MJ/m. A low heat input provided the highest rates of cooling of the HAZ metal and could demonstrate the effectiveness of heat insulation application to the utmost degree. The best correlation of the design thermal cycles with the experimental ones, as well as of penetration depth (H) and weld width was achieved with heat-transfer coefficient, W/(m^2·K),

$$a_{T_{ins}} = 10^{-7}T^3 + 8.3\cdot 10^{-5}\,T^2 + 2500. \qquad (3)$$

The found value of heat-transfer coefficient was used to simulate for open surfaces the variant of wet underwater welding with heat insulation of the weld surface (B_{ins} is the dimension of the insulating layer). The low heat transfer in the section with the heat-insulating material was achieved with the heat-transfer coefficient, J/(m^2·K),

$$a_{T_{ins}} = 1.04\cdot 10^{-4}\,T^2 + 60. \qquad (4)$$

The calculation results and the experimental data are given in the Table which shows that the model of the thermal processes provides the best correlation of the cooling rates in the temperature range of 800 to 500 °C under the weld center.

The penetration depth and the weld width turned out to be quite close to the experimental values. A much higher design cooling rate of the HAZ metal located on the surface compared to the experimental value, is attributable to the complex nature of temperature variation in this section. Experimental studies showed that the temperature gradient at 1 mm distance from the fusion line at the weld edge is 1000 °C/mm [6]. The diameter of the thermocouple junction comes out to be equal to 0.4 to 0.5 mm, this hindering the gradient falling exactly into the maximal temperature zone (above 800 to 850 °C). The appearance of the thermal cycles given in Figure 2, confirms the above peculiarities of the design and experimental data.

Analysis showed the high effectiveness of reduction of the heat transfer from the weld surface, this resulting in lowering of the cooling rate at the weld edge by 4.4 and 2.5 times in the temperature range of 800 to 500 °C. With further cooling of the HAZ metal in the temperature range of 500 to 300 °C, the effectiveness of the heat insulation is still high. The cooling rate is lowered by 2.6 and 2.0 times, respectively. The thermal cycle becomes less abrupt, the time of the metal staying at high temperatures and the time of cooling to low temperatures are longer. By its shape and characteristics it becomes closer to the thermal cycles produced in welding in air. The non-uniformity of the cooling rates distribution in the HAZ metal is eliminated.

In order to verify the adequacy of the mathematical model and search for the optimal width of the heat-insulating layer, calculations were performed and thermal cycles were recorded in welding of 12 mm metal with different heat inputs (1.6 to 3.2 MJ/m). Four welding current values were used, namely 150 ± 5; 170 ± 5; 200 ± 5; 230 ± 5 A which covered the entire range of currents applied for this electrode diameter. The welding speed was unchanged. Figures 3 and 4 give the results of processing the design and experimental data. The design and experimental values of the rate of metal cooling under the weld show the best correlation at a low heat input (1.6 to 2.0 MJ/m). The discrepancy between the data is from 3.3 up to 13.3 %. With the increase of the heat input up to q_i/v_w = = 3.2 MJ/m, the difference reaches 41.4 %, but the tendency of the cooling rate decrease is preserved. The design cooling rate of the HAZ metal

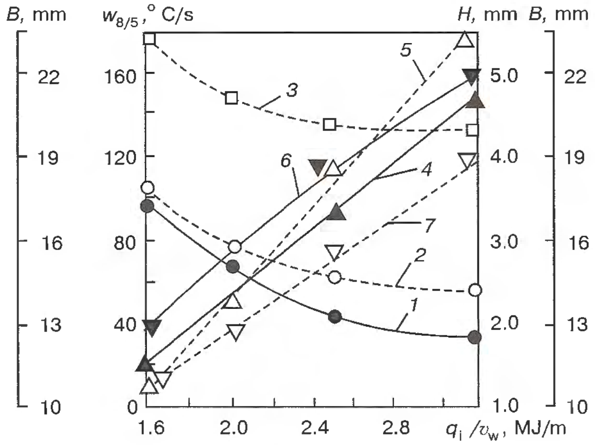

Figure 3. Influence of heat input in welding on weld parameters and cooling rate of HAZ metal: *1, 2* — experimental and design rates of HAZ metal cooling under the weld, respectively; *3* — design rate on the plate surface; *4, 5* — experimental and design penetration depth, respectively; *6, 7* — experimental and design weld width, respectively.

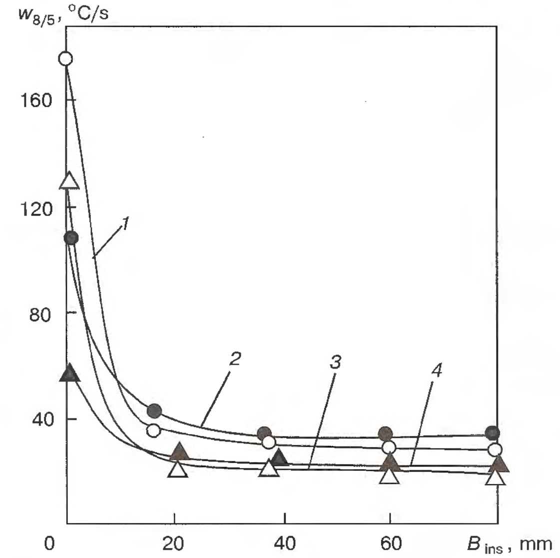

Figure 4. Influence of heat-insulating layer width on cooling rate of HAZ metal on plate surface (*1, 3*) and under the weld (*2, 4*): *1, 2* — q_i/v_w = 1.6; *3, 4* — q_i/v_w = 3.2 MJ/m.

on the surface remains to be higher than under the weld by 1.7 to 2.3 times, this being indicative of a great non-uniformity of its distribution in the plate cross-section. It grows with the increase of the heat input. This is related to the fact that a greater heat input enhances the heating of the deeper-lying metal layers (penetration depth is increased) and lowers the rate of its cooling. However, a concurrent increase of the area of the most heated region (the weld becomes wider) intensifies the heat transfer from the metal surface and slows down the pace of the cooling rate decrease at the weld edge.

Increase of the heat input at the expense of increasing the arc power (from 4200 up to 8300 W) lowers the rate of cooling of the HAZ metal from 100.0 to 33.6 °C/s (Figure 3), and can affect the type of its structure. In study [3] it is indicated that the effectiveness of the arc power influence on the cooling rate decrease is low on thin metal, but becomes higher with the greater thickness of the metal. However, in welding of 12.5 mm metal, when the power of 9500 W is achieved, the cooling rate is only lowered to 105 °C/s, this being insufficient to remove the quenching structures. Such a discordance of the data is attributable either to a higher welding speed (it is not given for this case), or the unsuitability of the design schematic (thin plate) for medium-thickness metal.

The design isotherm of the penetration temperature accurately enough coincides with the experimental one corresponding to the weld width and the penetration depth. The best correlation is observed at low heat inputs (1.6 to 2.2 MJ/m). With the increase of q_i/v_w above 2.2 MJ/m, the design penetration depth becomes greater than the experimental value, but does not exceed the natural variation of penetration in welding. The design value of the weld width in the entire heat input range turns out to be lower than that found experimentally. This is due to a strong influence of the higher heat-transfer coefficient in the design schematic and the impact of the liquid metal flows in the weld pool on the actual weld width, ignored in the model.

Simulation of heat insulation on the weld surface showed the high effectiveness of this technique also for 12 mm metal (Figure 4). The rate of the HAZ metal cooling at the weld edge becomes 4.8 to 5.0 times lower, and 1.9 to 2.5 times lower under the weld. Further spreading of the heat-insulating

Method of data generation	*Place of analysis*	*B_{ins}, mm*	*H, mm*	*B, mm*	*$w_{8/5}$, °C/s*	
					800 – 500 °C	*500 – 300 °C*
Experiment	Under the weld	–	1.4 – 1.8	12.0 – 13.0	103.2	72.5
	On the surface				104.2	63.5
Calculation	Under the weld	–	1.2	11.5	105.0	52.3
	On the surface				178.6	58.8
	Under the weld	16	6.5	16.5	42.2	25.4
	On the surface				40.8	22.7

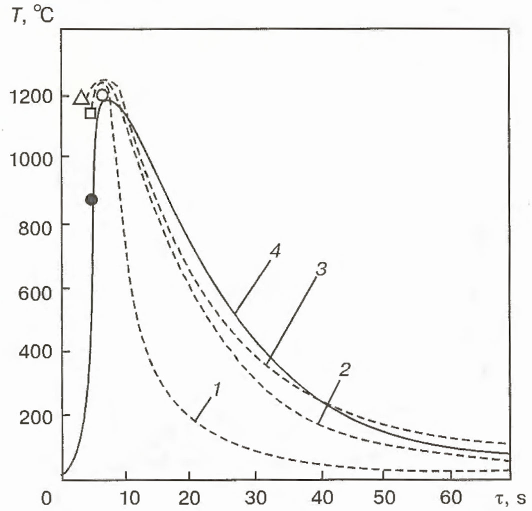

Figure 5. Influence of heat input and insulation from the water on thermal cycle of HAZ metal under the weld: *1 – 3* — in welding without insulation, with 16 and 80 mm wide insulation, respectively; q_i/v_w = 1.6 MJ/m; *4* — under regular conditions, q_i/v_w = 3.2 MJ/m.

layer to the base metal up to 60 mm, i.e. 3.8 times, leads to 1.2 times lowering of the cooling rate both on the surface and in the depth of the plate. Enlargement of the heat insulated area by another 20 mm lowers the rate by just 1.0 to 6.0 °C/s. The low effectiveness of the plate surface insulation from the water beyond the weld is confirmed by a small difference in the thermal cycles corresponding to the layer widths of 16 and 80 mm (Figure 5).

Heat insulation of the weld surface also improves the cooling rates distribution in the plate cross-section (see Figure 4): it becomes practically uniform, as in welding in air. The rate of cooling of the HAZ metal at the weld edge turns out to be by 13 to 18 % lower than under it. The nature of the cooling rates distribution does not change with the increase of the heat input.

The results of estimation of the effectiveness of heat insulation of the weld surface on medium-thickness metal are in good qualitative agreement with the data of [3]. On the other hand, it does mention a significant difference between the cooling rates of the surface and the lower-lying layers of the HAZ, which is, probably, attributable to heating of the entire thickness of thin metal (3.2 to 6.4 mm) up to a high temperature. This results in an intensive heat transfer not only from the face, but also from the reverse side of the thin plate. In such a case or in the case of a root pass of a multi-layer weld, heat insulation of the back surface with indubitably reduce the heat losses and the HAZ metal cooling rate. A significant improvement of the thermal cycle in the HAZ at application of oil paste on the face (except for the weld) and back side of the plate surface [4] was, probably, achieved exactly with such a temperature field in the metal.

In medium-thickness metal heat insulation of the surface of the weld and the adjacent base metal section of optimal width at minimal q_i/v_w = = 1.6 MJ/m lowers the HAZ metal cooling rate to 29.4 to 33.2 °C/s (see Figure 4). The same rate of the HAZ metal cooling under the weld can be also achieved with increase of q_i/v_w up to 3.2 MJ/m, but then the cooling rate in the surface layer is reduced just to 133.4 °C/s (see Figure 3). Heat insulation at a higher heat input (2.5 to 3.2 MJ/m) allows achievement of very low rates of the HAZ metal cooling (20.0 to 24.0 °C/s) both under the weld and on the surface (see Figure 4). Such cooling rates in the temperature range of phase transformations allow prevention of the formation of quenching structures in some low-alloyed steels [11] and at the expense of it, a significant improvement of the quality of welded joints in coated-electrode wet underwater welding.

The design-experimental procedure of investigations used in this study, allowed development of a mathematical model of the thermal processes occurring in wet underwater welding. The mathematical model based on FEM, provides an adequate description of the thermal cycles in the HAZ metal and distribution of the maximal temperatures over the cross-section of medium-thickness plates (12 to 16 mm). The calculation method was used to reveal the high degree of non-uniformity of the cooling rates distribution across the thickness in welding, which is 1.7 to 2.3 times higher on the surface than under the weld.

The proposed replacement of the complex boundary conditions of the metal heat exchange with the environment by simpler ones allowed simulation of the influence of thermal insulation of different sections of the welded joint on the thermal processes in the metal in wet underwater welding. Calculations showed that heat insulation of the weld surface from the water is the most effective and provides a lowering of the HAZ metal cooling rate in the temperature range of 800 to 500 °C by 4.4 to 5.0 times at the weld edge and by 1.9 to 2.5 times under the weld. Further spreading of heat insulation to the adjacent base metal is less effective and can further lower the cooling rate by 1.2 times. The optimal width of the layer of heat-insulating material should not exceed 80 mm.

Application of heat insulation eliminates the non-uniformity of distribution of the cooling rates over the plate cross-section and provides at a minimal heat input, the same rate of the HAZ metal cooling as in welding with the maximal heat input without the heat insulation. Heat insulation of weld surface at a higher heat input allows achievement of the region of cooling rates admissible for the low-alloyed steels in the temperature range of phase transformations in coated-electrode wet underwater welding and improvement of its quality.

REFERENCES

1. Gretsky, Yu.Ya., Maksimov, S.Yu. (1995) Structure and properties of joints of low-alloyed steels in coated-electrode wet underwater welding (Review). *Avtomaticheskaya Svarka*, **5**, 7 – 11.
2. Brawn, R.T., Masubuchi, K. (1975) Fundamental research on underwater welding. *Welding J.*, **6**, 178 – 188.
3. Tsai, C.-L., Masubuchi, K. (1980) Mechanism of rapid cooling and their design considerations in underwater welding. *J. of Petroleum Technology*, **10**, 1825 – 1833.
4. Hasui, F., Suga, Y. (1980) On cooling underwater welds. *Transact. of the Jap. Weld. Soc.*, **1**, 21 – 28.
5. Grivnyak, I. (1984) *Weldability of steels*. Ed. by E.L. Makarov. Moscow: Mashinostroyeniye.
6. Ustinov, A.V. (1998) Features of thermal cycle and distribution of maximal temperatures in wet underwater welding. *Vestnik Priazov State Techn. Univ.*, **6**, 232 – 235.
7. (1988) *Fundamentals of welding*. Ed. by V.V. Frolov. Moscow: Vysshaya Shkola.
8. Segerlind, L. (1979) *Application of the finite element method*. Ed. by B.E. Pobedri. Moscow: Mir.
9. Rykalin, N.N. (1951) *Calculation of thermal processes in welding*. Moscow: Mashgiz.
10. Pamar, R.S. (1977) Temperature distribution in underwater shielded metal arc welding of free flat plates. *J. Inst. Eng., Mech. Eng. Div.* (India), **1**, 38 – 47.
11. Zeyffarth, P., Gross, H.-G., Dovzhenko, V.A. *et al.* (1991) Structural transformations and properties of the metal of the HAZ of 10KhSND steel welded joints. *Avtomaticheskaya Svarka*, **8**, 12 – 16.

PECULIARITIES OF ARC TREATMENT OF QUENCHING STEELS WITHOUT MELTING

M.M. SAVITSKY, V.M. KULIK and **G.V. BURSKY**
The E.O. Paton Electric Welding Institute, NASU, Kyiv, Ukraine

ABSTRACT

The effect of conditions of argon-arc tungsten-electrode treatment of steels on the thermal cycle parameters is investigated. It is shown that to avoid incipient melting at an increase in amperage, it is necessary to raise the rate of treatment, increase the arc length to 7 – 15 mm and impart transverse oscillations to the arc. The treatment conditions allow the temperature of a short-time heating, duration of metal dwelling in a heated state and cooling rate to be controlled.

Key words: *arc treatment, high-strength steel, thermocouple, thermal cycle, heating temperature, cooling rate, austenization, transformation, structure, hardness, microhardness, hardening.*

Welding high-strength alloyed steels leads to formation of brittle quenching structures in the HAZ and the weld. This leads to a risk of delayed fracture in manufacture or brittle fracture in operation of parts. In particular, this is the case where the weld metal is close to the base metal in its carbon content and strength characteristics. To increase ductility and crack resistance of welded joints, as a rule they are subjected to postweld heat treatment in furnaces, which causes a substantial increase in power consumption and cost of operations, and it is not always technically feasible. Nor is it always possible to use traditional means for local heat treatment, which involves other sources of heat energy, materials, equipment, fixture and, hence, considerable complication of the process of fabrication of welded structures.

Argon-arc treatment with or without metal melting is carried out to improve geometry and structure of welded joints, improve impact toughness and performance of the joints and working surfaces of parts [1 – 3]. This treatment can be done using the same equipment and the same consumables as those used for welding, and can readily be built-in into the welding production line, in many cases being an integral part of welding. In treatment with surface melting, the probability exists of variation of chemical composition of metal, deterioration in surface appearance and finish and formation of stressed and cast brittle structures of metal remelted. Multiple surface melting can also be accompanied by hydrogenation of metal, thus leading to embrittlement and porosity. Argon-arc treatment without surface melting is free from such drawbacks. It leads to refinement of the metal structure and improvement in impact toughness of a welded joint in high-strength steel [3]. The surface of iron-carbon alloys [4] can be hardened by the magnetically-impelled arc with a tungsten cathode, moving at a high speed (60 – 180 m/h). It is likely that the effect achieved by arc treatment without melting depends primarily upon the thermal cycle with controllable parameters (temperature of heating, rate and time of cooling). Almost no data are available on thermal cycles of arc treatment without incipient melting, although by analogy with fusion welding [5, 6] they should be determined by the heat source (arc) power q, treatment rate v_{tr}, heat input q/v_{tr}, thermal-physical properties and thickness of metal treated.

The aim of this work was to find a possibility and basic solutions for a purposeful change in structure and state of metal of the welded joints in high-strength steels using arc treatment without melting. Investigations were conducted to study thermal cycles and zones of structural changes of metal in arc heating under different conditions.

Normally, the welded joints have different thickness in transverse and longitudinal sections and are characterized by a complex structure. The welded joints in high-strength steels, in addition, are hard to treat by cutting or by applying pressure. This makes preparation and conducting of experiments much more difficult, causes random changes in input and propagation of heat from the arc, and hampers revealing the zones of structural transformations in metal in arc treatment. On this basis, treatment was done to samples of plate steel 30KhGSA and 42Kh2GSNM, 3 and 5 mm thick, having different susceptibility to quenching, homogeneous structure and hardness in the as-received state, which is several times lower than hardness of the weld metal.

Arc heating of metal was done using tungsten electrode and the machine of the ARK-1 type, equipped with the VSVU-315 welding rectifier. The steel plates were clamped horizontally in a fixture having no cooling elements, the distance between the clamps being 50 mm. The plates were heated to temperatures above the critical ones, normally without melting (for steel 30KhGSA A_{c_1} = = 735 °C and A_{c_3} = 850 °C), by varying over wide ranges the amperage, arc length, electrode oscillation amplitude and frequency.

Thermal cycles in heating the face and back sides of the plates of steel 30KhGSA, 3 mm thick, were recorded using the KSP-4 potentiometers of continuous and striking types, by a signal received from the WRe 20/5 tungsten to rhenium-tungsten to rhenium thermocouples with a diameter of 0.35 mm. Thermal electrodes of one pair were spaced at 3.5 mm across the treatment direction, passed via the through holes (with diameters varied from 1.6 to 0.4 mm at a distance of 0.2 – 0.3 mm from the face surface) and spot welded to the metal by the argon-arc method. Metal shunting of the thermal electrodes was prevented using ceramic splints with a diameter of 1.5 mm in an expanded portion of the holes. The conventional thermocouples were caulked in a blind hole with a diameter of 0.8 mm on the back side of the plates. This lay-out the thermocouples provided the high accuracy of measurements of the temperature [7].

Characteristic thermal cycles of arc treatment at low and increased rates are shown in Figure 1. It can be seen that local heating of the face side to a maximum temperature occurs almost immediately, while that of the back side to lower temperatures occurs more slowly (80 – 230 °C/s). A decrease in the temperature and rate of heating is characterized by the value of $c\gamma/\lambda$, which is inverse to the value of thermal diffusivity. The latter determines the rate of levelling of the temperature at unsteady thermal conductivity and distance from the heating surface, like in welding. Metal cooling occurs much slower and longer than heating. Delay in heating the back side causes a shorter duration of cooling, as compared with the face side. However, the rate of its cooling at different temperatures may be either higher or lower than that of the face side, depending upon the heating conditions, which is caused by a lower heating temperature. Naturally, upon reaching the same temperatures, cooling of both sides and deep layers of metal occurs at the same rates.

Prevention of incipient melting and decrease in the temperature of arc heating are provided by a decrease in density of the thermal energy (on retention of the total power value), caused by transverse oscillations of the electrode. Thus, in treatment at a current of 130 – 140 A and rate of 38 m/h, the face and back sides are heated without the electrode oscillations to temperatures of 1120 – 1380 and 600 – 680 °C, and with the electrode oscillating to an amplitude of 10 – 12 mm — to temperatures of 770 – 1120 and 450 – 630 °C, respectively. Naturally, with an increase in the oscillation amplitude the heating temperature is decreased, and with a frequency varied from 1 to 4 Hz/s it hardly changes.

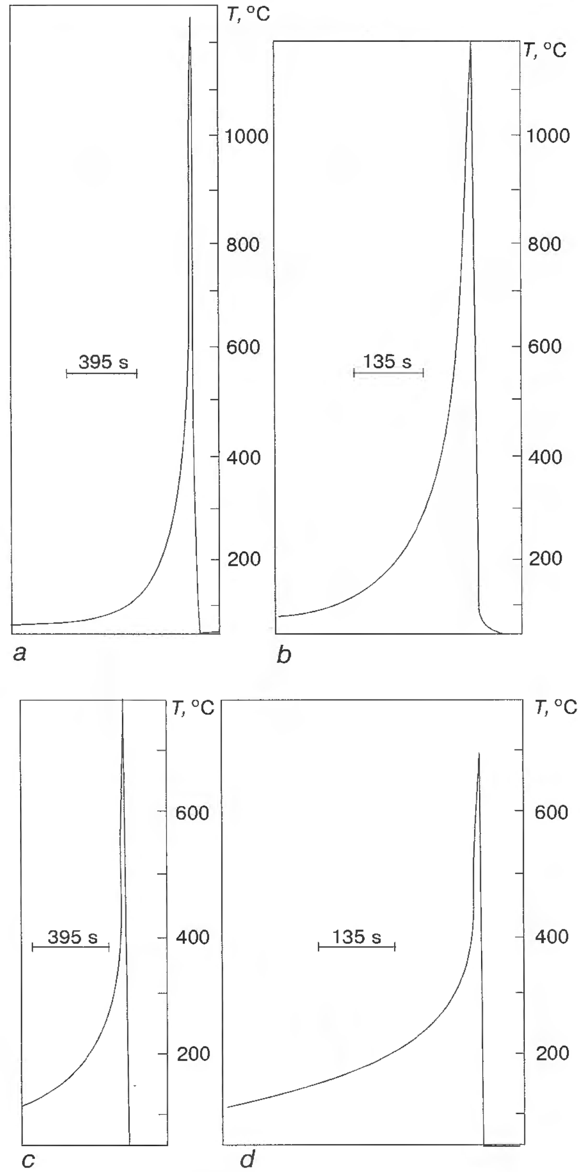

Figure 1. Thermal cycles of arc treatment of steel 3 mm thick on the face (*a*, *b*) and back (*b*, *d*) sides under conditions: v_{tr} = = 4.8 m/h, I = 60 A (*a*, *b*) and v_{tr} = 60 m/h, I = 180 A (*c*, *d*).

Dispersal of the arc can also be provided by increasing its length to 7 – 15 mm, which causes a decrease in its stability, while at a length of more than 15 mm there is a risk of spontaneous interruption of the process. Therefore, it is advisable to perform argon-arc heating without melting by using the transversely oscillating arc 8 – 12 mm long. In this case the value of the current, below which there is no incipient melting, increases with an increase in the treatment rate:

v_{tr}, m/h	4.5 – 4.8	12.0 – 12.5	37.0 – 38.0	60.0 – 62.0
I, A	60 – 65	110 – 120	150 – 160	210 – 230

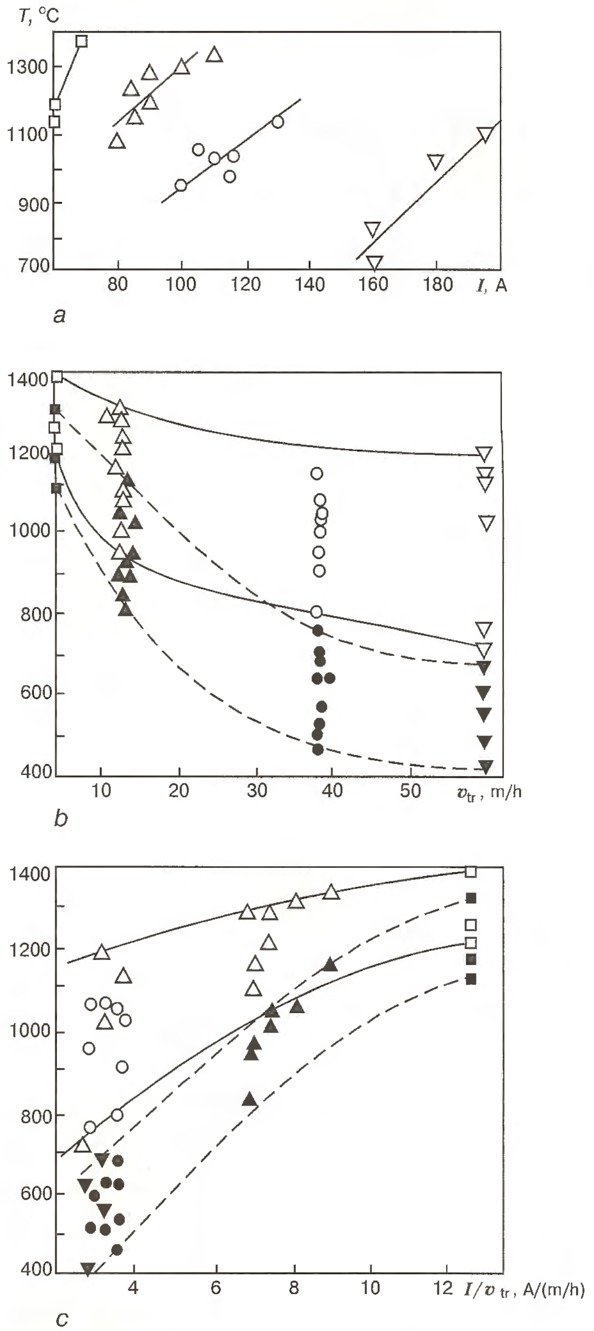

Figure 2. Effect of current (*a*), rate of treatment (*b*) and their ratio (*c*) on temperature of short-time heating of the face (light designations) and back (dark designations) sides of thin-sheet steel at v_{tr}, m/h: □, ■ – 4.8; ▲ – 12.5; ○, ● – 37 – 38; ▽, ▼ – 60 – 62.

It should be noted that the intensity of heating a solid metal with an increase in the arc length decreases but insignificantly: with an increase of 1.5 time at a current of 85 A (v_{tr} = 12.5 m/h) the temperature of a short-time heating decreases from 1100 – 1235 to 940 – 1090 °C, i.e. by 13 – 17 %. Therefore, a simple reduced value of I/v_{tr} was used instead of heat input to establish peculiarities of variations in the thermal state of metal and em-

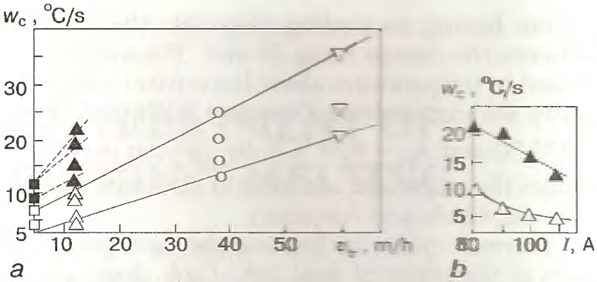

Figure 3. Cooling rate within a temperature range of minimum stability of austenite depending upon the rate of arc treatment (*a*) and current (*b*) (v_{tr} = 12.5 m/h) (see designations in Figure 2).

ploy the treatment conditions as the technological parameters.

As shown by multiple measurements (Figure 2, *a*), the temperature of heating without incipient melting of metal is proportional to the amperage and substantially decreases with an increase in the treatment rate v_{tr}, i.e. in general it is proportional to I/v_{tr}. To heat steel 30KhGSA to critical temperatures A_{c_1} and A_{c_3} at a rate of 60 and 38 m/h, it is necessary that the electric current be 150 – 170 and 60 – 90 A, respectively. With an increase in v_{tr}, it is necessary to increase the amperage to some extent to keep the temperature of heating the face side unchanged; whereas a decrease in I/v_{tr} is indicative of a decrease in the electric power consumption of the process. Difference in temperatures through thickness of the metal increases with an increase in v_{tr}. Transverse oscillations of the electrode are accompanied by an increase in spread of values of the heating temperature, which can be caused, among other things, by non-uniformity of heating due to reciprocal movement. The latter is evidenced by the presence of alternating transverse zones with different tempering colours, which are formed with an increase in the treatment rate. To increase uniformity of heating, it is advisable to increase frequency of transverse oscillations of the arc and decrease the general treatment rate.

Rise in the heating temperature, decrease in the treatment rate and increase in the amperage are accompanied by an increase in time during which the non-melted metal remains in a heated state, reaching several tens of seconds at temperatures of austenization (above A_{c_3} = 850 °C), the latter being always higher on the face side (Table 1). At a treatment rate of more than 37 – 60 m/h, the metal on the back side is heated to a temperature

Table 1. Time (s) of non-melted metal dwelling at temperatures above 850 °C

Side of the sample	*Treatment rate, m/h*			
	4.8	*12.5*	*38.0*	*60.0*
Face	15 – 45	2 – 10	1 – 2	≈1
Back	14 – 17	1 – 8	–	–

Table 2. Hardness of steel 30KhGSA and size of the zone of visual changes in structure after arc heating

Variant of treatment	*Conditions*			*Visual parameters, mm*			*HRC*	
	I, A	v_{tr}, *m/h*	I/v_{tr}, *A/(m/h)*	*Depth*	*Width*		*Top*	*Bottom*
					Top	*Bottom*		
1	60	4.5	13.3	3.0	20	16 – 18	$\frac{31.00 - 42.50}{37.25}$	$\frac{37.50 - 41.50}{39.83}$
2	75	4.5	16.7	–	–	–	$\frac{43.00 - 55.00}{49.25}$	$\frac{51.00 - 55.50}{53.25}$
3	70	12.0	5.8	1.0 – 1.5	10 – 12	–	$\frac{41.00 - 45.00}{42.62}$	$\frac{13.00 - 17.00}{16.37}$
4	100	12.0	8.3	3.0	11 – 15	8 – 10	$\frac{47.50 - 50.50}{48.87}$	$\frac{46.00 - 50.50}{48.20}$
5	110	12.0	9.2	–	–	–	$\frac{50.00 - 55.00}{53.25}$	$\frac{41.50 - 43.00}{42.25}$
6	100	38.0	2.6	1.0 – 1.5	5 – 10	–	$\frac{51.00 - 53.00}{52.25}$	$\frac{14.00 - 16.00}{14.75}$
7	150	38.0	3.9	1.0 – 1.5	8 – 10	–	$\frac{48.00 - 54.00}{51.00}$	$\frac{23.00 - 24.50}{23.37}$
8	150	60.0	2.5	0.5 – 1.0	8 – 10	–	$\frac{31.00 - 37.50}{32.25}$	$\frac{18.00 - 22.00}{19.62}$

Notes: 1. Hardness of untreated steel — *HRC* 10 – 12. 2. Variants *2* and *5* — metal surface.

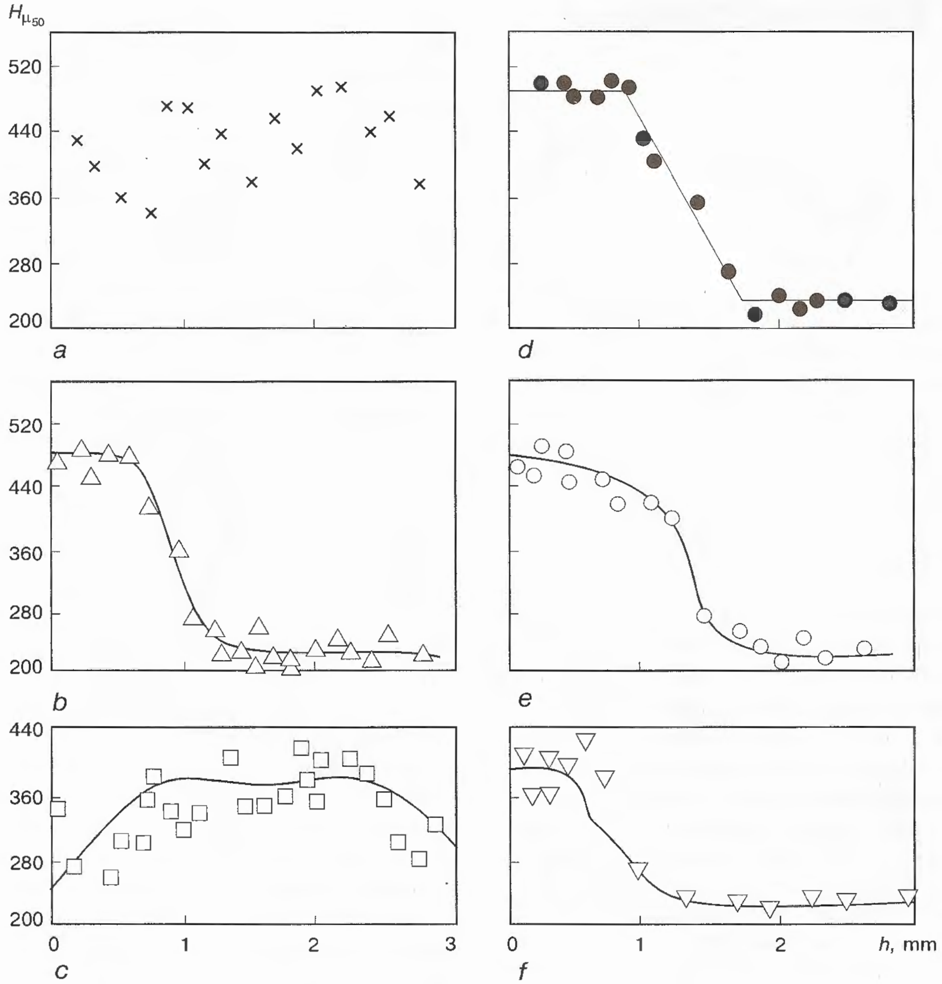

Figure 4. Distribution of microhardness through thickness of the plate of pre-tempered steel 30KhGSA after arc treatment at I/v_{tr}, A/(m/h): *a* — 60/4.5; *b* — 70/12; *c* — 100/12; *d* — 100/38; *e* — 150/38; *f* — 150/60.

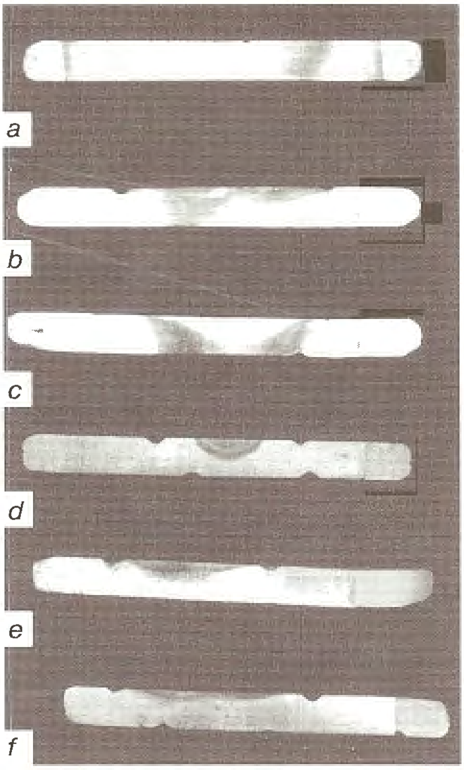

Figure 5. Variation in macrostructure of steel 30KhGSA in arc treatment (see designations in Figure 4).

which is lower than the transformation point, and the time of surface heating to more than 850 °C can be insufficient for its austenization to occur also on the face side.

The time of heating the face and back sides of the plate to a temperature of 150 °C, which can be assumed to be the lower limit of transformations for steels under investigation, is 130 – 360 and 70 – 230 s, depending upon the heating conditions. In this case, cooling from 300 °C (temperature conditionally assumed to be the point of beginning of martensitic transformation), at which the possibility exists of self-tempering of the quenched metal, lasts 100 – 180 and 50 – 100 s. At the same time, natural cooling to room temperature takes several minutes.

The cooling rate (w_c) of the thin-sheet metal within a temperature range of minimum stability of austenite (650 – 400 °C) is proportional to the treatment rate, inverse to the amperage (Figure 3) and equals 4 – 35 °C/s, where the probability exists of formation of quenching structures. More rapid cooling of the back surface suggests formation of structures with a rather high hardness of metal. However, since at the back surface the austenization temperature during treatment at a rate of 37 – 60 m/h and more is never achieved, allowance for the cooling rate in this case does not make sense.

Analysis of thermal cycles of argon-arc treatment indicates to a possibility of changing the aggregate state and polymorphic state of the metal treated, regulation of temperature, depth and rate of a short-time heating and time of the metal dwelling in the heated state, which is a prerequisite for the controlled change of structure and properties of the metal. This postulate is confirmed by the results of metallography and measurements of hardness (Table 2, Figures 4, 5).

In treatment at a low rate (4.5 m/h) at a current of 60 A, where the metal is heated through the entire thickness to more than A_{c_3} = 850 °C and cooled at low quenching rates, hardness of the metal on the face and back sides is increased to *HRC* 37.25 and 39.83, respectively, and microhardness is increased to $H_{\mu_{50}}$ 280 – 480. This corresponds to the formation of the bainitic-martensitic structure. The width of the zone of a visible structural change amounts to 16 – 20 mm. An increase in the amperage to 75 A, which is accompanied by surface melting, general increase in the heating temperature, homogeneity and austenite stability, as well as by a decrease in the transformation temperature of austenite, causes an increase in hardness of the metal on both sides to *HRC* 49.25 and 53.25, because of an increased martensite component content of the structure. Higher hardness of the back side of the sample is attributable to a higher cooling rate during transformation of austenite.

Treatment of the metal at a rate of 12 m/h, where the cooling rate within a temperature range of minimum stability of austenite is substantially higher, creates conditions for achieving a higher hardness. If the amperage is kept at a low value (70 A), microhardness in the subsurface layer about 0.5 mm thick on the face surface will increase to $H_{\mu_{50}}$ 460 – 500, while the lower part will hardly be hardened. Visually, the zone of the structural changes is 10 – 12 mm wide and about 2 mm deep. At this v_{tr}, an increase in the amperage to 100 A (1.5 times) that causes an increase in the heating temperature and depth and stability of austenite, leads to an increase in hardness to *HRC* 48 and microhardness to $H_{\mu_{50}}$ 380 – 500 through the entire thickness (despite some decrease in the cooling rate). The visible zone of structural changes propagates through the entire thickness, although it hardly changes in width. Heating accompanied by surface melting, extra increase in stability of austenite and general decrease in the cooling rate causes an increase in hardness, which is higher on the face surface (to *HRC* 53.25) and lower on the back surface (to *HRC* 42.25).

Further three-fold increase (to 38 m/h) in the treatment rate at currents of 100 and 150 A, where the metal is heated far above A_{c_3} on the face surface and in most cases below A_{c_1} on the back surface, and then cooled at a rate increased 2.5 – 3.0 times causes surface hardening to a depth of 1.0 –

1.2 mm. At the amperage increased within the above limits, hardening on the face side falls from *HRC* 52.25 to 51.00 and from $H_{\mu_{50}}$ 470 – 500 to 400 – 490, whereas on the back side it grows from *HRC* 14.75 to 23.37.

After arc treatment at a rate of 60 m/h and a current of 150 A, where the metal on the face side is subjected to indirect austenization, and that on the back side is not austenized at all, surface hardening occurs only to a value of *HRC* 35.25 and $H_{\mu_{50}}$ 350 – 420 to a depth of 0.5 – 0.6 mm on the face side, while on the back side both hardness and microhardness remain almost unchanged. Analysis of thermal cycles, variations in hardness and microhardness of the metal after treatment under different conditions also indicates that heating of the face surface above A_{c_1} can be eliminated by further increasing the treatment rate and decreasing the amperage. This allows hardening of the tempered metal to be avoided and softening of the metal quenched, i.e. by welding, to be achieved.

Similar changes in microhardness and its distribution through thickness were found to take place on 5 mm thick medium-alloyed steel 42Kh2GSNM, susceptible to quenching in air, which was treated at currents of 60 – 180 A at a rate of 5.5 – 80.0 m/h. Arc treatment provides hardening of this steel to $H_{\mu_{50}}$ 400 – 850, while at a treatment rate of 60 and 80 m/h and current of 60 A there is almost no hardening.

Therefore, by varying the rate and current of arc treatment, it is possible to regulate parameters of the thermal cycle of the process over wide ranges and favourably affect the structure and hardness of metal without its surface melting, which suggests corresponding changes in mechanical properties. Depending upon the treatment parameters, it is possible to harden metal to a different depth, cause self-tempering of different duration and short-time tempering. Treatment at a low rate (accordingly, at a high heat input) is indicated for a relatively deep heating, treatment at an increased rate is indicated for one-sided hardening and that at a high rate is recommended for surface hardening or local tempering of a welded joint or other part. Apparently, arc treatment can be used to improve a stressed state and increase crack resistance of a welded joint. Locality, short duration, low consumption of energy and simplicity of arc heating are good reasons to use it as a basis to develop new energy-saving technologies for the fabrication of weldments.

REFERENCES

1. Asnis, A.E., Ivashchenko, G.A., Frenkel, I.Kh. *et al.* (1980) Argon-arc treatment — a reserve for decreasing metal consumption of welded structures. *Avtomaticheskaya Svarka*, **6**, 69 – 70.
2. Chernyshov, A.I., Kaplina, I.I., Seranin, M.I. (1996) Surface quenching by remelting of working surfaces of cast iron camshafts. *Metallovedeniye i Term. Obrabotka Metallov*, **10**, 26 – 28.
3. Kulik, V.M., Savitsky, M.M., Novikova, D.P. *et al.* (1999) Investigation of arc treatment of welded joints of high-strength steel. *Avtomaticheskaya Svarka*, **5**, 19 – 25.
4. Safonov, E.N., Zhuravlyev, V.I. (1997) Surface hardening of iron-carbon alloys by arc quenching. *Svarochnoye Proizvodstvo*, **10**, 30 – 32.
5. Rykalin, N.I. (1951) *Calculations of thermal processes in welding*. Moscow: Mashgiz.
6. Prokhorov, N.I. (1968) *Physical processes in metals during welding*. Moscow: Metallurgia.
7. Cherenin, V.T. (1968) *Experiments in physical materials science*. Kyiv: Tekhnika.

PECULIARITIES OF FRICTION WELDING OF DISSIMILAR METALS AND ALLOYS

I.V. ZYAKHOR
The E.O. Paton Electric Welding Institute, NASU, Kyiv, Ukraine

ABSTRACT

Peculiarities of friction welding of different grades of steels, non-ferrous metals and their alloys in dissimilar combinations, as well as metals to some ceramic materials are considered. Factors affecting formation of the joints made by different methods of friction welding, such as conventional, inertia and combined, are analysed on the basis of experimental data. Some techniques which ensure optimization of thermal-deformation conditions of the formation of the joints are described. Peculiarities of producing the joints in hard-to-weld metals and alloys using intermediate layers are studied.

Key words: *friction welding, technology, dissimilar joints, conventional friction welding, inertia friction welding, combined friction welding, heating and forging stages, process parameters, pressure, rotation speed, upsetting, heating time, braking time, equipment, quality of joints.*

Structures of composite materials are widely applied in many industries. In this connection, joining of dissimilar metals is among the most important problems of welding science and technology.

One of the most efficient methods for joining different grades of steels and non-ferrous metals in dissimilar combinations is friction welding. In friction welding, a welded joint is formed in a solid state as a result of the combined plastic deformation of workpieces joined. Heat is generated through a direct conversion of mechanical energy released on the mating surfaces of workpieces pressed to each other under a certain load and participating in relative displacement.

Friction welding is successfully used to join materials which drastically differ in their mechanical and thermal-physical characteristics, as well as materials which, when heated, enter into chemical interaction to form brittle intermetallic compounds [1]. Combinations of dissimilar metals and alloys made by friction welding can be conditionally classified as hard/hard and hard/soft. They can either form or not form intermetallic compounds [2]. For example, joints between corrosion-resistant steel and low-carbon steel are a hard/hard combination which does not form intermetallics, whereas joints between corrosion-resistant steel and titanium are a hard/hard combination which does not form intermetallics. An example of the hard/soft combination which does not form intermetallics is a steel–copper joint and the hard/soft combination which does form intermetallics is a steel–aluminium joint.

In development of a friction welding technology, depending upon the combination of materials joined, different requirements are imposed on surface preparation, selection of ranges of variations in welding parameters and utilization of different technological procedures to ensure optimal thermal-deformation conditions for the formation of the joints.

Friction welding of dissimilar metals and alloys with equal or different cross sections is characterized by asymmetry of temperature and deformation fields [3]. This asymmetry is caused by a different intensity of removal of heat and its input into billets because of different thermal-physical and mechanical characteristics of materials welded.

Welding of materials which, when jointly heated, enter into chemical interaction to form a transition layer of intermetallic compounds, causing a drastic decrease in mechanical properties of the joints or making direct welding of these materials impossible, presents a special problem. In such cases it is necessary to perform friction welding through an intermediate insert.

Welding of high-strength alloyed steels to carbon steels. In manufacture of components of hydraulic systems, such as casings of hydraulic cylinders, piston rods, plungers, shafts of axial-piston machines, it is necessary to join billets with different cross sections (T-joints) made from different grades of steels. Working sections of components are made from high-strength alloyed steels, such as 12KhN2A, 30KhGSA, 35KhGSA, 30KhGSN2A, 38Kh2MYuA or 25Kh5M, and welded to smaller diameter billets made from carbon steels of the 45 or 40X grades.

In friction welding, metal of a smaller-diameter billet is transferred to a larger-diameter billet because of asymmetry of temperature fields. This causes «displacement» of the friction surface into the carbon steel billet and formation of a deposited metal layer on the high-strength steel billet. The value of the «displacement» increases with a decrease in pressure during heating and circumferential speed [4]. Quality of the joints thus produced depends in many respects upon the initial conditions of the welding process, primarily upon the perpendicularity of the edge of the high-strength steel billet.

Combined friction welding is an efficient method which allows consistency of the quality of the joints to be improved. In combined welding, the billets start heating as in the case of conventional friction welding. Then the rotation drive is turned off and the energy accumulated in the rotating parts of the machine is released into the joint until the spindle is fully stopped. However, the method of combined friction welding using a standard conventional friction welding machine can be employed only for a limited range of cross sections, where the total moment of inertia of the rotating parts of the machine is optimal [5].

Upgrading these machines [6] makes it possible to control the final stage of heating by setting the acceleration (time) of braking irrespective of the diameter of workpieces welded. Welding parameters, including the time of braking, are set so that the effect of «reverse displacement» of the friction surface takes place at the final stage of heating. The layer of metal transferred to the high-strength steel billet is removed to flash at the braking stage, thus providing the high-quality of the joints, i.e. with properties at a level of those of the base metal (carbon steel).

Welding of high-speed steels to structural steels. Friction welding of high-speed steels to structural steels is extensively used in tool-making industry for the manufacture of metal-cutting point tools. Working sections of the tools are made from high-alloy steels R6M5, 02R6M5, R9, R18 or R9K5, while tailing parts of the tools are made from inexpensive structural steels of the 45 or 40X grades.

Difficulties in providing sound joints between these steels are associated with a dramatic difference in their chemical composition and physical-mechanical properties. It is this fact that is responsible for susceptibility to formation of a peripheral circumferential lack of penetration, defects of the type of «shining rings» and a transition layer which causes a decrease in mechanical properties of the joints [1, 3, 7].

Formation of the transition layer is a result of transfer of the high-speed steel particles to the surface of structural steel, which causes fracture of the so-called adhesion bridges [3]. Maximum thickness of the transition layer at the end of the heating stage is 0.3 – 1.0 mm; its structure after welding and cooling in air consists of austenite + martensite + carbides. Chemical composition of the transition layer is an intermediate between those of high-speed and structural steels. To produce the sound joints, it is necessary to remove the transition layer to flash during welding, which can be provided by increasing the heating and forging pressure.

According to [8], a decrease in strength properties of the joints is associated with precipitation of carbides of alloying elements at the transition layer — high-speed steel interface. The optimal structure and high mechanical properties of the joints can be achieved at a relatively low rotation speed and a substantial pressure which increases with an increase in diameter of the workpieces.

The forced weld formation using the upsetting die is employed to avoid peripheral circumferential lack of penetration. It should be noted that the use of the upsetting die adds complexity to the design of the machine (this requires the use of the cooling system for the die) and the welding technology, and increases the risk of cracking of the welded joints due to intensive heat removal.

According to [7, 9], inertia or combined friction welding provides removal of the transition layer to flash, substantially decreases the probability of formation of defects and allows the use of the upsetting die to be avoided. After appropriate heat treatment the joints meet the requirements imposed on strength of welded metal-cutting tools.

To realize the technology of combined friction welding of tools for a wide range of their diameters using the conventional friction welding machines, it is necessary to regulate the acceleration (or time) of braking at the final stage of the process. Technological parameters of the welding process are set so that thermal-deformation conditions similar to those of inertia friction welding and optimized for a given diameter to be welded are provided at the stage of braking. The characteristic feature of this technology, as compared with the classical technology of inertia welding, is a longer time heating, as the process of heating occurs at lower values of the circumferential speed and pressure.

Standard machines for conventional friction welding subjected to appropriate upgrading can be used to realize the technologies for combined friction welding of metal-cutting point tools. For example, the standard machine of the MST-2001 type was used to apply the technology for combined friction welding of metal-cutting point tool 25 – 40 mm in diameter (Figure 1).

Welding of heat-resistant steels to structural steels. The need for joining these combinations of materials arises in the manufacture of rotors of turbo-compressors of diesels and valves of internal combustion engines.

Wheels of rotors of turbo-compressors are made from austenitic heat-resistant steel 14Kh20N25V5M and shafts are made from pearlitic

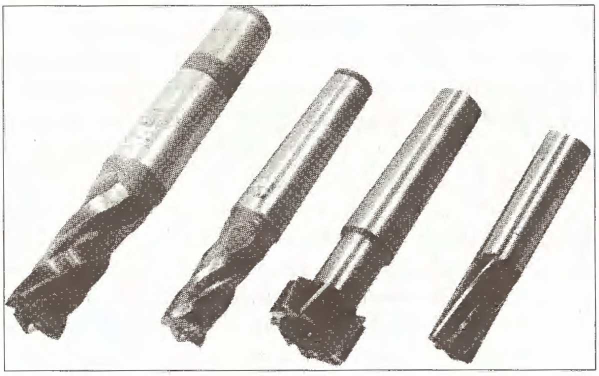

Figure 1. Welded metal-cutting tool.

steel 40G. Problems in welding steels of the austenitic and pearlitic grades are caused by differences in many of their thermal-physical properties, including thermal expansion coefficients. Metallography of the friction welded joints reveals an interlayer with the intermediate structure, which causes deterioration to strength and ductility properties [1].

In conventional friction welding, sound joints are provided by using rigid welding conditions (forging pressure should be not less than 200 MPa) combined with the use of an upsetting die, which is installed on the side of structural steel. Inertia friction welding carried out under a constant pressure within a wide range of the process parameters fails to provide joints of a satisfactory quality. The joints are characterized by a central or circumferential peripheral lack of penetration. This lack of penetration can be eliminated by using the programmed welding cycle with an axial force applied stepwise [10]. Uniform heating of the mating surfaces of pearlitic and austenitic steels is achieved at increased rotation frequencies and a low axial force, while at the final stage of the process the welded joint in its finished form is completed at an increased axial force.

The developed technology for inertia welding of rotors of turbo-compressor (Figure 2) [11], carried out using the machine equipped with the electromagnetic power drive [12], provides a high quality of the joints without the use of the upsetting die. Analysis of the microstructure of the joining zone (Figure 3) reveals the presence of microregions with heterogeneous chemical composition, having an austenitic-martensitic structure. After heat treatment the HAZ on the side of austenitic steel undergoes no visible changes, while that on the side of steel 40G has a ferritic-sorbitic structure. When subjected to static tensile tests, the welded joints fracture in the base metal of the shaft.

Welded valves with plates made from materials with high heat- and corrosion-resistant properties (steels 45Kh14N14V2M or 55Kh20G9AN4) and rods made from wear-resistant steels with high thermal conductivity (steels 40G or 40Kh9S2) have an

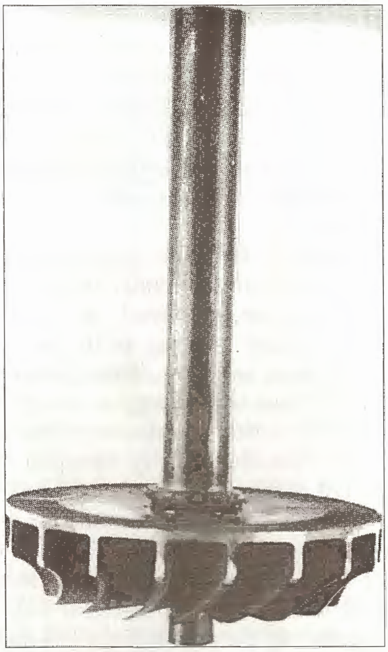

Figure 2. Rotor of turbo-compressor for tractor diesel engines.

increasingly wide application in internal combustion engines.

Conventional friction welding using the upsetting die, which is favourable for levelling the degree of heating and deformation of billets within the joint, as well as for elimination of lack of penetration on its periphery, is employed for the manufacture of bimetal valves [13]. However, the use of the die often causes cracks in the welded joint due to an intensive removal of heat to the die.

Inertia friction welding is characterized by certain values of pressure P and specific energy w. Below this values it is impossible to produce joints with the guaranteed consistent strength properties, which is attributable to a peripheral lack of penetration. For example, for valves with a shaft diameter of 16 and 18 mm, these values are $P =$ $= 150$ mm and $w = 80$ MJ/m^2 [14].

Character of application of the axial force was found to have a considerable effect on consistency of mechanical properties of the joints. Thus, in welding billets of the valves with a diameter of 18 mm, at the same pressure and specific energy values the spread of values of impact toughness of the joints was +5 and −20 J/cm^2 at a single-step application of the axial force and within a range of +5 J/cm^2 at a two-step application of the axial force. The conditions with a two-step application of the axial force are characterized by a wider HAZ and lower microhardness. Therefore, heat treatment of such joints after welding is unnecessary [15].

The programmed welding cycle with a stepwise application of the axial force used for inertia welding of bimetal valves for the «Tavria» car provided regulation of the thermal welding cycle, so that

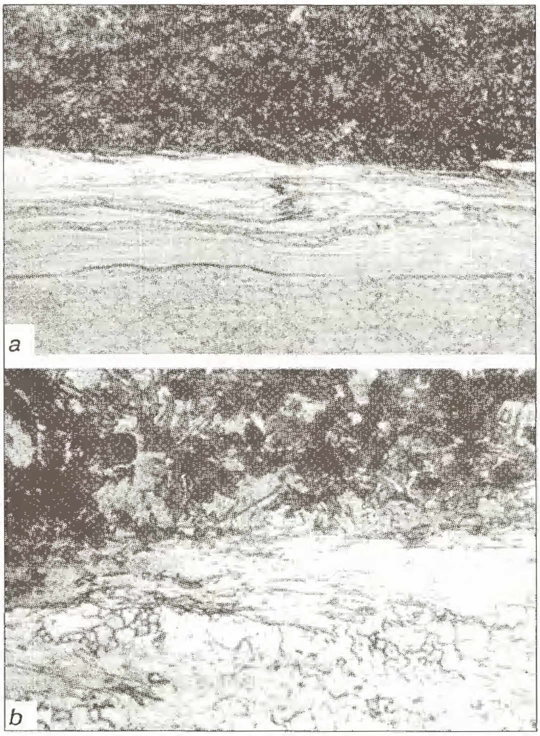

Figure 3. Microstructure of a welded joint in rotor of turbocompressor: *a* — as welded (×500); *b* — after tempering (×400) (reduced by 0.80).

defects were eliminated and formation of brittle quenching structures were avoided [16].

The developed technologies for friction welding of valves of different standard sizes (Figure 4) were realized using equipment fitted with the electromagnetic drive for generation of the axial force [12].

Welding of copper to steel. Steel–copper bimetal transition pieces are utilized for the manufacture of electrodes for resistance welding machines and heating elements for electric furnaces, and are an example of the hard/soft combination of materials, forming no intermetallic compounds.

Friction welding of this combination of materials is characterized by the fact that in heating one of the materials joined (steel) undergoes almost no deformation, while overall upsetting occurs due to the other material (copper). This imposes very stringent requirements on surface preparation.

Thus, in inertia friction welding of austenitic corrosion-resistant steel 304L to oxygen-free copper OFHC (99.99 %) the edges to be welded were machined immediately before welding to produce sound welded joints [17]. If more than 24 h pass after machining of the surfaces to be welded, defects in the form of lack of penetration are formed within the welding zone. In addition, contaminants present on the surfaces to be joined also cause formation of defects.

One of the problems in welding steel to copper is the probability of formation of a martensitic structure in the HAZ of steel. To produce ductile

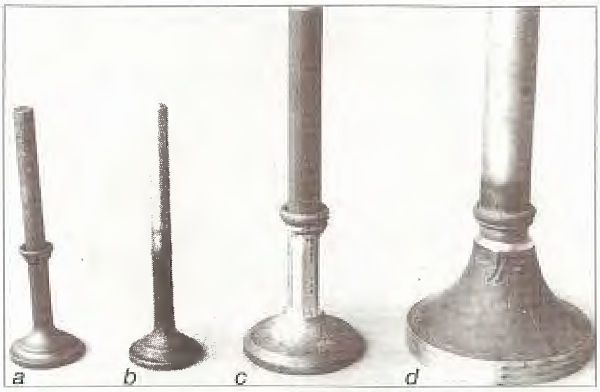

Figure 4. Welded valves: *a* — «Tavria» car engine; *b* — same with removed flash; *c* — pipe-laying machine engine; *d* — locomotive engine.

joints, the martensitic structure formed should be limited to a sufficiently narrow zone. In friction welding, this can be achieved by reducing the time of heating. Reduction of the heating stage has another positive effect, consisting in the fact that only pearlite grains undergo martensitic transformation, whereas ferrite grains retain their structure [18]. Therefore, the joints having a sufficiently narrow zone with the ferritic-martensitic structure, which hardly has an effect on their ductile properties, can be provided by choosing the appropriate welding parameters.

In welding St.2 to electrotechnical copper M1, based on high thermal conductivity of copper, the optimal parameters of the heating stage are characterized by a high linear speed and comparatively low pressure [3]. High pressure values are typical of the forging stage. To provide optimal conditions for the formation of the joints, it is advisable to use the upsetting die on the side of copper.

Welding of aluminium to steel and copper. The need to join aluminium to steel arises in the manufacture of bimetal adapters utilized in aerospace engineering and metallurgy. Difficulties in producing sound welded joints between these materials are associated with a dramatic difference in their physical-mechanical properties and with chemical interaction, leading to the formation of a brittle intermetallic layer Al_nFe_m within the joining zone.

It was found as a result of processing numerous data on strength properties that the smaller the thickness of the intermetallic layer, the higher the strength of a welded joint between steel and aluminium [19]. Embrittlement of steel–aluminium joints can be avoided only in those cases where thickness of the intermetallic layer is no more than 1 μm [2].

Intensity of the chemical interaction processes depends upon the temperature and time of heating. As experimentally found, at each temperature there is a latent period during which no intermetallics are seen within the contact zone. According to [20],

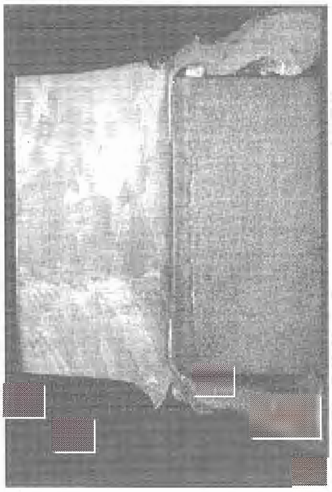

Figure 5. Macrosection of a welded joint in bronze Br.012 to steel 40X through a copper interlayer.

intermetallics in the steel 12Kh18N10T + aluminium AD1 joints were fixed at a temperature of 540 °C after 1 h annealing. The time of the latent period is decreased with an increase in the temperature. In addition, thickness of the intermetallic layer and the time-temperature limit of its formation depend upon chemical composition of components of bimetal. For example, in the 12Kh18N10T + AD1 joints the intermetallic phases were detected at a temperature of 540 °C, while in the St.3 + AD1 joints the brittle interlayer was fixed at a temperature of 450 °C.

To produce a sound steel–aluminium welded joint, it is necessary to minimize or eliminate the probability of formation of the brittle intermetallic interlayer. This requirement can be met only if a joint is heated during welding to a temperature which is sufficient for the formation of the joint, and the time of influence of this temperature on the contact zone is shorter than the latent period of formation of the intermetallic phases.

In friction welding, the required temperature in the joint, at which no brittle intermetallic interlayer is formed, can be provided by varying the process parameters. For example, for a pair of 12Kh18N10T + AD1, the joints of a satisfactory quality are produced by heating a joint to 360 – 450 °C, while for a pair of St.3 + AD1, this temperature is about 320 – 420 °C.

In terms of formation of brittle intermediate phases in the joint, development of the friction welding technology should be based on using the comparatively low frequency of rotation of billets. The optimal circumferential speed for a pair of 12Kh18N10T + AD1 is 1.0 m/s, and for a pair of St.3 + AD1 it is 0.7 – 0.9 m/s [20].

Variation in the heating pressure within a wide range has no effect on the character of the welding cycle, it rather leads to a change in the gradient of growth of temperature at the beginning of the process and a slight change (by 25 °C) in the maximum temperature. An increase in the heating pressure to a certain level accelerates the process of equalizing of a temperature in the joint plane during friction, decreases the time of contact of steel and aluminium and, thus, increases strength of the joint. An increase in the forging pressure causes removal of intermetallics from the joint, which has a favourable effect on the joint quality.

Stringent requirements are imposed on surface preparation [21]. It is recommended that the edge preparation of a steel billet be done using the same welding machine in a rotating chuck by means of a special cutting carriage. This makes it possible not only to clean the surface to be welded, but also to eliminate the end play of the billet which deteriorates quality of the joints. Surface finish of the steel billet prepared for welding should be not lower than of class 5. The aluminium billet edge should be cleaned from grease or other adsorbed films.

The joints between aluminium and stainless steels of the austenitic grade produced by friction welding under optimal conditions have satisfactory performance at 500 °C and those between aluminium and carbon steels – at 400 °C [20].

Peculiarities of producing welded joints through an interlayer. This method is employed in the cases where direct welding fails to ensure the sound joints [22].

Welding of anti-friction bronze to steel. Welding bronze Br.012 to steel 40X is applied for the manufacture of blocks of cylinders of the axial-piston hydraulic machines. Friction welding of anti-friction bronze directly to steel fails to provide welded joints or at least to achieve adhesion [23]. The friction process is accompanied by polishing, heating and brittle fracture of the bronze billet. Low heat release caused by a low friction coefficient does not allow the temperature required for welding to be achieved.

Friction welding through an intermediate copper insert was used to produce the joint between bronze and steel (Figure 5). The technology for making combined welded joints ensures the sound joints in bronze to copper and copper to steel, and provides the preset consistent final thickness of the copper insert which determines strength and ductility of the combined joints. The optimal relative thickness of the copper insert (ratio of thickness of the insert layer to diameter of the test specimen), at which a maximum strength of the welded joint in provided, is 0.07 – 0.20.

The highest strength and the lowest percentage of defects were exhibited by the joints produced by conventional friction welding with instantaneous forced braking. Joints made by combined and inertia friction welding had substantial lack of penetration, which is attributable to a low heat release at the end of the heating cycle.

The qualitative difference in the character of dependence of the upsetting speed upon thickness of the insert layer during the welding process was noted in the case of different sequence of welding the copper insert to both billets. In the case of welding bronze Br.012 with the copper interlayer to steel 40X, variations in the upsetting speed do not depend upon thickness of the interlayer. In the case of welding steel with the copper interlayer to bronze, a dramatic variation in the upsetting speed was noted after the interlayer reached certain thickness. The method of friction welding with the controlled upsetting speed was developed on the basis of this phenomenon. It provides an improvement in quality of the joints through increasing consistency of the interlayer thickness [24].

The developed friction welding technology makes it possible to produce billets of bimetal blocks of cylinders for axial-piston hydraulic machines with strength at a level of service requirements.

Welding of steel to titanium and niobium. Titanium-steel transition pieces used in special structures enable their metal consumption to be reduced, reliability to be improved and service life to be extended. However, direct welding of titanium to steel fails to produce sound welded joints because of the formation of brittle and hard intermetallic compounds and carbides.

The currently available methods for welding titanium to steel are based on the use of interlayers made from some metals or alloys. Friction welding of transition pieces from titanium VT1-0 and stainless steel 12Kh18N10T using aluminium AD1 as the interlayer resulted in production of sound joints (Figure 6) within a wide range of the welding process parameters [25]. No intermetallic phases were detected within the joining zone of the transition pieces subjected to X-ray microanalysis. A drastic difference in the concentrations of aluminium, titanium and steel is indicative of the absence of diffusion.

Fracture of the titanium-aluminium-steel joints subjected to tensile tests occurs in aluminium, strength of the joint made through the aluminium interlayer 5 mm thick being 140 – 150 MPa. This is approximately 50 % higher than strength of AD1. Flattening of the tubular transition pieces leads to cracking of steel. The extra tests showed that the transition pieces thus produced were air tight.

In inertia friction welding of VT1-0 to steel 30, the sound joints were produced using a copper interlayer. This interlayer is partially or totally pressed out by upsetting [26]. The best test results on strength were obtained with the welded joints in which a steel piece had a preliminarily deposited galvanic coating of copper 0.01 mm thick, i.e. in the case where the interlayer was totally pressed out from the joint by upsetting.

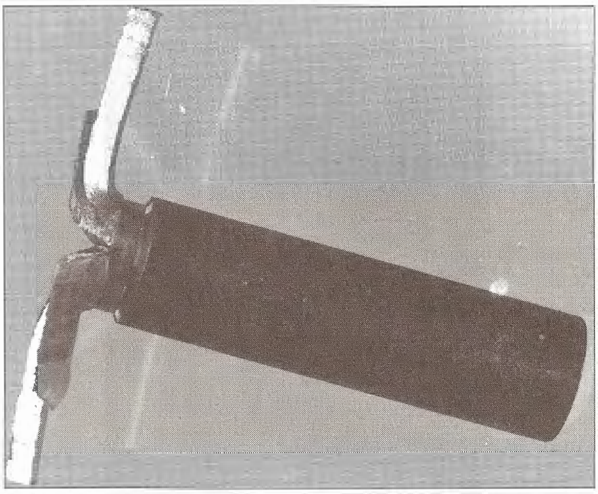

Figure 6. Sample of the titanium to stainless steel friction welded joint made through an aluminium interlayer after bending test.

Friction welded joints of steel 10Kh18N9T to niobium are characterized by low strength, which is attributable to the presence of microcracks within the contact zone [27]. The microcracks are formed during cooling of the joint and caused by a large difference in thermal expansion coefficients of niobium and 10Kh18N9T.

The iron (0.025 % C) interlayer was used to join niobium to 10Kh18N9T. Thermal expansion coefficient of iron is in between those of niobium and 10Kh18N9T. In tensile tests of the niobium–iron interlayer–steel 10Kh18N9T joints made under optimal conditions (σ_t = 550, 360 and 440 MPa, respectively), fracture occurs in the base, less strong metal. The character of fracture depends upon thickness of the iron interlayer. At a relative thickness of the interlayer equal to more than 0.1, fracture occurs in the iron layer and at that less than 0.1 — in niobium.

Welding of metals to ceramic materials. Brazing is used to advantage in many cases to join ceramics to metals. Friction welding employed for this purpose makes it possible to use less stringent requirements to surface preparation, simplify mechanization and automation of the process and improve its hygienic aspects.

Mobile contacts of high-voltage switches are made bimetallic, i.e. a copper rod is joined to a metal-ceramic tip (80 % W + 20 % Ni). Sound joints made by conventional and inertia friction welding of these materials are provided by using a substantial pressure of heating and forging (above 200 MPa) and a linear speed of over 2 mm/s [28]. The more favourable conditions for the formation of the joints were achieved in friction welding involving a copper layer preliminarily deposited on the metal-ceramic billet (Figure 7). For this, thickness of the deposited layer should be not in excess of 3 mm. Otherwise, the joints may contain dis-

Figure 7. Joint between copper and metal–ceramic (80 % W + + 20 % Ni).

Figure 8. Microstructure of the joint between copper and metal–ceramic (×100) (reduced by 0.80).

continuities caused by non-uniform pressing out of the heated metal to flash.

Metallography of the joints produced under optimal conditions did not reveal any defects or structural heterogeneity. The zone of joining copper to metal–ceramic has a clearly defined interface (Figure 8). X-ray microanalysis showed a substantial difference in the concentration of copper, tungsten and nickel within the joining zone, which is indicative of the absence of diffusion. In tensile tests of the welded joints fracture occurred in the base metal.

Satisfactory results were obtained in welding AD1 to silicon nitride (Figure 9). The use of thorough surface preparation for welding (machining or etching of the aluminium piece edge, degreasing the ceramic piece edge) is the required condition for production of the sound joints.

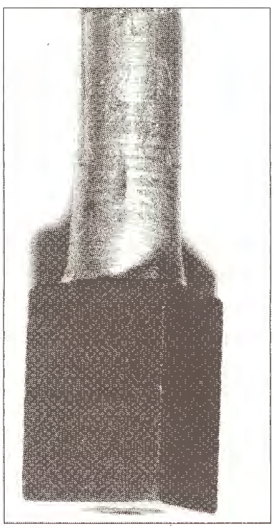

Figure 9. Joint between aluminium AD1 and silicon nitride Si_3N_4.

The feasibility of friction welding of titanium aluminides was proved by preliminary investigations [29]. Resolving the problem of welding titanium aluminide based alloys and their joining to steels will allow the manufacture of pieces from a new class of heat-resistant materials, intended for the fabrication of high-efficiency power engineering structures.

Welding of steel to aluminium alloys. The problem of producing such joints is topical for the manufacture of transition pieces for aerospace engineering.

Low-alloy aluminium alloys are known to have good weldability when joined to steels. The quality of the joints decreases with an increase in the alloying elements content of alloys. According to data of [30], satisfactory results were obtained in friction welding of St.3 and 10Kh18N9T to aluminium alloys which contain 0.6 % Mg, 1.6 % Mn and 1.0 % Si, e.g. alloys of the AMts or AV type. To join steel to high-alloyed aluminium alloys, it is necessary to use an intermediate material which has good weldability when joined to steel or aluminium alloy [31].

According to data of [32], in the manufacture of cryogenic structures for space shuttles, it is necessary to join stainless steel 304L to alloy 2219-T351 (6.2 % Cu, 0.3 % Mn). Good results were obtained in inertia welding of these materials through an insert of alloy 6061-T6 (1.0 % Mg, 0.6 % Si, 0.2 % Cr, 0.2 % Mn). Testing the samples to strength by hydraulic pressure, to thermal shock by immersion into the liquid nitrogen bath and to vacuum tightness in liquid helium proved the welded joints to be fit for purpose.

Direct friction welding of high-strength aluminium-lithium alloy 1420 (5.0 % Mg, 1.8 % Li) to stainless steel 12Kh18N10T cannot provide

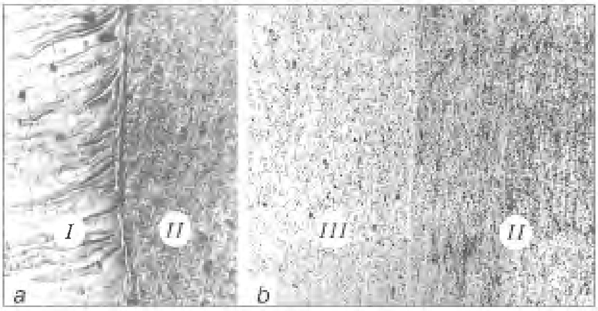

Figure 10. Microstructure of the welded joint: *a* — aluminium AD1 (*II*) to steel 12Kh18N10T (*I*) (×320); *b* — aluminium AD1 (*II*) to alloy 1420 (*III*) (×200) (reduced by 0.50).

joints of a satisfactory quality. Conditions for the formation of sound joints between 12Kh18N10T and alloy 1420 through an intermediate insert were determined in [33]. These conditions provide an optimum relationship between strength and ductility of the joints. For this, aluminium AD1 was used as the intermediate insert.

It was established that at a certain combination of the welding process parameters it is possible to produce the desirable value of temperature in the joints of 12Kh18N10T + AD1 and AD1 + 1420, which ensures the quality joints and the absence of an intermetallic layer in the joints (Figure 10). Mechanical properties of the combined welded joints can be effectively affected by varying thickness of the aluminium interlayer that persists in the joint.

The machine available for conventional friction welding [34] allows the combined joints with thickness of the persisting aluminium interlayer equal to several tens of microns to be produced at the final stage of the process by controlling the process parameters (pressure, rotation speed, braking acceleration and friction moment in the joint) (Figure 11). Static rupture strength of such joints is close to tensile strength of alloy 1420. It is apparent that development of the welding technology that involves low-alloyed aluminium alloys used as the intermediate inserts will make it possible to produce transition pieces with required service strength and ductility.

CONCLUSIONS

1. Friction welding provides sound welded joints in different grades of steels, non-ferrous metals and their alloys in dissimilar combinations, as well as between some ceramic materials and metals.

2. In welding dissimilar metals which form a transition layer or brittle intermetallic compounds during welding, the sound welded joints can be produced by creating rigid thermal-deformation conditions at the stage of forging, which can be provided by completing the process with inertia.

3. In all cases of friction welding of dissimilar materials, very stringent requirements are imposed on preparation of the mating surfaces for welding, while in a number of cases to produce the sound welded joints it is required that surface preparation be conducted immediately before welding.

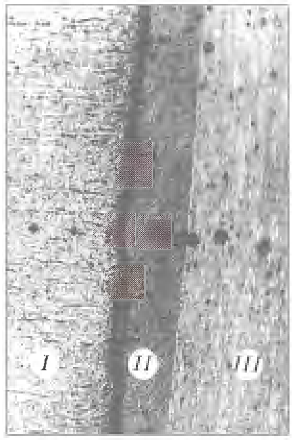

Figure 11. Microstructure of the steel 12Kh18N10T (*I*) — aluminium AD1 (*II*) — alloy 1420 (*III*) combined joint (×100) (reduced by 0.80).

4. Friction welding using interlayers is successfully applied for joining hard-to-weld materials. Transition pieces with desirable service properties are produced by varying thickness of the interlayer that persists in the joint.

5. Further in-depth investigations are required to study the known modifications of friction welding of advanced materials, such as new high-strength aluminium alloys, alloys on the titanium aluminide base, composite and ceramic materials in similar or dissimilar combinations.

REFERENCES

1. Vill, V.I. (1970) *Friction welding of metals*. Leningrad: Mashinostroyeniye.
2. Jessop, T.J., Nicholas, E.D., Disndale, W.O. (1978) Friction welding dissimilar metals. In: *Proc. of 4th Int. Conf. on Advances in Welding,* Harrogate, England, 1978, May 9 – 11. Harrogate.
3. Lebedev, V.K., Chernenko, I.A., Vill, V.I. *et al.* (1987) *Friction welding*. Handbook. Leningrad: Mashinostroyeniye.
4. Lebedev, V.K., Mirgorod, Yu.A., Tsurul, I.A. (1989) Friction welding of cylindrical billets of different cross sections. *Avtomaticheskaya Svarka*, **4**, 66 – 69.
5. Chernenko, I.A., Reshetnyak, A.V., Filatov, V.E. (1989) Properties of friction welded joints in steel billets of different cross sections. *Ibid.*, **7**, 68 – 71.
6. Chernenko, I.A., Zyakhor, I.V. (1999) Friction welding of dissimilar metals and alloys. *Svarshchik*, **1**, 10 – 12.
7. Lebedev, V.K., Mirgorod, Yu.A., Gordonnaya, A.A. (1988) Causes of formation of defects of the «bright ring» type in friction welding. *Avtomaticheskaya Svarka*, **12**, 12 – 15.
8. Pilarczik, Ya., Pietras, A. (1998) Mechanism of release and propagation of heat in friction welding of high-speed steels to structural steels. In: *Proc. of Int. Conf. on Welding and Related Technologies for the XXI century.* Kyiv: PWI.
9. Chernenko, I.A., Mirgorod, Yu.A., Ivanov, L.I. (1984) Inertia friction welding of steel R6M5 to steel 45. *Avtomaticheskaya Svarka*, **6**, 53 – 55.
10. Chernenko, I.A., Litvin, L.V., Chovnyuk, V.I. (1981) Inertia friction welding of parts of turbo-compressors. *Ibid.*, **9**, 51 – 53.
11. Kuchuk-Yatsenko, S.I. (1998) State of the art and prospects of development of friction welding. In: *Proc. of*

Int. Conf. on Welding and Related Technologies for the XXI century. Kyiv: PWI.
12. Lebedev, V.K., Prodan, S.K. (1979) Electromagnetic drive for welding machines. *Avtomaticheskaya Svarka*, **7**, 63 – 66.
13. Domnin, V.D., Gritsenko, L.A., Repin, F.F. (1978) Investigation and development of technology for manufacture of ship engine valves using friction welding. *Transact. of the Gorky Institute for Water Transport Engineers*, **162**, 29 – 33.
14. Litvin, L.V., Chernenko, I.A., Androshchuk, I.A. *et al.* (1989) Inertia friction welding of heat-resistant steel EI69 to steel 40X. *Avtomaticheskaya Svarka*, **12**, 45 – 48.
15. Chernenko, I.A., Litvin, L.V. (1989) *Inertia friction welding of bimetal valves for car engines.* Kyiv: PWI.
16. Chernenko, I.A., Forostovets, B.A., Litvin, L.V. (1990) Inertia friction welding and heat treatment of bimetal valves. *Avtomaticheskaya Svarka*, **3**, 53 – 58.
17. Bell, R.A., Lippold, J.C., Adolphson, D.R. (1984) An evaluation of copper-stainless steel inertia friction welds. *Welding J.*, **11**, 325 – 332.
18. Kreye, H., Reiners, G. (1986) Metallurgical aspects and application of friction welding. In: *Proc. of Int. Conf. of Trends in Welding Research on Advances in Welding Science and Technology,* Gatlinburg, USA, 1986, May 18 – 22. Gatlinburg.
19. Ryabov, V.R. (1983) *Welding of aluminium and its alloys to other metals.* Kyiv: Naukova Dumka.
20. Chernenko, I.A., Ryabov, V.R., Reshetnyak, A.V. (1988) Friction welding of aluminium AD1 to steel 12Kh18N10T. *Avtomaticheskaya Svarka*, **5**, 60 – 65.
21. Sarginson, N.M. (1979) A review of the development of friction welded anode hangers. In: *Exploiting Friction Welding in Production.* Abington.
22. Sassani, F., Neelam, J.R. (1988) Friction welding of incompatible materials. *Welding J.*, **11**, 264 – 270.
23. Chernenko, I.A., Mirgorod, Yu.A., Tsurul, I.A. (1990) Friction welding of bronze Br.012 to steel 40X through a copper interlayer. *Avtomaticheskaya Svarka*, **9**, 50 – 52.
24. Lebedev, V.K., Mirgorod, Yu.A., Tsurul, I.A. (1993) Peculiarities of friction welding of bronze Br.012 to steel 40X through a copper interlayer. *Ibid.*, **4**, 11 – 14.
25. Litvin, L.V., Kharchenko, G.K., Chernenko, I.A. *et al.* (1986) Friction welding of titanium-steel transition pieces using an aluminium interlayer. *Ibid.*, **5**, 73 – 74.
26. Kharchenko, G.K., Prodan, S.K. (1983) Inertia friction welding of titanium to steel. *Ibid.*, **4**, 70.
27. Lebedev, V.K., Kharchenko, G.K., Gurevich, S.M. *et al.* (1979) Inertia friction welding of niobium to iron and steel Kh18N9T. *Ibid.*, **6**, 35 – 36, 42.
28. Litvin, L.V., Chernenko, I.A., Kolosok, N.A. (1990) Friction welding of electrical equipment contacts. *Ibid.*, **8**, 71 – 72.
29. Baeslack, W.A., Threadgill, P.L., Nicholas, E.D. *et al.* (1995) Linear friction welding of Ti–4Al–2Cr–2Nb (at %) titanium aluminide. In: *Proc. of Titanium'95 8th Int. Conf. on Science and Technology,* Birmingham, 1995, Oct. 22 – 29. Birmingham.
30. Shternin, L.A. (1965) Friction welding of dissimilar metals. *Svarochnoye Proizvodstvo*, **3**, 11 – 13.
31. Elliott, S., Wallach, E.R. (1981) Joining aluminium to steel. Part 2. Friction welding. *Metal Construction*, **4**, 221 – 225.
32. Wadleigh, A. (1991) Joining dissimilar metals. *Fabricator,* **9**, 14 – 16.
33. Zyakhor, I.V., Kuchuk-Yatsenko, S.I. (1997) Friction welding of steel 12Kh18N10T – aluminium alloy 1420 transition pieces. In: *Proc. of Welding'97 Russian Sci.-Tech. Conf. on Advances in Welding Science and Technology*, Voronezh, 1997, Sept. 16 – 18. Voronezh.
34. Zyakhor, I.V. (1999) New equipment for friction welding. *Svarshchik*, **2**, 20.

NEW ELECTRODES FOR WELDING AND SURFACING OF STEEL 110G13L

V.V. SNISAR, E.L. DEMCHENKO, O.I. BREDNEVA and **E.V. IVANCHENKO**
The E.O. Paton Electric Welding Institute, NASU, Kyiv, Ukraine

ABSTRACT

Data are given on new electrodes of the ANVM-1 grade intended for welding and surfacing of high-manganese steel 110G13L, as well as for welding it to low-carbon steels. Results of evaluation of mechanical properties and structure of weld metal and welded joints made using the ANVM-1 electrodes are presented. These electrodes are recommended for welding and surfacing of the mentioned steels in fabrication and repair of mining equipment and parts of rolling stock coupling devices.

Key words: *high-manganese steel, electrodes, weld metal, deposited metal, fusion zone, structure, mechanical properties.*

Cold-workability of steel 110G13L in the process of a cold plastic deformation stipulated its wide application for castings of components which operate under the conditions of impact-abrasive wear (teeth of excavator buckets, track links of caterpillar machines, railway switches, frogs, bodies of energy absorbers, armour plates of crushers, etc.). Due to high content of carbon and manganese the steel 110G13L is characterized by a relatively stable austenitic structure [1, 2].

The wear resistance of components is provided at the expense of a high hardness of the working surface. The characteristic property of steel 110G13L is peculiar by the fact that the increased hardness (up to *HB* 550 – 600) and, consequently, the wear resistance of the surface layers of components of this steel are acquired during service under the action of impact loads and abrasive actions, due to an increased ability to a strain hardening of a high-manganese austenite characterized by lower values of energy of stacking faults as compared with a ferritic-pearlitic structure of the carbon steel. In addition, the high wear resistance of steel 110G13L is combined with high values of strength, ductility and impact strength. To provide the above-mentioned combination of properties the parts are subjected to quenching from 1050 – 1100 °C in water that will retain the austenite structure and prevent the precipitation of carbides.

A delayed cooling from high temperatures or an isothermal soaking of steel 110G13L within the 400 – 800 °C temperature interval leads to the decay of austenite according to the reaction $\gamma \rightarrow \gamma + \alpha + K$. The latter is one of the main reasons of a poor weldability of steel, embrittlement and hot crack formation in HAZ metal during welding at an unfavourable thermal cycle [3 – 5]. In some cases, to prevent the mentioned phenomena a forced cooling of the welded joint (welding zone) with a compressed air or a water irrigation is recommended.

It is established that the fracture of welded specimens during tensile test occurs in HAZ. This is caused by a precipitation of a carbide phase along the grain boundaries, which embrittles and weakens this region of the welded joint [1].

For welding steel 110G13L the electrode materials are used which can be divided conditionally into three groups by the compositions [3 – 5]: chrome-nickel austenitic; complex-alloyed austenitic and high-manganese.

In accordance with recommendations given in [5] the low-carbon chrome-manganese and chrome-nickel electrodes are preferred for welding of critical products, because, as to the technological strength, they are superior to high-carbon electrodes, and the mechanical properties of the welded joints made by these materials, which provide the deposited metal of 10Kh14G18M and 10Kh19N9G2 type, are similar to the properties of the parent metal. The high-carbon chrome-manganese and manganese-nickel steels of grades 35Kh10G18N2 and 90G13N4 are used only for the restoration hardfacing.

In welding steel 110G13L with low-carbon steels the different kinds of brittle and low-plastic layers [6], which are inevitable at the regions of a transition composition, may initiate in the zone of their fusion. Their properties differ greatly from the properties of steels welded and the deposited metal. All these factors cause the occurrence of a chemical, structural and mechanical inhomogeneity of the welded joints.

At present the high-alloyed austenitic chrome-nickel welding materials, for example, electrodes of grade OZL-6 (E-10Kh25N13) and NII48G (E-10Kh20N9G6S) GOST 10052–75 have found wide

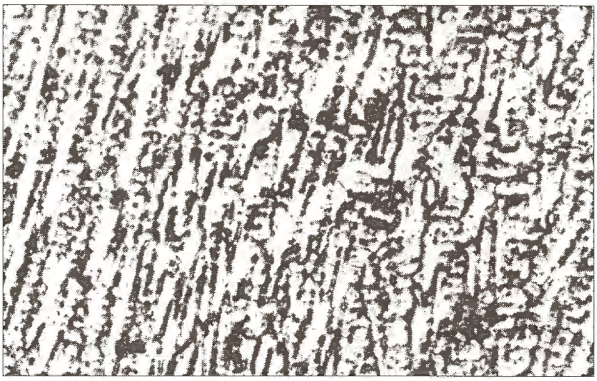

Figure 1. Microstructure of weld metal of a dissimilar joint of 110G13L + 09G2S, made with electrodes ANVM-1 (×320) (reduced by 0.80).

application for welding steel 110G13L with low-carbon steel 20 and low-alloyed steel 09G2S. These electrodes make it possible to prevent the embrittlement at the regions of a transition composition in the zone of fusion with a pearlitic steel. However, there are data about the successful application of chromium-free high-manganese welding materials, sparsely-alloyed with nickel, such as flux-cored wire PP-G13N4 and electrodes of E-G13N4 grade, for the solution of the mentioned problem [5, 6].

The authors suggested electrodes of ANVM-1 grade for manual arc welding and hardfacing of steel 110G13L and its combinations with carbon and low-alloyed steels to produce the austenitic weld metal without using such expensive alloying elements as chromium and nickel.

To provide the austenitic structure and required complex of mechanical properties of the deposited metal (weld metal) the following alloying elements are introduced into its composition, %: 0.20 – 0.40 C, 19.0 – 21.0 Mn, 0.08 – 0.13 Ti and 0.12 – 0.18 N.

Taking into account that it is impossible now to manufacture the steel wire of the above-mentioned composition, a low-carbon steel wire of Sv-08 or Sv-08A type was used as an electrode core. The necessary alloying of the deposited metal in this case is provided by introducing the alloying components to the electrode coating composition in the form of powders of pure metals and ferroalloys. A slag base, consisting of basic oxides (CaO, MgO, CaF), promotes an effective arc transition of alloying elements to the weld. The offered electrodes are characterized by a high stability of the arc process and allow welding to be performed both at direct and alternating currents. In addition, the quality formation of the deposited metal, resistance to pore formation and easy removal of a slag crust are provided.

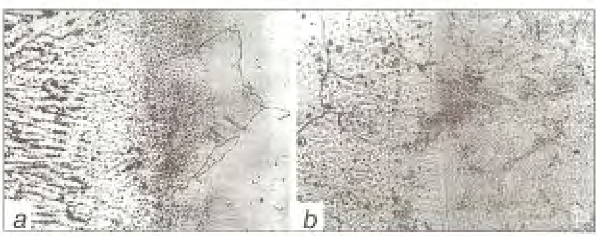

Figure 2. Microstructure of fusion zones of a dissimilar joint of steels 110G13L (*a*) and 09G2S (b), made with electrodes ANVM-1 (×320) (reduced by 0.80).

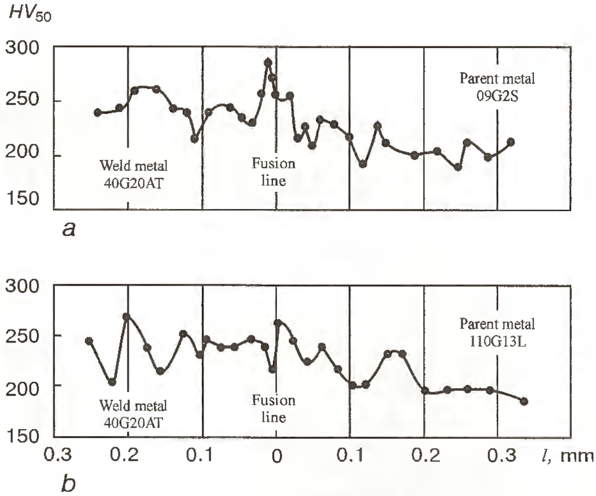

Figure 3. Distribution of microhardness in fusion zones of a dissimilar joint of 110G13L + 09G2S with a weld metal made using electrodes ANVM-1: *a* — steel 09G2S; *b* — steel 110G13L; *l* — distance from the fusion line.

The mechanical properties of metal deposited with electrodes ANVM-1, are almost at the level of properties of steel 110G13L ($\sigma_{0.2}$ = 270 – 360 MPa, σ_t = 570 – 630 MPa, δ = 18 – 26 %, ψ = 28 – 35 %, KCU^{+20} = 80 – 100 J/cm^2), including the susceptibility to hardening at mechanical cold working. According to data of measurements of hardness of metal, deposited with electrodes ANVM-1, it is *HV* 220 – 360 in initial state and *HV* 480 – 550 after cold plastic deformation.

The structure of the deposited metal is austenitic with a precipitation of carbonitrides; microhardness is at the level HV_{50} = 185 – 240; there are no liquation clusters and pores, typical of steel 110G13L (Figure 1), hardness of weld metal is *HV* 221 – 260.

In HAZ of steel 110G13L a structure of austenite with a coarse grain is formed (Figure 2, *a*). Hardness of HAZ metal does not differ greatly from that of the parent metal.

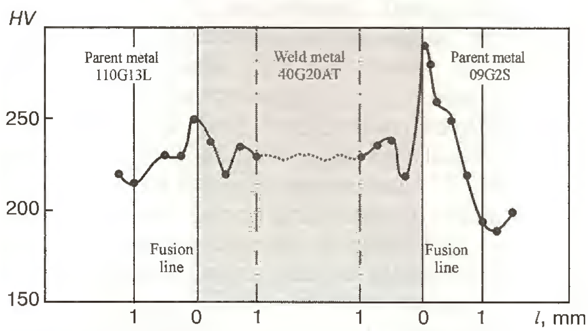

Figure 4. Distribution of hardness in a dissimilar joint of 110G13L + 09G2S, made with electrodes ANVM-1.

At the fusion line with steel 09G2S a martensite fringing of 5 – 15 μm width is formed, its hardness is *HV* 296 – 327. The HAZ metal is characterized by a structural mixture of ferritic, pearlitic and bainitic constituents (Figure 2, *b*). Hardness of metal of overheated region is *HV* 236 – 260. Results of measurements of microhardness in the fusion zones and HAZ of welded joints of steels 110G13L and 09G2S with a weld metal made with electrodes ANVM-1 are shown in Figure 3. Hardness distribution in a dissimilar welded joint is given in Figure 4.

Welded joints of steel of 110G13L grade and also dissimilar welded joints of 110G13L + 09G2S made with electrodes ANVM-1 are resistant to the formation of cold and hot cracks if the preset temperature conditions of welding are followed.

Electrodes ANVM-1 were first designed for the manual arc welding and hardfacing of steel 110G13L and also its dissimilar combinations with low-carbon steel 20 and 09G2S in manufacture and repair of components of mining equipment subjected to impact-abrasive wear. However, the comprehensive evaluation of properties of different welded joints, made with electrodes examined, allowed the field of their application to be widened significantly. Thus, for example, it was established that electrodes ANVM-1 provide the quality, hot crack-resistant welded joint of steels saturated with a hydrogen sulphide in the process of a long-term service of petroleum refining plants (pipelines, column membranes, etc.). The satisfactory results were obtained during testing electrodes as hardfacing materials for the restoration of necks of bodies of energy-absorbing mechanisms (steel 30GSLB) of couplings of railway rolling stock subjected to the intensive impact wear.

Electrodes ANVM-1 have passed the industrial testing at Krivoj Rog Central Ore and Machinery Repairing Factory and also were highly evaluated during testing railway cars at the Darnitsa Repairing Factory.

The electrodes developed are characterized by a good adaptability to manufacture. They are now serial-produced.

Concerning technological recommendations and purchase of electrodes ANVM-1, please, contact:
Prof. L.M. Zhadkevich, Deputy Director,
The E.O. Paton Electric Welding Institute
(for Dept. No. 11)
11, Bozhenko str., Kyiv, 03680, Ukraine
Tel. (380 44) 261 50 86; 261 54 39

REFERENCES

1. Davydov, N.G. (1979) *High-manganese steel*. Moscow: Metallurgia.
2. Goldshtein, M.I., Grachev, S.V., Veksler, Yu.G. (1985) *Special steels*. Moscow: Metallurgia.
3. Morozovskaya, E.N. (1964) About prevention of tears in hardfacing steel of G13L type on carbon steel. *Avtomaticheskaya Svarka*, **12**, 38 – 41.
4. Belyashin, P.A., Motus, E.P., Tarlinsky, V.D. (1990) Improvement of weldability of high-manganese cast steel 110G14L. *Khim. i Neft. Machinostroyeniye*, **3**, 23 – 25.
5. Berezovsky, A.V., Barmin, L.N., Shumyakov, V.I. (1967) Effect of electrode material composition on properties of welded joints of steel 110G13L. *Svarochnoye Proizvodstvo*, **7**, 26 – 27.
6. Bukrina, N.I., Volkonsky, A.I. (1971) Weldability of high-manganese steel 110G13L with steels of pearlitic class. In: *Manufacture of large machines. Welding of steel structures*. Moscow: Metallurgia.

TECHNOLOGY OF BRAZE WELDING OF FLANGES TO TUBES

A.S. PROKOFIEV and **A.S. PISMENNY**
The E.O. Paton Electric Welding Institute, NASU, Kyiv

ABSTRACT

New technology of manufacture of flanged joints, made from carbon steels, using a braze welding is considered. Data for calculation of the process parameters and results of testing the joints are given. The technology of braze welding is characterized by a high efficiency, adaptability to mechanization and automation for manufacture of flanged joints. No high-skill personnel is required.

Key words: *braze welding, flanges, joints, structures, edge preparation, weld area, strength.*

A large amount of carbon steel tubular metal structures with flanged elements are widely used in manufacture of different-purpose pipelines, gas and other equipment (counters of gas, water, heat, etc.), in repair of old pipelines and laying of new pipings in housing sectors, in gasification of populated areas. However, the problem of their manufacture is still actual.

In some cases the brazing is used successfully for joining the tubular structures [1]. It is interesting to describe some designs of flanged joints of pipelines, methods of their manufacture from pipes and branch pipes of a limited length using brazing or braze welding.

As a rule, in designs of pipelines an intermediate (middle) fittings in the form of T-joints and cross-pieces with welded-on flanges are used. The fittings are manufactured by casting, stamping with a subsequent mechanical treatment. Here, the material utilization factor is very high, and the labour content for the manufacture of fittings has even reserves to be reduced.

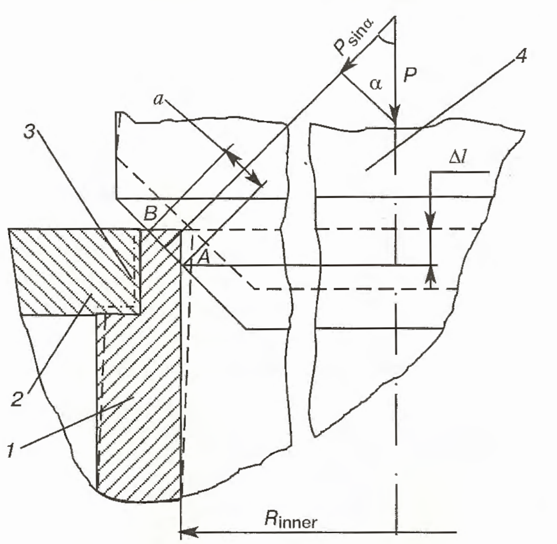

Figure 1. Joining of flange to pipe with a grooving: *1* — pipe; *2* — flange; *3* — mixture of a brazing alloy with a flux; *4* — welding punch. Here and in Figure 2 a dash line shows an initial arrangement of parts to be joined and a welding punch.

The manufacture of flanged joints of the pipelines by brazing and braze welding can decrease the total mass of piping systems and labour content for their manufacture.

Method, described in application patent, includes a preliminary preparation of the pipe end to be joined to a pipe using a step grooving along the outside diameter of the pipe. This requires a negligible mechanical treatment of the pipe end. Then, the flanged joint is assembled in the clamps of the welding machine, the brazing alloy and flux are fed to the joint zone; the zone of flange joining to the pipe is heated with a next applying of the upset force to an inner surface of the pipe with a flange mounted on it, and the weld zone is deformed. The shaping of the weld zone of the flanged joint is determined with allowance for the required degree of forming.

Thus, the technology of manufacture of a flanged joint includes the following operations (Figure 1): mechanical treatment (facing) of a pipe with a formation of step grooves along the outside diameter of the pipe; flange mounting on a step groove of the pipe and introducing the brazing alloy and flux into the joint zone; heating of the joint zone from induction or other heating unit; shaping of the weld zone of the flanged joint with a profile welding punch at applying upset force along the conical surface *AB* by punch displacement for a preset distance Δl.

During experimental investigation of the above-described technology two types of designs of flanged joints made with the technology of braze welding were considered and tested (Figures 1 and 2). Sizes of the experimental specimens are given in Figures.

The joint, given in Figure 2, requires, except the step grooving of the pipe, the conical grooving along the inner hole of the flange (surface AB with a generating a). Further, in calculations the surface AB with a generating a is a width of an area of a contact bearing strain and defines the size of zone of a required deformation.

It should be noted that the grooving in the flange for the second type of the joint can be made not only in the form of a cone, but also in the form of a part of a spherical or other surface depending on special requirements to the flanged joint.

In the first type of the joint (Figure 1) the pipe should deform from inside at a minimum expansion of the flange during upsetting with a welding punch, thus leading to a stress-strain state of the metal of the joint zone, to extrusion of the brazing alloy and flux, to the contact of the surfaces joined and, respectively, to the minimizing the alloy thickness at the joint spot.

In the second type of the joint (Figure 2) the pipe will deform during upsetting with producing of a joint along the conical surface formed after grooving in the flange, thus leading to the increase in the joint surface and its strength. Initially, the brazing alloy, made in the form of a ring, was located in the flange groove in the section of ABC triangle.

As the upsetting force of the welding conical punch is distributed into constituents, directed tangentially and radially with respect to the pipe axis, then this influences greatly the type and quality of the joint due to the occurrence of a complex-type deformation.

The calculation of a required upset force is made coming from the following considerations. It is known, that to determine the forces required for a contact bearing strain and developing the plastic deformation the results of the fourth theory of strength can be used. It follows from the theory that in the center of the contact area the maximum compressive stress σ_{max}, normal to the weld surface, is [3]

$$\sigma_{max} = 5\sigma_y, \tag{1}$$

where σ_y is the yield strength for the given steel grade at the given temperature.

From the other hand, the maximum stress can be determined by a distributed linear loading q and a width of a contact bearing strain area a using a formula given in [2]:

$$\sigma_{max} = 1.27q/a. \tag{2}$$

Equating the formulae (1) and (2), we shall obtain

$$q = \frac{5\sigma_y/a}{1.27} = \frac{5\sigma_y \Delta l}{1.27\cos\alpha}. \tag{3}$$

The distributed loading can be calculated as a ratio of normal (to the bearing strain area) force P_a to the weld length L determined along the center of the bearing strain area

$$q = P_a/L, \tag{4}$$

where $L = 2\pi\,(R_{inner} + 0.5\,\Delta l \,\mathrm{ctg}\,\alpha)$; α is the angle between the axis of pipe and flange and a normal, made to the surface of the welding punch; Δl

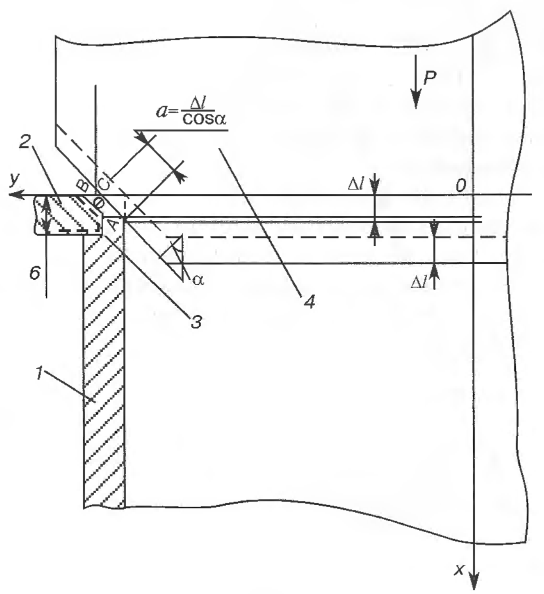

Figure 2. Joining of flange with a grooving to a pipe with a grooving: *1* — pipe with a grooving; *2* — flange with a grooving; *3* — brazing alloy in a formed joint; *4* — welding punch.

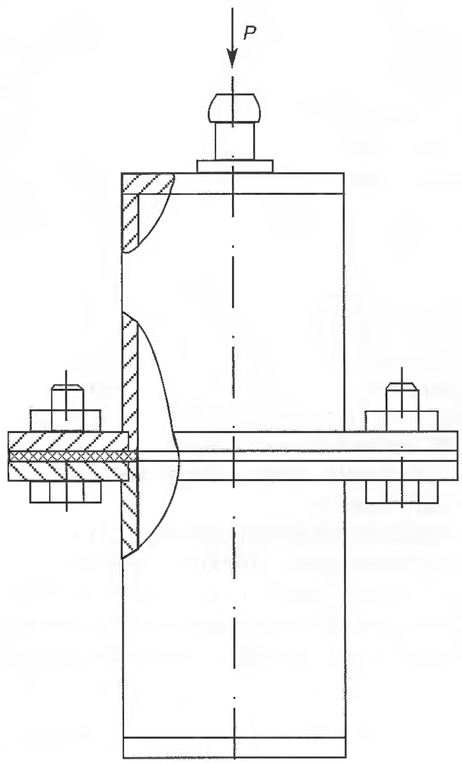

Figure 3. Scheme of assembly of flanged joints for tests.

is the upsetting along the axis of pipe and flange (displacement of the welding punch); R_{inner} is the radius of the pipe inner surface.

From solution of equations (3) and (4) we shall obtain the formulae for determination of a normal force P_a applied to the bearing strain area and force P which should be applied to the welding punch along its axis to provide the preset deformation of the weld zone:

$$P_a = \frac{10\sigma_y\pi\,(R_{inner} + 0.5\,\Delta l\ \mathrm{ctg}\ \alpha)\,\Delta l}{1.27\cos\alpha}, \quad (5)$$

$$P = \frac{P_a}{\cos\alpha} = \frac{10\sigma_y\pi\,(R_{inner} + 0.5\,\Delta l\ \mathrm{ctg}\ \alpha)\,\Delta l}{1.27\cos^2\alpha}. \quad (6)$$

It is seen from formulae (5) and (6) that the upset force depends greatly on the angle α, radius of the pipe joined, and also on the punch displacement Δl. The sizes of an outside diameter of the groove on the pipe and the shape of grooving on the inner diameter of the flange also influence the results of calculations by these formulae as it is associated with a selection of angle α and a size of the zone of a required deformation a (generatrix and determinant of the width of the contact bearing strain area).

The upsetting was calculated coming from the conditions that at temperature of alloy melting within the range 1000 – 1100 °C the deformation resistance is 8 – 5 MPa. The full upset force reached 2.5 kN for the first type of the joint and 7.8 kN for the second type.

During upsetting the force was applied to the joint zone by a welding punch. Here, the punch displacement Δl was from 0.25 (Figure 1) to 0.65 (Figure 2) of the pipe wall thickness. Thus, for example, the displacement was 1.6 (first type of the joint) and 4.9 mm (second type of the joint) at 70 mm pipe diameter and 6 mm wall thickness and 120 mm OD flange of 6 mm wall thickness, respectively. The further increase in Δl to 2 and 5 mm led to cracking of edges at the pipe inner surface.

When testing the braze welding for producing the above-described designs two methods of brazing alloy deposition were used: a powder-like mixture of alloy and flux with a binder was deposited on the pipe surface joined; the alloy was placed into a conical groove of the flange in the form of an embedded element.

In experiments a brass powder of L63 grade was used as a brazing alloy for the first type of the joint and a 2.5 mm diameter brass wire of L63 grade (GOST 16130–72) was used for the second type. Powder of borax Na_2BrO_7 was used as a flux in both cases. Material of pipe and flange was steel 20 (GOST 1050–52).

Best results (from the point of view of filling the joint spot with an alloy) were obtained at vertical location of parts to be joined. In this case the upset force was applied to the inner surface of the vertically-located pipe. The flange perpendicularity with respect to the pipe was provided at the expense of the quality of a mechanical treatment of both the pipe and the flange, and also a proper welding equipment.

The braze welding process was performed at a direct contact of parts to be welded, namely a pipe, fixed in the welding machine clamp, and a flange, located at a step outside grooving of the pipe and pressed against it by a welding punch. In addition, the spot of joining was heated by a single-turn circular inductor at 2500 Hz current frequency. The displacement value during upsetting was set by a movable part of the machine. During formation of joints of the first and second types the flow section of the pipe was not subjected to any changes.

Specimens of the flanged joints were fracture tested with an inner hydrostatic pressure (Figure 3). During tests the induced hydrostatic pressure in the specimens tested exceeded significantly a standard test pressure of 2.5 MPa at a working pressure of 1.6 MPa.

It should be noted in conclusion that the above-described technology of braze welding the flanged joints of pipes guarantees structures which are similar in strength and air-tightness to those made by the arc welding.

Increase in weld area sizes when designing the flanged joint (Figure 2) contributes to the increase in strength and air-tightness of the joint and improvement of the quality. The estimation of its strength showed that the use of the joints of such type is feasible in manufacture of load-carrying metal structures and heavy-duty units, for example, when joining the tubes to the tube sheets in heat exchangers, etc.

The technology of braze welding is more efficient than many other technologies of manufacture of the flanged joints (arc welding, for example). It does not require high-skill personnel and is more adaptable to mechanization and automation of the manufacture.

REFERENCES

1. Khorunov, V.F. (1991) High-temperature brazing in the USSR: achievements and problems. In: *Materials and technology of brazing*. Kyiv: PWI.
2. (1973) *Resistance of materials*. Ed. by G.S. Pisarenko. Kyiv: Vyshcha Shkola.

PROPERTIES OF HYPEREUTECTOID COMPLEX-ALLOYED STEELS AFTER LASER HEAT-TREATMENT

V.Yu. KHASKIN[1], **S.Yu. PAVLOVSKY**[1], **V.P. GARASHCHUK**[1], **V.D. SHELYAGIN**[1], **A.K. TSARYUK**[1], **T.G. SOLOMIJCHUK**[1] and **T.G. CHIZHSKAYA**[2]
[1]The E.O.Paton Electric Welding Institute, NASU, Kyiv, Ukraine
[2]«KPI» National Technical University of Ukraine, Kyiv, Ukraine

ABSTRACT

Laser heat-treatment of hypoeutectoid complex-alloyed steels has been studied for the case of diesel engine crankshafts and parts of steam-distribution units of steam turbines. A procedure is proposed for selection of the treatment modes. A technology of laser hardening of crankpins of crankshafts made of this steel grade has been developed.

Key words: *laser heat-treatment, partial melting, steels, parts being hardened, thermophysical problem, modes, metallography, residual stresses, wear resistance.*

Hypereutectoid complex-alloyed steels, due to their high strength and antifriction properties, are applied in industry for fabrication of complex and critical parts, namely crankshafts of powerful automotive, heat locomotive and ship diesel engines (40KhN2MFA steel is the material of the crankshaft of the KAMAZ lorry), parts of turbine steam distribution units (25Kh1M1FTR steel), etc. In order to improve the wear resistance, the parts of these steels are hardened by the traditional methods (bulk heat-treatment in furnaces, chemical heat treatment, HFC quenching). However, their service life is not always satisfactory in economic terms. The comparatively high cost of the parts necessitates an extension of their service life by 1.5 to 2.0 times, but the cost of hardening performed with this purpose should not exceed 10 to 30 % of the cost of the part being hardened [1].

Extension of the service life in the case being considered can be achieved by different processes (detonation- and ion-plasma, coating deposition by electroplating, etc.). Hardening performed by application of high power density sources, namely laser, electron beam and plasma is a well-established method [2]. Among the enumerated processes laser heat-treatment (LHT) is notable for its highly local nature and high efficiency, ability to conduct the technological process in any atmosphere transparent for the laser radiation.

In this study LHT of 40KhN2MFA and 25Kh1M1FTR steels with the aim of improvement of wear resistance of the friction surfaces of parts by increasing the metal hardness was investigated. The first steel was studied for the case of crankshafts of diesel engines operating at the temperature of about 100 °C, and the second one for parts of steam distribution and regulation units (valves, bushings, rods of steam turbines operating at the temperature of 540 to 570 °C and high vapour pressure of up to 12 MPa).

According to [3] high stresses can develop in the strips of LHT of 40KhN2MFA steel under the impact of the thermal energy source and the residual stressed state as a result of structural transformations. In the zones of LHT strip overlapping the residual stresses become higher because of recrystallization. Therefore, in order to eliminate the above phenomenon, as well as achieve a damping effect at shock service loads on the crankshaft, a schematic of LHT performance along a spiral was accepted with the following geometry of the hardened strips: strip width on the surface being treated was 6 to 9 mm, strip spacing being 1 to 2 mm, and strip depth 0.8 to 1.0 mm.

In order to achieve in the LHT strips a uniform structure with isotropic properties, it is rational to perform laser hardening without partial melting. However, as the allowance for the finish cylindrical grinding of the hardened crank pins was 0.1 mm to the side, the presence of a zone of partial melting to the depth of not more than 0.1 mm from the surface of the hardened strip was allowed, in order to improve the stability of LHT process. The strip hardness should not be lower than *HRC* 54 to 59 with the base metal hardness of *HRC* 40 to 44 [1].

The required power of laser radiation was estimated by the dependence given in [4]:

$$T\,(y,\,z,\,t) = \frac{2PA}{v c \rho}\,\frac{\exp\left\{-\left[z^2/4at + y^2/4a\,(t_0+t)\right]\right\}}{\sqrt{4\pi a t}\,\sqrt{4\pi a\,(t+t_0)}},$$

where y and z are the coordinates of a point which belongs to a plane passing through the center of the thermal source of power P normal to the direction of its displacement; t is the duration of the thermal source impact calculated from the moment

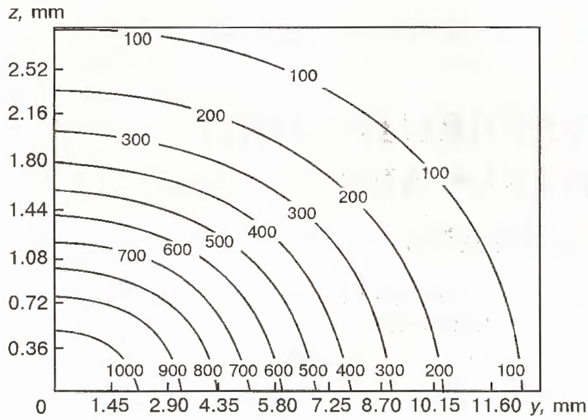

Figure 1. Temperature distribution (°C) along y, z co-ordinates during LHT of 40KhN2MFA steel with surface melting.

it crosses this plane with the speed v; A is the average value of absorptance in the temperature range being considered; c is the specific heat capacity of the steel being treated; ρ is its density; $a = \lambda / c\rho$ is the thermal diffusivity; λ is the thermal conductivity of steel; $t_0 = 1/4ak$ is the time constant, and k is the coefficient of concentration in Gauss law.

The given relationship was first used to calculate the required values of consumed power PA for heating a point with coordinates $y = 0$ and $z = 1 \cdot 10^{-3}$ m up to the temperature $A_{c_3} = 780$ °C [5] under the conditions of our experiment ($v = 1.7 \cdot 10^{-2}$ m/s, light spot diameter $d = 8$ mm with corresponding coefficient of concentration $k = 6.25 \cdot 10^4$ m^{-2} and duration of thermal source action $t = 0.35$ s). Value of k was estimated by impact on acrylic plastic of a focused laser beam with the same position of its focus relative to the irradiated surface and treatment speed as in LHT of steel. The duration of impact t of the source was estimated with an optical pyrometer «Spectropir P1-003» by the position of the light spot point in which the maximal temperature was achieved. It was approximately at $0.75d$ distance from the front edge of the beam, this resulting in $t = 0.75d/v \approx 0.35$ s.

The following values of the steel thermophysical properties were used in calculations [5]: thermal conductivity factor $\lambda_{800\,°C} = 28$ J/(m·K); average heat content (in the temperature range of 20 to 800 °C) $c = 697$ J/(kg·K); steel density $\rho = 7900$ kg/m^3. The temperature field in the case of $t = 0.35$ s is shown in Figure 1.

Calculation showed that the required value of absorbed power of the laser beam should be $PA = 1.69$ kW; absorptance of the studied steel is $A = 0.2$; so the laser radiation power should be approximately 8 kW. Therefore, it is rational to apply a coating with the absorptance of not less than 0.5. Such a coating is zinc phosphate [6] which was applied onto the sample surface by the method of cold chemical etching. The absorptance of this coating for a 10.6 μm wave of CO_2-laser varies from 0.90 to 0.55 with the temperature increase from 20 °C up to the iron melting temperature of ~1500 °C [7, 8].

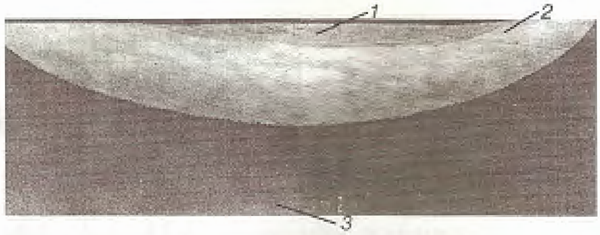

Figure 2. Cross-sectional structure of LHT strip of 40KhN2MFA steel: *1* — cast (dendritic) zone; *2* — zone of quenching from the hard phase; *3* — base metal (×25) (reduced by 0.67).

As a result, the following mode was selected for LHT of 40KhN2MFA steel: $P = 3.3$ kW; $v = 16.67$ mm/s, $d = 8$ mm. Treatment was performed with the focal point lowering by (60 ± 5) mm with 300 mm focal length.

On 25Kh1M1FTR steel (according to the statement of work) the requirement was to produce a hardened surface layer not less than 0.5 mm deep with the hardness not lower than *HRC* 48 with the base metal hardness *HRC* 20 to 23. In this case the surface layer was to consist of individual not overlapping strips, in order to prevent metal recrystallization in the overlapping zones. The latter can lead to undesirable properties [3]. The spacing of the adjacent strips should be minimal (approximately 0.1 to 0.3 mm).

As the internal diameter of the surface being hardened was 60 mm, and laser radiation was transmitted to it by means of a rotary mirror introduced inside, it was necessary, instead of using an absorbing coating, to concentrate the energy by reducing d, in order to prevent the spatter from the beam impact zone depositing on the mirror. Therefore, the version of LHT with partial melting, i.e. quenching from the liquid phase, was accepted [6].

Proceeding from the above dependence and its subsequent more precise determination through experiments, the following mode was selected for LHT of 25Kh1M1FTR steel: $P = 1.5$ kW, $v = 23$ mm/s, $d = 1$ mm. Treatment was performed close to the focal point.

Experiments were conducted in a process CO_2-laser LT-104 [9]. A screw-cutting lathe FT-11 specially modified for the purpose, was used as the rotator. The samples were cylindrical simulators of KAMAZ lorry crankshaft pins of 80 mm dia. and 60 mm length and 95 mm dia. and 40 mm length of 40KhN2MFA steel and bushings of 100 mm and 60 mm dia. and 50 mm length of 25Kh1M1FTR steel.

Experiments showed that for LHT of 40KhN2MFA steel with the strip width of 8 to 9 mm, the partial melting zone width of 5 to 6 mm and its depth of 0.07 to 0.10 mm, the total depth of the strip is 0.8 to 1.0 mm (Figure 2). If the

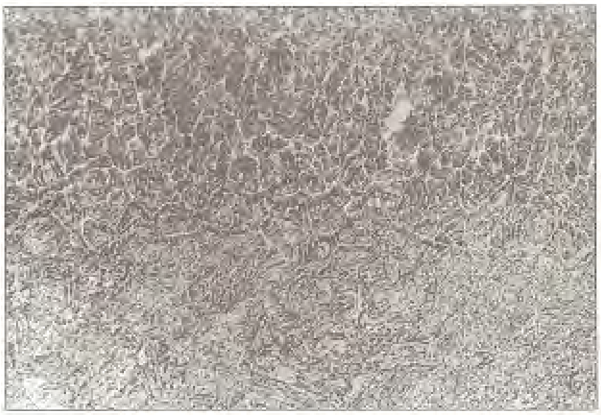

Figure 3. Microstructure of the columnar crystallite-dendrite zone (top) and transition to a fine-grained acicular martensite of the zone of quenching from the hard phase (bottom) (×320) (reduced by 0.60).

partially melted zone is absent, the maximal depth of LHT strip is up to 0.7 to 0.8 mm.

The base metal has the structure of beinite (predominantly lower beinite) with the characteristic forging bands. The partially melted (cast) zone has a well-defined dendritic structure (Figure 3) with microcracks 0.01 to 0.02 mm wide (Figure 4). These cracks remain within the cast zone and do not propagate into the quenching zone area, thus permitting their removal together with the allowance, in finish machining. The structure of the quenching zone metal is the so-called structureless martensite [10] with a uniform hardness of approximately *HRC* 65 to 66 (Figures 3, 5). A transition zone 0.04 to 0.06 mm wide with a gradual lowering of the hardness is located between this zone and the base metal (Figure 5).

The presence of the transition zone provides a smooth transition from the quenching structure to the base metal, which should prevent the strip chipping in service with cyclic impact loads. A characteristic distribution of microhardness in LHT zones by the depth of the sample of 40KhN2MFA steel is given in Figure 6.

The presence of microcracks in the cast zone points to the action of temporary thermal stresses

Figure 4. Microstructure of the dendrite region of the hardened strip with microcracks and HV_1 microhardness indentations (×156) (reduced by 0.67).

Figure 5. Microstructure of the zone of transition from finely-dispersed acicular martensite of the zone of quenching from the hard phase (top) to the base metal (bottom) (×400) (reduced by 0.60).

during LHT of the samples [11]. As LHT strips can develop inadmissibly high residual stresses, stresses of the first kind (zone macrostresses) were determined by X-ray diffraction analysis on unmachined strip surfaces [12]. The roentgenograms were taken in «Dron-3» unit.

Investigations revealed on the unmelted surface of LHT strips (40KhN2MFA steel) compressive stresses $\sigma = (-763 \pm 380)$ MPa, this being equal to 0.3 to 0.6 of ultimate strength: $[\sigma_t] = 1710 - 1750$ MPa (quenching at 840 to 850 °C in oil with subsequent tempering from 200 °C). When combined with the cyclic alternating loads characteristic of the conditions of the crankshaft operation, they can lead to premature fatigue failure of the part [1, 13]. No residual stresses were found in the partially melted (cast) zone of LHT strips, as temporary stresses which exceed the ultimate strength of the cast zone metal are acting in it at the moment of its solidification. The formed solidification cracks lead to a complete relaxation of the temporary stresses and, as a result, to the absence of the residual stresses.

It is found that the bulk heat-treatment of samples of 40KhN2MFA steel after LHT, which includes heating up to 200 to 250 °C, soaking for 3 to 4 h and subsequent cooling in air, allows complete elimination of the above residual stresses. After such a tempering which relieves the stressed

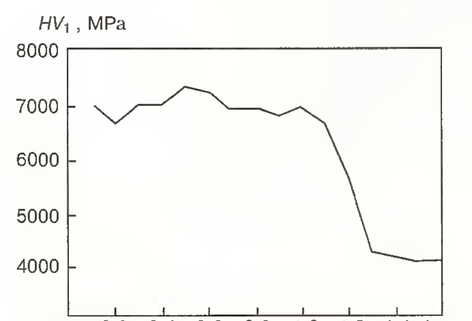

Figure 6. HV_1 microhardness distribution by depth *h* in the strip center shown in Figure 2.

state, the hardness of the samples metal is somewhat reduced and is about *HRC* 60.

According to the theory of fatigue fracture of crankshafts [13], accumulation of residual stresses and formation of fatigue cracks proceed in a comparatively thin (0.5 to 1.0 mm) near-surface layer on the shaft pins. The most critical locations in this respect (stress raisers) are the fillets. They do not work in wear, but experience alternating cyclic loads under the impact of the torque. Therefore, it can be assumed that despite the heat-treatment which allows relieving of the residual stresses, in LHT of the crankshaft pins the laser beam falling on the fillet is not desirable.

Testing of LHT samples of 40KhN2MFA steel for wear resistance by the dry friction method was conducted in a specially made friction machine by the cylinder-pin schematic, which accurately enough simulates the actual conditions of operation of the diesel crankshafts. The mating bodies were made of steel 45 with subsequent quenching up to the hardness of about *HRC* 55. Specific pressure was set to be within 10 to 16 MPa, rotation frequency of the sample being tested was 50 to 1600 min^{-1}, linear friction speeds being 1600 to 4000 m/h. Sample wear was measured by the change of diameter with a micrometer with 0.01 mm scale division, as well as by the change of weight by weighing in MTZ No. 206 beam balance (1965) with ±10 mg error. The duration of friction was increased in order to improve the measurement accuracy. Testing results showed that wear resistance of the hardened samples exceeds that of samples cut out of a standard crankshaft, by 2 to 3 times.

In investigation of LHT strips of 25Kh1M1FTR steel it was found that application of energy concentration resulted in deep but narrow strips. Their depth was 0.7 to 0.9 mm with 1.1 to 1.3 mm width on the surface. The strip spacing was 0.2 to 0.3 mm. The hardness of the produced cast structure of the hardened strips varied from *HRC* 48 to 54. The width of the zone of transition to the base metal was not more than 0.04 mm. HV_1 hardness of the metal of this zone was 300 to 350 MPa.

The thus hardened bushings were tested for heat resistance of the hardened layer by a long-term soaking in the furnace at the temperature of 540 to 570 °C. The samples were periodically taken out of the furnace (after 10 to 20 h), their microstructure was studied and hardness of the LHT strip metal was measured. The assessment criterion was provision of the initial structure and hardness of the hardened layer metal after LHT during the control soaking time (up to 500 h) at the working temperature.

Testing showed that at 540 to 570 °C, softening of the quenching structures of the hardened layer occurs within 50 to 60 h, after which these structures correspond to the initial condition of the base metal.

CONCLUSIONS

1. Residual compressive stresses (0.3 to 0.6)σ_t develop from the hard phase of the hardened strips in the quenching zone in the case of LHT of 40KhN2MFA steel without partial melting. No residual stresses were found in the base metal remelted by laser radiation.

2. In order to eliminate the residual stresses in LHT strips, it is recommended to perform bulk heat-treatment, including heating up to 200 to 250 °C, soaking for 3 to 4 h and subsequent cooling in air.

3. A considerable (2 to 3 times) improvement of wear resistance allows LHT technology with minimal surface melting to be recommended for industrial application in the items exposed to temperatures reaching 100 °C in service.

4. LHT application for hardening of the surfaces of friction parts of steam distribution and regulation units of 25Kh1M1FTR steel operating at considerable steam temperatures of 540 to 570 °C, does not provide the required wear resistance in the case of long-term operation. Apparently, laser surfacing with self-fluxing alloy powders can be a rational variant of hardening of the above part surfaces.

REFERENCES

1. Kanarchuk, V.E., Chigrinets, A.D., Golyak, O.L. *et al.* (1993) *Technology and equipment for automotive part reconditioning*. Kyiv: ISDO.
2. Shchur, E.A., Voinov, S.S., Klesheva, I.I. (1982) Improvement of structural strength of steels in laser quenching. *Metallovedeniye i Term. Obrabotka Metallov*, **5**, 36 – 38.
3. Gladky, P.V., Makhnenko, V.I., Oleinik, V.A. *et al.* (1993) Features of stressed state of rollers of slab-casting machines in their cladding with 15Kh13 steel. *Avtomaticheskaya Svarka*, **5**, 20 – 24.
4. Rykalin, N.N., Uglov, A.A., Anishchenko, L.M. (1985) *High-temperature technological processes: thermophysical fundamentals*. Moscow: Nauka.
5. Sorokin, V.G., Volosnikova, A.V., Vyatkin, S.A. *et al.* (1989) *Guidebook of steels and alloys*. Moscow: Mashinostroyeniye.
6. Abilsiitov, G.A., Golubev, V.S., Gontar, V.G. *et al.* (1991) *Process lasers*. Reference book. 2 vol. Vol. 1. Design and operation. Moscow: Mashinostroyeniye.
7. Arata, Y., Maruo, H., Miyamoto, I. (1978) Application of laser for material processing. Heat flow in laser hardening. *IIW Doc. IV-241*, 1–24.
8. Harth, G.H., Leslie, W.C., Gregson, V.G. *et al.* (1976) Laser heat treating of steels. *J. of Metals*, **4**, 5.
9. Garashchuk, V.P., Shelyagin, V.D., Nazarenko, O.K. *et al.* (1997) Process CO_2-laser LT 104 of 10 kW power. *Avtomaticheskaya Svarka*, **1**, 36 – 39.
10. Gulyaev, A.P. (1963) *Metal science*. Moscow: Oborongiz.
11. Grigoryants, A.G., Shiganov, A.N. (1988) Laser equipment and technology. In: *Laser welding of metals*. Manual for higher educational establishments. Moscow: Vysshaya Shkola.
12. Gorelik, S.S., Rastorguyev, L.N., Skakov, Yu.A. (1963) *Radiographic and electron diffraction analysis of metals*. Moscow: Metallurgizdat.
13. Mishin, I.A. (1976) *Service life of engines*. Leningrad: Mashinostroyeniye.

SELECTION OF SPARSELY-ALLOYED SURFACING MATERIALS FOR DIFFERENT IMPACT-ABRASIVE CONDITIONS

V.V. CHIGAREV and **V.L. MALINOV**
Priazov State Technical University, Mariupol, Ukraine

ABSTRACT

The absence of an objective quantitative estimate of the conditions of impact-abrasive wear is noted. It is proposed to use the dynamism coefficient (K_d) as the criterion of the intensity of impact-abrasive wear. The applicability of K_d criterion has been verified for the case of development of PL-Np-160Kh12G5 flux-cored strip for restoration of the plates of jaw crushers.

Key words: *impact-abrasive wear, coefficient of dynamism, relative wear resistance, regressional dependence, alloying element, deposited metal, flux-cored strip.*

A large number of various parts of machines are currently operating under the conditions of impact-abrasive action, resulting in their intensive wear which requires considerable expenses for their restoration or replacement. One of the most widely accepted technologies of part restoration and improvement of their fatigue life is electric-arc surfacing. Increasing the requirements to fatigue life of surfaced parts operating under the conditions of impact-abrasive wear, improvement of cost-effectiveness and adaptability of surfacing materials to fabrication are urgent. In this connection, the use of procedures allowing greater effectiveness of development or selection of surfacing metals satisfying these requirements, appears to be important.

The publications on impact-abrasive wear resistance of deposited metal contain a lot of incomparable and contradictory data. One of the reasons for it is the fact that the conditions of impact-abrasive wear, which can differ essentially, are only qualitatively evaluated. The definitions used for this purpose, namely «insignificant», «moderate», «considerable» impact loads, are conventional, not based on any objective testing procedures, reflecting the actual conditions of the parts service. No standard methods of determination of impact-abrasive wear resistance are available now. This, on the one hand, makes laboratory evaluation more difficult, and on the other, makes selection of materials for certain operational conditions more complicated. Now the full-scale tests of the surfaced parts which yield valid results, are highly labour- and time-consuming [1].

As a result, surfacing materials of different degree of alloying and structure are applied for the same conditions of impact-abrasive wear, and expensive and deficit alloying elements are used inefficiently.

Proceeding from the above, an objective quantitative estimation of the conditions of impact-abrasive wear is required. Already in 1965, I.V. Petrov suggested a quantitative criterion of intensity of impact-abrasive action, called the coefficient of dynamism K_d by him, which is determined as the ratio of the hardness of 110G13L steel sample working surface after wear under specific conditions to its initial hardness. The author believes that this steel is capable of accumulating the external action energy, while becoming strengthened, whereas the values of strengthening are a measure of integral intensity of impact-abrasive action of the particles [2].

It is known that the energy of the action of abrasive particles in wear, absorbed by the metal, is consumed for elastic and plastic deformation, as well as its fracture [3]. On the other hand, K_d objectively characterises the energy of such an impact, absorbed by 110G13L steel during wear under specific conditions. The greater the energy of impact-abrasive action, the greater the degree of work hardening. However, assessment using K_d did not become widely accepted in selection and development of surfacing materials.

This study is devoted to a procedure of development of advanced sparsely-alloyed surfacing materials for different impact-abrasion conditions characterised by K_d. Five different procedures of testing for impact-abrasive wear [4] used in investigations, allowed variation of the coefficient of dynamism in a broad range from 1.2 up to 3.5.

In the first procedure, abrasive particles move between the cylindrical surface of the rotating disc and the flat surface of the sample, which particles are entrapped by the disc, thus wearing the sample. Formally this testing procedure corresponds to purely abrasive wear [4]. Considering, however, Deposited metal composition providing the highest impact-abrasive wear resistance for the considered K_d values

Procedure #	K_d	Composition, %			Relative wear resistance, ε
		C	Mn	Cr	
1	1.1	2.2	2.4	12.0	1.85
2	1.4	2.2	2.8	12.0	1.80
3	1.7	2.0	3.2	12.0	1.65
4	2.0	1.8	3.6	12.0	1.60
5	3.5	1.6	5.2	12.0	1.50

that the metal surface has a microrelief, it can be stated that a certain part of abrasive particles have an impact action, the evidence of which is small strengthening of 110G13L steel (K_d = 1.2).

In keeping with the second - fourth procedures, wear is produced by abrasive particles transported by the air flow. In this case the samples being tested were mounted at an angle of 30, 60 and 90° to the abrasive flow, while K_d was 1.4, 1.7 and 2.0, respectively. These testing procedures formally belong to gas-abrasive wear [1], but essentially they implement a combination of impact and abrasive action of the particles. The intensity of abrasive particle impact and the rate of materials wear, respectively, greatly depend on the angle of incidence, which is indicated by different degree of strengthening of 110G13L steel and K_d.

According to the fifth procedure, the samples fastened to the disc, rotate at a high speed (1500 rpm) and collide with the free-falling shot. In this case the highest value of K_d = 3.5 is achieved, this being the consequence of a great energy of the abrasive particles impact on the deposited metal surface. In this case, similar to the previous ones, the action of the abrasive particles is both abrasive and impact. The second prevails, the proof of which is a great strengthening of 110G13L steel (hardness rises from *HB* 140 – 150 up to *HB* 490 – 520).

In order to verify the applicability of K_d for assessment of various conditions of impact-abrasive wear in the testing procedures used in this study, wear resistance of a number of materials (ETN-2, Sormite-1, etc.) tested by I.V. Petrov by his procedures [2] was compared at close values of K_d. Approximately the same values of wear resistance were derived, this leading to the conclusion that not the testing procedure proper, but the energy of the abrasive particles impact and its share absorbed by the metal and estimated using K_d, respectively, is the determinant factor for characterisation of the wear conditions.

The object of study were surfacing alloys of Fe–Cr–Mn–C alloying system. Flux-cored strips were used to produce the deposited metal. The alloying elements content in the deposited metal was varied in the following ranges, %: C — 1 – 3, Mn — 2 – 6, Cr — 6 – 12. A mathematical model of the second order, namely a symmetrical orthogonal composition plan 2^3, was selected for description of the alloying elements influence on wear resistance.

The regressional dependencies for relative wear resistance were calculated from the derived experimental data. The regression equations were represented by second order polynomial:

$$\varepsilon_{(K_d = 1.2)} = 0.98 + 0.68 \cdot C + 0.087 \cdot Mn - 0.027 \cdot Cr + 0.021 \cdot C \cdot Cr - 0.2 \cdot C^2 - 0.017 \cdot Mn^2, \quad (1)$$

$$\varepsilon_{(K_d = 1.4)} = 0.93 + 0.6 \cdot C + 0.11 \cdot Mn - 0.018 \cdot Cr + 0.017 \cdot C \cdot Cr - 0.18 \cdot C^2 - 0.019 \cdot Mn^2, \quad (2)$$

$$\varepsilon_{(K_d = 1.7)} = 1.17 + 0.41 \cdot C + 0.044 \cdot Mn - 0.018 \cdot Cr + 0.017 \cdot C \cdot Cr + 0.025 \cdot C \cdot Mn - 0.16 \cdot C^2 - 0.015 \cdot Mn^2, \quad (3)$$

$$\varepsilon_{(K_d = 2.0)} = 1.19 + 0.36 \cdot C + 0.023 \cdot Mn - 0.015 \cdot Cr + 0.017 \cdot C \cdot Cr + 0.037 \cdot C \cdot Mn - 0.18 \cdot C^2 - 0.012 \cdot Mn^2, \quad (4)$$

$$\varepsilon_{(K_d = 3.5)} = 0.77 + 0.866 \cdot C + 0.002 \cdot Mn - 0.014 \cdot Cr + 0.031 \cdot C \cdot Mn + \ldots + 0.01 \cdot Cr \cdot Mn - 0.34 \cdot C^2 - 0.017 \cdot Mn^2. \quad (5)$$

These equations were used to determine the composition of the deposited metal, providing the highest impact-abrasive wear resistance for each of the considered coefficients of dynamism (Table).

A procedure of selection of the optimal composition of the surfacing material was proposed proceeding from the derived mathematical models, which consists of the following:

determination of K_d, for which purpose test samples of 110G13L steel are placed onto the wearing surface of the part;

selection of an appropriate mathematical model and determination of the required composition of the deposited metal based on the derived K_d;

determination of the composition of the flux-cored strip filler providing the required composition of the deposited metal, using a developed computational program [5].

An example of application of the proposed procedure is development of a flux-cored strip for restoration of plates of a jaw crusher of Kalchik query. These plates are mass-produced of 110G13L steel. In order to select the deposited metal composition, K_d was determined under the actual conditions of service. Samples cut out of the plates were used for measurement of surface hardness before and after operation. These values are HB 140 – 150 and HB 490 – 520, respectively. Proceeding from that, K_d = 3.5. Although the laboratory testing procedure differs from that implemented in operation of the jaw crushers, the same values of K_d (3.5) were derived in either case, however. This leads to the conclusion that under the conditions of laboratory testing and under the actual conditions of service, 110G13L steel absorbs the same energy of impact-abrasive action. The latter allows an appropriate mathematical model (equation (5)) to be used for selection of the deposited metal composition providing the highest wear resistance under these conditions of impact-abrasive wear. This was taken into account in calculation of the composition of PL-Np-160Kh12G5 flux-cored strip filler [6].

Proceeding from the results of preliminary studies the following surfacing parameters were selected: I_w = 600 – 650 A; U_a = 28 – 32 V; v_w = = 35 m/h. Submerged-arc surfacing was performed with AN-26 flux to improve the quality of the deposited metal and reduce the evolution of harmful substances. A stable arcing and a good fusion with the base metal were observed. The developed PL-Np-160Kh12G5 flux-cored strip has good surfacing-technological characteristics:

melting process efficiency, g/h	12600 – 13650
specific efficiency of the surfacing process α_η, g/(A·h)	20 – 22
coefficient of losses ψ, %	4.5 – 4.9

The deposited metal has an austenitic-martensitic-carbide structure. The amount of austenite is 60 – 65 % with 25 – 30 % of martensite, the balance being carbides. The hardness in this case is 39 to 40 HRC.

Application of the flux-cored strip developed by the authors based on laboratory investigations, provided an improvement of wear resistance of the surfaced parts by 1.5 times, compared to the series-produced materials. This is another proof of the need to use the coefficient of dynamism as an objective quantitative criterion of the conditions of impact-abrasive wear. In this case a number of essential advantages are provided, namely an objective assessment of the actual conditions of the parts operation; ability to compare the experimental data of various researchers using different procedures of wear resistance determination; ability to choose the most effective surfacing materials for the specific conditions of service; application of mathematical models to establish the dependencies of wear resistance on hardness, phase and chemical composition.

CONCLUSIONS

1. Use of K_d allows quantitative estimation of different conditions of impact-abrasive action and elimination of the widely used qualitative evaluation characterised by great vagueness. This will permit selection of the most effective surfacing materials for the specific conditions of service.

2. Regressional mathematical dependencies of wear resistance on the deposited metal composition were derived for different conditions of impact-abrasive wear characterised by the coefficient of dynamism, varied in the range of 1.2 to 3.5.

3. PL-Np-160Kh12G5 flux-cored strip was developed for the conditions of wear of jaw crusher plates (K_d = 3.5), proceeding from the appropriate regressional dependence.

REFERENCES

1. (1974) *Technology of electric fusion welding of metals and alloys*. Ed. by B.E. Paton. Moscow: Mashinostroyeniye.
2. Petrov, I.V. (1965) *Investigation of wear resistance of surfacing materials in abrasive wear under the impact of dynamic loads*. Thesis of Candidate of Science. Moscow.
3. Popov, V.S., Brykov, N., Dmitrichenko, N.S. (1971) *Wear resistance of moulds in refractory materials production*. Moscow: Metallurgia.
4. Tenenbaum, M.M. (1966) *Wear resistance of structural materials and machine parts*. Moscow: Mashinostroyeniye.
5. Malinov, V.L., Chigarev, V.V. (1997) Procedure of computation of flux-cored strip. *Vestnik of Priazov State Technical University*, **3**, 164 – 166.
6. Malinov, V.L., Chigarev, V.V. (1998) Procedure of optimisation of the composition of Fe–Cr–Mn–C surfacing materials for different conditions of impact-abrasive wear. *Ibid.*, **6**, 153 – 154.

EFFECT OF HYDROELECTRIC PULSE TREATMENT ON STRUCTURE OF WELDED JOINT METAL

L.I. MARKASHOVA[1], V.V. ARSENYUK[1], V.S. OPARA[2], N.A. ONATSKAYA[2] and L.Ya. REZNIKOVA[2]
[1]The E.O. Paton Electric Welding Institute, NASU, Kyiv, Ukraine
[2]Institute for Pulse Processes and Technologies, NASU, Kyiv, Ukraine

ABSTRACT

It is shown that hydroelectric pulse treatment can provide an efficient stabilization of the dislocation structure and, accordingly, the HAZ metal of welded joints in steel 09G2S through regulating the energy of loading pulses without increasing their amplitude. It is noted that in this characteristic the method of hydroelectric pulse treatment is similar to ultrasonic peening.

Key words: *welded joints, hydroelectric pulse treatment, energy flow density, pressure wave, amplitude, dislocation density.*

Reliability and service life of metal products are known to greatly depend upon the state of the dislocation structure of metal. This is a pressing problem for metal of the welded joints, and in particular of the HAZ metal, which is characterized by extreme instability of the dislocation structure [1]. Based on the relationship between the fine structure and properties of the metal, it can be suggested that one of the promising methods for improvement of the above properties is subjecting the metal to treatment to ensure stabilization of the said structure. According to results of special investigations, the hydroelectric pulse treatment (HEPT) can be used for this purpose [2]. In this connection, of interest is to determine the possibility of enhancing the effect of HEPT primarily by increasing the energy of the pulses, i.e. without increasing their amplitude. This is very important for practical purposes, as the capabilities of HEPT in terms of regulation of the pulse energy are much wider than in terms of variation of amplitude [3].

To find answers to the questions that might arise in this case, investigations were conducted to reveal variations in the dislocation structure of the HAZ metal of welded joints in steel 09G2S (samples 200 × 600 × 40 mm) depending upon the pulse energy. This was done by increasing the energy of the pulses almost without any change in their amplitude, in particular by varying capacitance of the capacitors [3]. The effect of two modes was compared. The modes differed, according to the calculation data [3], in the regions characterized by a high level of local internal stresses and the corresponding dislocation density, as well as the energy flow density which was approximately 1.5 times higher ($E_1 = 3.37$ and $E_2 = 4.35$ kJ/m^2) and close in amplitude ($P_{m_1} = 2.13 \cdot 10^8$ and $P_{m_2} = 2.3 \cdot 10^8$ Pa).

The dislocation structure was studied on ferritic grains in the HAZ located at a depth of 10 mm in the discharge regions. The studies were carried out using the JEOL transmission electron microscope JEM-200CX (Japan) at an accelerating voltage of 200 kV. It was established that samples in the as-welded condition were characterized by an extremely non-equilibrium gradient structure with regions featuring a high level of local internal stresses and corresponding dislocation density $\rho = (0.8 - 1.2) \cdot 10^{11}$ cm^{-2}. Rare unstressed regions with $\rho = (5.0 - 6.0) \cdot 10^9$ cm^{-2} were found. Grain boundaries were non-equilibrium either and characterized by local stress gradients.

Mode *I* of HEPT conducted at $E_1 = 3.37$ kJ/m^2 leads to a relatively low development of the relaxation processes through the entire volume both in the bulk of the grains and at the grain boundaries. This is evidenced by delayed dislocation configurations of the type of the Lomer-Cottrell barriers [4]. Individual dislocation threshold lines with fractures, which are indicative of an intensive interaction of mobile dislocations of different sliding systems in redistribution of relaxation occurring in the course of the process, as well as initial stages of formation of the ball-cellular structures (~10 vol. %), are noted. Sizes of the latter characterizing the free path of the dislocations vary from 0.05 to 0.10 μm. Cells (0.2 – 0.5) μm in size are also found. Density of the dislocations in the more completely formed substructures is about $\rho \sim 10^9$ cm^{-2}; while in the locations of initiation of new structural elements it is $\rho \sim 10^{11}$ cm^{-2}. The in situ relaxation takes place in a grain boundary region.

An increase in density of the energy flow by the pressure wave in mode *II* to $E_2 = 4.35$ kJ/m^2 leads to the mostly cellular structures that are

Variations in the dislocation structure of the HAZ depending upon the pulse energy

Sample state	*Dislocation structure type*	*Dislocation density, ρ, cm^{-2}*	*Free path length, μm*	*Grain boundary state*
Prior to HEPT (as-welded)	Extremely non-equilibrium with local heterogeneity	$(0.8 - 1.2)\cdot 10^{11}$	–	Non-equilibrium with thermal stresses of the 2nd kind
After HEPT	Configuration of the type of Lomer-Cottrell barriers	~ 10^9	0.05 – 0.10	Relaxation of stresses of the 2nd kind (in-situ relaxation)
Mode *I*	Ball-cellular type (~ 10 % through the entire volume)	~ 10^{11}		
Mode *II*	Cellular without clearly defined boundaries (~ 50 %); regions with 100 % formation of cellular structures	$(4.6 - 6.0)\cdot 10^9$	0.7 – 1.0	Relaxation of stresses causing formation of regular structures (dislocation networks, walls)

formed through the entire volume (approximately 50 %). In some locations their amount increases to 100 %. However, judging from the presence of irregular dislocation clusters in regions of the subgrain boundaries and the absence of stable dislocation configurations of these boundaries, the cellular structure formed in this case lacks equilibrium and stability. The length of the free path of dislocations also increases and amounts to (0.7 – 1.0) μm. Active relaxation takes place in the grain boundaries to form more equilibrium regular structures (dislocation networks and walls). The dislocation density is $\rho = (4.0 - 6.0)\cdot 10^9$ cm^{-2}. Summary of the investigation results is given in the Table. It can be seen from comparison of the results on variations in the dislocation structure in HEPT that mode *II* provides a much more efficient stabilization of this structure, as compared with mode *I*, a larger decrease in the intensity of locally distorted regions both in the bulk of the grain and along their boundaries, and an increase in size of the substructural components. However, the results presented are not in all aspects in agreement with the opinion of other investigators concerning the decisive effect of the pulse amplitude on the relaxation processes occurring in metals.

In this connection, it is of interest to compare the effects of HEPT and ultrasonic treatment of metals, as there is no common opinion concerning the mechanism of influence of the latter on the microstructure and, accordingly, properties of materials treated. For example, it is the opinion of some investigators that in static deformation of metals superimposed by ultrasonic oscillations the activation of this process is caused by the addition of wave and static stresses [6], whereas other investigators think that this hypothesis does not have enough grounds [7], as it fails to explain the revealed 100 % decrease in the static deformation force. In addition, as it is indicated, the metals lose all their strength under the sound pressure, which is by two orders of magnitude lower than static yield strength of these metals. This strong effect of the ultrasound is attributable to the fact that various structural defects absorb too much energy. The latter is indicative of the similarity in many respects of the hydroelectric pulse and ultrasonic effects, and proves the presented experimental results.

Therefore, it can be concluded on the basis of the abovesaid that the effect of HEPT on the dislocation structure of metal of the welded joints and its stabilization, in particular, can be achieved through regulation of the energy of the loading pulses without increasing their amplitude. Also, this accounts for the earlier established possibility of increasing the effect on the dislocation structure through multiple repetition of the pressure pulses [8].

REFERENCES

1. Prokhorov, N.N. (1976) *Physical processes occurring in metals during welding. Internal stresses, strains and phase transformations*. Moscow: Metallurgia.
2. Petushkov, V.G., Opara, V.S., Yurchenko, E.S. (1984) Effect of hydroelectric pulse treatment on the dislocation structure of welded joints. *Svarochnoye Proizvodstvo*, **10**, 10 – 11.
3. Krivitsky, E.V. (1986) *Dynamics of electric explosion in fluid*. Kyiv: Naukova Dumka.
4. (1990) *Structural levels of plastic deformation and fracture*. Ed. by E.E. Panin. Novosibirsk: Nauka.
5. Kotsyubinsky, O.Yu. (1974) *Stabilization of sizes of cast iron ingots*. Moscow: Mashinostroyeniye.
6. Konon, Yu.A., Pervukhin, A.B., Chudnovsky, A.D. (1987) *Explosion welding*. Ed. by V.M. Kuznetsov. Moscow: Mashinostroyeniye.
7. Zandeneker, B. *Method for strengthening. Metals*. Patent **3276918** USA. Publ. 28.06.70.
8. Opara, V.S., Petushkov, V.G., Onatskaya, N.A. (1993) Effect of duration of hydroelectric pulse treatment on the dislocation structure of welded joints. *Avtomaticheskaya Svarka*, **3**, 53 – 54.